博士論文

Heat transfer enhancement in a parallel, finless heat exchanger

（フィンレス熱交換器における熱伝達向上に関する研究）

李 霽陽

Contents

Index i
Chapter 1. Introduction 1
1.1 Research background 1
1.1.1 Evolution of refrigerant 1
1.1.2 Evolution of heat exchanger in air conditioner 2
1.2 Research objective 5
1.3 Previous research 6
1.3.1 Refrigerant side 6
1.3.2 Air side 9
1.3.3 Distribution of two phase flow in parallel tubes 12
Chapter 2. Refrigerant side performance of flat tubes with various cross sections 18
2.1 Experimental setup and methodology 18
2.1.1 Experimental Setup 18
2.1.2 Experimental methodology 19
2.2. Results and discussion 23
2.2.1 Heat transfer characteristics of tubes A and B 23
2.2.2 Effect of cross section dimension on heat transfer 26
2.2.3 Pressure drop of tubes A and B 27
2.2.4 Assessment of predictive methods for heat transfer coefficient 28
2.3. Conclusions 32
Chapter 3. Air side performance of fin-tube parallel heat exchangers 33
3.1. Experimental setup and methodology 33
3.1.1 Experimental Setup 33
3.1.2 Test sections and Experimental conditions 34
3.1.3 Experimental data reduction 35
3.2. Results and discussion 37
3.2.1 Dry conditions 37
3.2.2 Wet conditions 38
3.2.3 Frosting/defrosting condition 40
3.3. Conclusions 42
Chapter 4. Air side performance of a finless heat exchanger 44
4.1 Numerical model 45
4.2. Comparison between TLVG, RLVG and DTLVG 49
4.3 Parameter analysis of DTLVG 54
4.3.1 Gap between the DTLVG and finless heat exchanger 55
4.3.2 Tube width 55

4.3.3 Air velocity 56
4.3.4 Robustness analysis 56
4.4. Experimental investigation on the performance of finless heat exchanger with DTLVG 58
4.4.1 Dry conditions 59
4.4.2 Wet conditions 60
4.4.3 Frosting/defrosting conditions 62
4.5 Conclusions 64
Chapter 5. Design of a novel manifold for parallel heat exchangers 66
5.1 Design of manifold 66
5.2 experimental verification 67
5.2.1 Design of experiment 67
5.2.2 Experiment results 72
5.3 Conclusions and future work 76
Chapter 6. Conclusions 77
Acknowledgement 80
References 82

Index

Nomenclature

A_a Total air-side surface area, m^2

A_c cross section of the flat tube, m^2

A_w Inner tube wall area, m^2

A_{unit} tube inner surface area of a specific unit, m^2

b_a, b_w Slopes of saturated air enthalpy, defined in Eq. (3.11), J $kg^{-1}K^{-1}$

C_p Specific heat, J $kg^{-1}K^{-1}$

C_r Capacity ratio

G mass flux, kg $m^{-2}s^{-1}$

H Heat transfer coefficient, W $m^{-2}K^{-1}$

h_{lg} heat of evaporation of R1234yf, J kg^{-1}

h_{ref} heat transfer coefficient of refrigerant, kW $m^{-2}K^{-1}$

I current, A

i Enthalpy, kJ kg^{-1}

L tube length, m

m Mass flow rate, kg s^{-1}

NTU Number of transfer unit, refer Eq. (3.8)

Q Heat transfer rate, W

Q_{up} the heat transfer rate to a specific unit form the upper flat tube, W

Q_{down} the heat transfer rate to a specific unit form the under flat tube, W

q heat flux, kW m^{-2}

q_{unit} heat flux in a specific unit of flat tube, kW m^{-2}

R electric resistance, Ω

T Temperature, K

T_a, T_a, T_c temperature of tube surface defined in Figure. 4, K

T_{ref} refrigerant temperature, K

T_w mean tube wall temperature, K

U_oA_o Overall thermal conductance, W K^{-1}

$U_{ow}A_{ow}$ Overall transport coefficient based on enthalpy difference, kg s^{-1}

x_p vapor quality of refrigerant at the tube length of p

x_{in} vapor quality of refrigerant at inlet

Greek letters

ε Effectiveness

η Surface effectiveness

Subscript

1 Inlet

2	Outlet
a	Air side
max	Maximum value
min	Minimum value
s	Saturation state of moisture air
w	Water side

Chapter 1. Introduction

1.1 Research background

Nowadays, the balance between social development and environment protection is placed at a strategic position from all over the world. In the last century, significant development was achieved by human beings but with a penalty of natural resource and environment degradation. In the 21th century, eco-friendly technologies are the targets for the researchers. Under the background of global warming, for the air conditioner which occupies a considerable part of domestic electric consumption, two parts of new technologies are being explored by the researcher in this area. Firstly, new refrigerants with a low global warming potential are being investigated for replacing the traditional refrigerants. The second is the enhancement of COP of air conditioner by improving the performance of each parts in the system.

1.1.1 Evolution of refrigerant

Increasing concerns regarding the global warming and Ozone depletion have resulted in the evolution of refrigerants in air conditioners from Chlorofluorocarbons (CFCs) which has been phased out under the Montreal Protocol because of its large global warming potential (GWP) and Ozone depletion potential (ODP), and hydro-chlorofluorocarbons (HCFCS) which will be phased out until 2020 in developed countries and 2030 in developing countries because of its medium global warming GWP and small ODP, to Hydro-fluorocarbons (HFCs) in developed and developing countries. Hydro-fluorocarbons (HFCs) refrigerants such as R134a proposed in automobile air conditioners and refrigerant mixture of R410a and R407a proposed in household air conditioners, have no ODP so that they are beneficial for the Ozone protection. However, their GWP cannot be ignored. Figure 1.1 shows CO_2 discharge quantity until 2050. Without Montreal Protocol and Kyoto Protocol, the CO_2 discharge quantity of HFC will account for 19% of total CO_2 discharge quantity, which has significant influence on the global warming. Hence, the low GWP refrigerants are desired in the refrigeration industry.

From the beginning of 2017 the use of refrigerants with global warming potential (GWP) exceeding 150 in all types of mobile air conditioners is banned in the EU market, which has triggered a exploration for new low-GWP refrigerants. Recently, HFOs refrigerant R1234yf, developed by Honeywell and DuPont, has emerged as a promising candidate. Comparing to R134a with a GWP of 1430, R1234yf has a much lower GWP value of 4 and similar thermal properties to R134a which be used in the car air conditioner. However, for promoting the application of R1234yf, two aspects need to be carefully considered. Firstly, R1234yf has a mildly flammability. In the atmosphere, R1234yf degrades to trifluoroacetic acid, which is a mildly phytotoxic strong organic acid. In case of fire it releases highly corrosive and toxic hydrogen fluoride and the highly toxic gas carbonyl fluoride. For safety, the charge amount of R1234yf need to be decreased to a critical point. Secondly, Comparing to R410a

(GWP=2088) which is commonly used in the household air conditioner, the latent heat of R1234fy at an evaporating temperature of 15 ℃ is 153 kJ/kg, which is 26% less than that of R410a with a value of 206 kJ/kg. Therefore, for achieving equivalent cooling capacity, the cycling rate of R1234yf should be larger than that R410a, which induces almost double pressure drop in the heat exchangers. In the refrigeration system, the bigger pressure drop in heat exchangers causes lower COP and higher energy consumption.

The evaporator and condenser occupy the most inner volume in the air conditioner system. In order to compensating the two shortages of R1234yf, the heat exchangers with lower smaller inner volume and pressure drop need to be investigated.

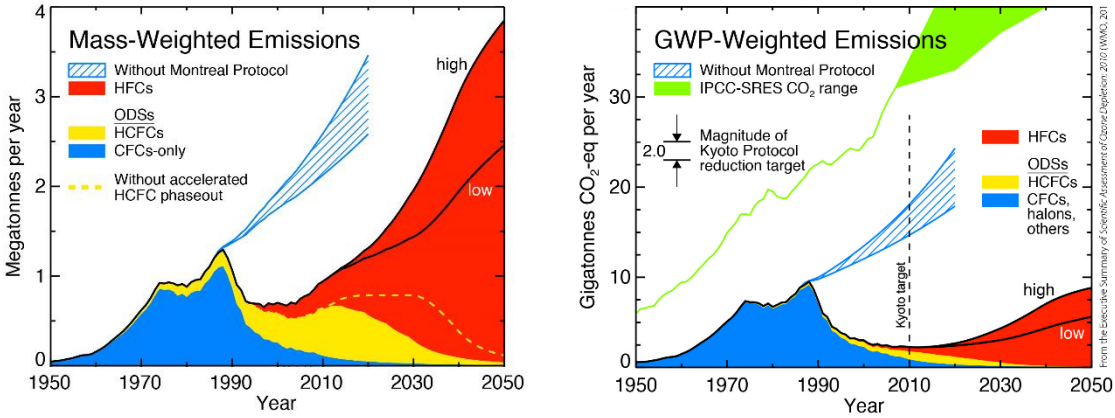

Figure 1.1 shows CO_2 discharge quantity until 2050

1.1.2 Evolution of heat exchanger in air conditioner

The conventional heat exchanger used in air conditioner is constrcted of cupper tube and aluminum fin, as shown in figure 1.2a. By decreaing the diameter of the cupper tube, the inner tube surface area and heat transfer coefficent can be increased, and the inner volume of heat exchanger can be reduced. However, the present diameter of cupper tube is close to the critical diameter of 3 mm, which is decided by the limitation of tube expansion tecnology. For keeping increasing heat transfer performance and decresing inner volume, new constrction of heat exchanger need to be proposed.

All-aluminum parallel multi-port heat exchangers shown in figure 1.2b are being developed for air conditioning systems so as to improve compactness and performance, and to reduce refrigerant charge refills, pressure drops, and total cost. As the name suggested, this type of heat exchanger is constructed of parallel aluminum flat tubes and aluminum fins brazed between flat tubes. The flat tubes are manufactured by extruding technology and each tube commonly contains tens of minichannels which has a hydraulic diameter around 1 mm. Comparing to conventional the heat exchanger, all-aluminum parallel multi-port heat exchangers has several advantages. Firstly, the small hydraulic diameter providing larger inner heat transfer coefficient and area, which enhance the heat transfer performance. Secondly, the flat tube occupy less heat exchanger face area, which provides a lower air side pressure drop.

Thirdly, no more but aluminum is used in the heat exchanger, which ensures the easy recycle and low weight. Moreover, the braze between the fins and flat tubes provides better heat transfer, while comparing to the contact between aluminum fins and cupper tubes in the conventional heat exchangers. In addition, because of the parallel arrangement, the refrigerant mass flux and the length of flow path is less than the conventional heat exchangers, though the hydraulic diameter is much smaller, the refrigerant side pressure drop may be smaller than that in conventional heat exchangers.

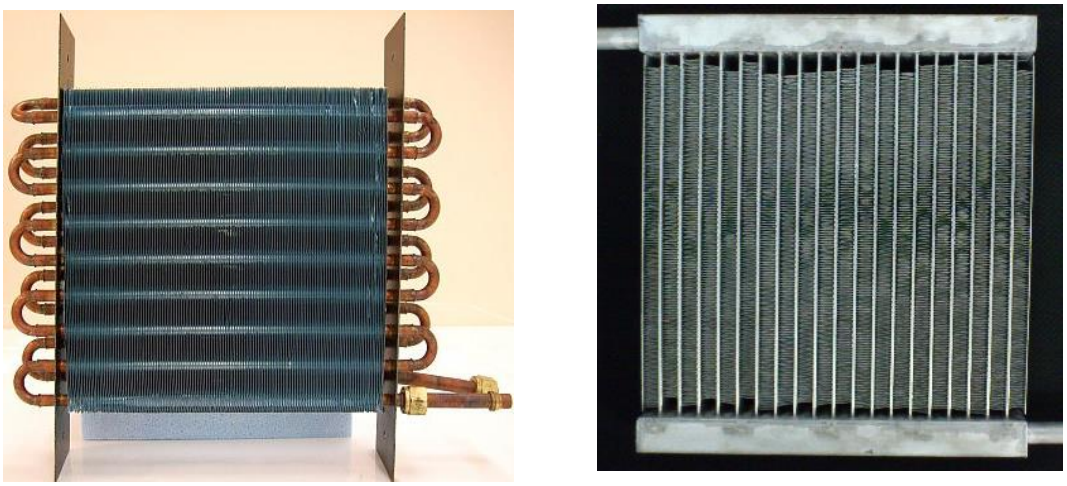

(a) (b)

Figure 1.2 conventional and all-aluminum parallel multi-port heat exchangers

However, the all-aluminum parallel multi-port heat exchangers are generally applied as a condenser in the car air condition, but rarely used in the household air conditioner. For the household air conditioner, in summer the indoor heat exchanger works as an evaporator while the outdoor heat exchanger works as a condenser. In winter, the opposite happens. Till now, the all-aluminum parallel multi-port heat exchangers barely used as an evaporator because of two shortages. The first one is the air side drainage problem, as shown in figure 1.3a. Generally, these heat exchangers consist of vertically set flat tubes, and horizontally mounted fins. When working as an evaporator in humid conditions, the condensed water accumulates on the fins, resulting in lower heat transfer performance, and a higher pressure drop. In winter, the drainage

problem is more serious for evaporators in the outdoor units, which may have an evaporating temperature below 0 ℃. Under such conditions, frosting and defrosting will periodically occur on the heat exchanger surface. If the defrosting water accumulates on the fins, ice will grow rapidly in the following frosting period, and dramatically reduce the performance. The second problem is the maldistribution of two phase flow in the parallel flat tubes. Figure 1.4 shows the distribution of refrigerant under two types of inlet arrangement. Because of the density difference and gravity, the liquid separates from the gas and leads to a stratified flow, which causes that one third of the tubes receive little liquid refrigerant. In an outlet manifold of the maldistributed evaporator, vapor from some tubes must be significantly superheated to compensate for two phase refrigerant coming from the other tubes, and provide sufficient bulk superheat for superheat controlled flow. Hence, the superheating vapor in some tubes causes significant reduction in evaporator performance.

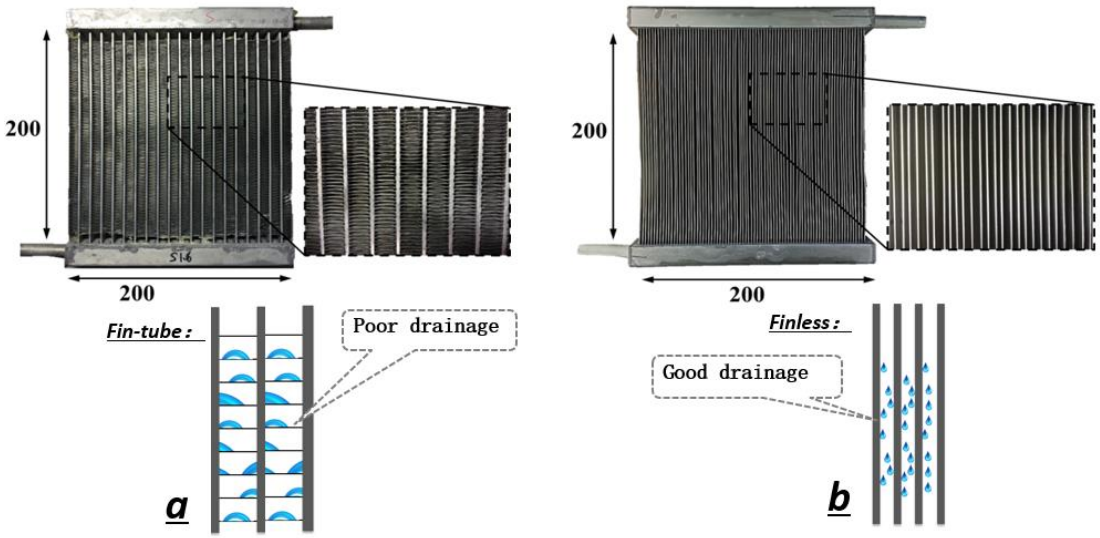

Figure 1.3 Drainage of fin-tube and finless heat exchangers

Modern techniques for manufacturing aluminum flat tubes are highly advanced, hence providing more design options for all-aluminum parallel heat exchangers. Considering the drainage problem described above, finless heat exchangers shown in figure 1.3b may have the potential for application in air conditioning systems. As the name suggests, finless heat exchangers consist of only vertically set, thin flat-tubes without any fins that provide excellent drainage performance in wet and frosting/defrosting conditions. However, although excellent drainage performance can be achieved by using the finless heat exchanger, their heat transfer performance in dry conditions is lower, when compared to that of the fin-tube parallel heat exchangers, for the following reasons. The first reason is that the smooth surface of the flat tube induces a thick flow boundary layer on it, which deteriorates its heat transfer performance. The second reason is that the total heat transfer area of the finless heat exchanger is lower as compared to the fin-tube parallel heat exchanger.

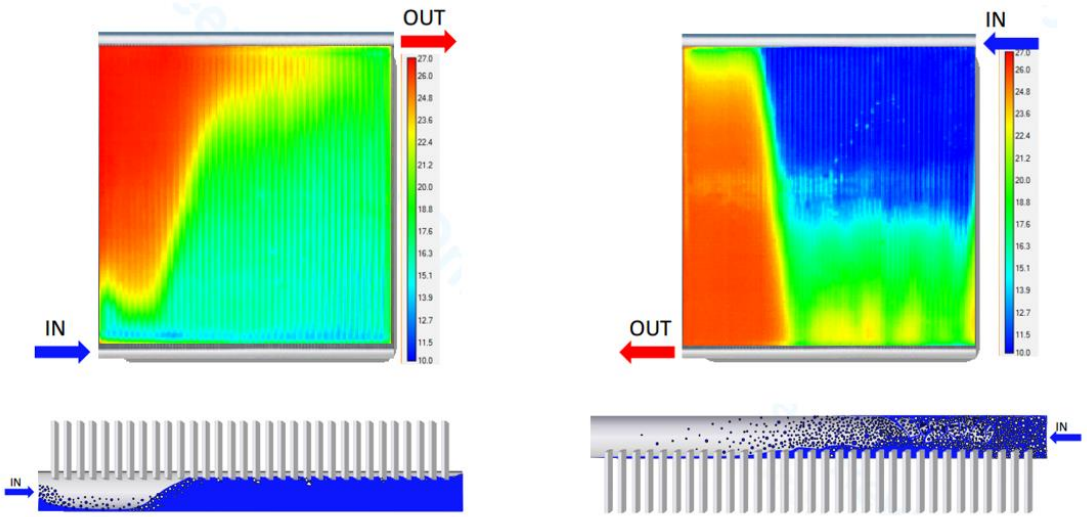

Figure 1.4 Maldistribution in parallel heat exchangers[1]

In conclusion, compared with the conventional heat exchanger with the same heat transfer capacity and pressure drop, both the parallel fin-tube and finless all aluminum heat exchanger may has lower inner volume, which make them have potential to be used for decreasing the charge amount of low GWP refrigerant.

1.2 Research objective

The performance of the parallel heat exchanger mainly includes three parts. The first part is the air side heat transfer coefficient and pressure drop under dry, wet and frosting/defrosting conditions. The fin-tube parallel heat exchanger may has deficiency on this part. The second part is the refrigerant side heat transfer coefficient and pressure drop. And the third part is the distribution of two phase flow in parallel flat tubes. In this dissertation, the study on these three parts are presented.

1. Air side

For the fin-tube heat exchanger, the air side performance is mainly determined by the structure of fin. Compared to the plain fin, slit- and louver-fins provided better heat transfer performance, by breaking boundary layers and mixing airflow. In this distribution, the heat transfer and pressure drop performance of five all-aluminum parallel multi-port heat exchangers, including three with slit fins with fin pitch of 1.2 mm, 1.4 mm and 1.6 mm, and the others with louver fins with the same fin pitches, were experimentally investigated under dry, wet and frosting/defrosting conditions.

For the finless heat exchanger, for enhancing the heat transfer performance of the finless heat exchanger, a longitudinal vortex generator (LVG) was installed in front of the finless heat exchanger with a narrow gap, which ensured that under wet and frosting/defrosting conditions, the condensed or defrosted water would not fall on the LVG, ensuring that the drain and defrosting

performance was not affected by the LVG. With numerical simulation, the optimal design and parameter analysis for LVG were finished. Moreover, the performance of finless heat exchanger with and without LVG under dry, wet and frosting/defrosting conditions were experimentally investigated, and compared to that of fin-tube heat exchangers.

2. Refrigerant side

The extruding technology provides possibility to manufacture various cross section of channel in flat tubes. In this study, two types of rectangular aluminum multi-port extruded tubes (here called tubes A and B) were manufactured, and the local heat transfer coefficient and pressure drop were measured. Tube A had 16 channels with a cross-section of 0.91 × 0.21 mm while tube B had 40 channels with a cross-section of 0.34 × 0.21 mm. The tested results were compared to that of another flat tube having 16 channels with a square cross-section of 0.9 × 0.9 mm, and a brief analysis of flow boiling pattern in each type of tube was presented. Furthermore, the comparison between the perdition results of several correlations and the experimental data was carried out.

3. Distribution of two phase flow in parallel tubes

In the parallel heat exchangers, all the flat tubes are connected to a manifold. The structure of the manifold has significant influence on the distribution performance. In this dissertation, a new design concept of manifold is proposed for achieving better distribution performance. This design was firstly verified by water and air, then the performance was further checked by refrigerant.

1.3 Previous research

1.3.1 Refrigerant side

All-aluminum parallel multi-port heat exchangers are being developed for air conditioning systems to improve compactness and performance, and to reduce refrigerant charge amount, pressure drop, and total cost. When working as an evaporator, the refrigerant side flow boiling heat transfer and pressure drop performances are the crucial characteristics that need to be studied in-depth. Although numerous studies of flow boiling in mini-channels have been previously conducted, only a limited number have employed low heat and mass flux conditions that are typically found in air conditioning systems. As a result, the flow boiling mechanism inside multi-port extruded tubes of air conditioning systems has not yet been elucidated.

As introduced in the last section, R1234yf is a candidate of the future refrigerant. Due to increasing concerns regarding all-aluminum parallel multi-port heat exchangers, there is a demand for clarification of the heat transfer performance of R1234yf in multi-port extruded tubes. Currently, limited data are available in the literature on evaporative heat transfer of R1234yf in mini-channels. Some researchers reported the thermal performance of R1234yf with comparison of R134a. Zilio et al. [2]represented an experimental study with R1234yf and R134a in a compact European automotive air conditioning system, they reported 3-7% lower

cooling capacity and 1−3% lower coefficient of performance (COP) comparing with R134a. Jarall[3] reported an experimental study with R134a and R1234fy in a small refrigeration system. The results showed lower COP, smaller cooling capacity and lower compressor efficiency for R1234yf. An experimental study of boiling heat transfer with R134a and R1234yf with mass flux of 20−100 kg/m^{2}s and heat flux of 2−15 kW/m^2 in a rectangular multiport channel was reported by Mortada et al[4]. Higher heat transfer coefficient was found for R1234yf, and convective boiling dominance was observed. Del Col et al.[5] carried out flow boiling experiments of R1234yf at a saturated temperature of 31 ℃ with mass flux of 200−600 kg/m^{2}s and heat flux of 2−15 kW/m^2 in a circular channel with a diameter of 1 mm, and compared with R134a. The heat transfer coefficient was highly dependent on the heat flux while the mass velocity is found to have no effect. With regard to vapor quality, the heat transfer coefficient decreased with quality up to 0.3, then it remained pretty constant. No significant differences between the flow boiling performance of R1234yf and R134a was reported. Saitoh et al.[6] reported an experimental study on flowing boiling of R1234yf at a saturated temperature of 15 ℃ with mass flux of 100−400 kg/m^{2}s and heat flux of 6−24 kW/m^2 in a 2 mm diameter horizontal tube. The results showed that nucleate boiling dominated the heat transfer performance at low vapor quality region, whereas at high vapor quality region the heat transfer coefficient was decided by both nuclear boiling and convective heat transfer. Zahid et al.[7] carried out flow boiling heat transfer, pressure drop and dryout characteristics of R1234yf in vertical stainless steel tube with a diameter of 1.60 mm and a length of 245 mm. The mass flux was in the range of 100−500 kg/m^{2}s while the applied heat flux was in the range of 5−130 kW/m^2. The results showed that the boiling heat transfer was strongly controlled by the applied heat flux with insignificant effect of mass flux and vapor quality, and almost identical heat transfer performance was reported comparing with R134a. The heat transfer coefficient could be satisfactorily predicted by correlations from Gungor and Winterton[8] and Mahnoud and Karayiannis[9]. Otherwise, in order to apply R1234yf to residential air-conditioners, Li et al. [10][11]proposed refrigerant mixtures of R1234yf and R32 for enhancing performance, and their flow boiling heat transfer performances were investigated at two mass fractions (80/20 and 50/50 by mass%) in a smooth horizontal tube with an inner diameter of 2 mm. The results showed that the heat transfer coefficients of the mixture with an R32 mass fraction of 20% were 10–30% less than those of pure R1234yf for various mass and heat fluxes. When the mass fraction of R32 increased to 50%, the heat transfer coefficients of the mixture were 10–20% greater than those of pure R1234yf under conditions of large mass and heat fluxes. Moreover, based on the experimental results they proposed a new semi-empirical correlation for pure refrigerants as well as refrigerant mixtures.

For flow boiling heat transfer in mini- and micro-channels, a plenty of reviews have been proposed in the literatures[12][13][14][15][16][17][18]. The previous works mostly focus on the circular channel, and the research on rectangular channel is relatively limited. Actually, the flow boiling

mechanism in rectangular channel is quite different from circular channel reported by the previous visualization researches. Enoki et al.[19][20] conducted visualization and heat transfer measurement of flow boiling with R410A in a circular, a triangle, and a rectangular channel with an identical hydraulic diameter of 1 mm. The mass flux ranged from 30 to 400 kg/m^{2}s, and the heat flux was in a range of 2−24 kW/m^2. They observed that the heat transfer coefficient in rectangular channel was higher than that in circular channel, especially in low mass flux and low vapor quality region. The reason was revealed by the visualization: because of surface tension, most liquid accumulated in the four corners while thin liquid film formed on the two channel sides, which provided excellent heat transfer performance. Yen et al.[21] visualized the flow boiling of HCFC123 in transparent circular and rectangular glass tubes which heated by semi-transparent ITO/Ag thin film. Comparing to the research of Enoki et al., higher heat flux ranged from 25.32 kW/m^2 to 84.72 kW/m^2 was imposed to the refrigerant. They found that the liquid accumulated in the four corners, which created a superb condition for nuclear boiling. Hence, the heat transfer performance of rectangular channel was better than that in circular channel. Tanaka et al.[22] visualized flow boiling of R1234yf in rectangular and half circular copper multi-port channels with an identical hydraulic diameter of 0.9 mm, and measured the heat transfer coefficient in the multiport aluminum tubes having the rectangular and circular channels for the mass flux range of 60−120 kg/m^{2}s and the heat flux range of 4−16 kW/m^2. They reported that the heat transfer performance in rectangular channels was better than that in circular channels, which could be explained with the same reason as Enoki et al.[19][20] reported. Furthermore, they reported that in the rectangular channel, the heat transfer performance in low mass flux and low heat flux region was higher than that in general mass and heat flux conditions. Chanyoot et al.[23] investigated the flow patterns and heat transfer characteristics of R134a during flow boiling in a single rectangular micro-channel with a hydraulic diameter of 0.68 mm at a heat flux range of 7.63–49.46 kW/m^2 and a mass flux range of 600–1400 kg/m^{2}s. They reported that six different flow patterns were observed during boiling of R134a: bubbly flow, bubbly-slug flow, slug flow, throat-annular flow, churn flow, and annular flow, which took significant influence on the heat transfer performance. Some other researchers investigated the heat transfer performance of refrigerants in multiport tubes with rectangular channels. Generally, they reported the influence of heat flux, mass flux, vapor quality and saturated temperature on the heat transfer performance, and several correlations were developed based on the experimental results. Particularly, Soupremanien et al.[24] studied the influence of aspect ratio on flow boiling of Forane® 365 HX in rectangular channels with a hydraulic diameter of 1.4 mm. They reported that the change of aspect ratio has significant influence on heat transfer coefficients and pressure drop.

Using R1234fy as refrigerant under low heat and mass flux conditions, Tanaka et al.[22] reported the local heat transfer and pressure drop performances of two kinds of multi-port extruded tubes having five channels with a rectangular cross-section of 1.05 × 2.6 mm, and

having 16 channels with a square cross-section of 0.9 × 0.9 mm. They concluded that under the specific working conditions, the vertical up-flow boiling heat transfer performance was significantly influenced by the channel geometries and the effect of surface tension. The tube with a square cross-section showed better heat transfer performance than that with a rectangular cross-section. These results implied that there was a potential to improve performance by decreasing the cross-sectional area.

1.3.2 Air side

On the air side, drainage problem is the main problem restricting these compact heat exchangers from being widely used in air conditioners. Generally, these compact heat exchangers consist of vertically set flat tubes, and horizontally mounted fins. When working as an evaporator in humid conditions, the condensed water accumulates on the fins, resulting in lower heat transfer performance, and a higher pressure drop. In winter, the drainage problem is more serious for evaporators in the outdoor units, which may have an evaporating temperature below 0 ℃. Under such conditions, frosting and defrosting will periodically occur on the heat exchanger surface. If the defrosting water accumulates on the fins, ice will grow rapidly in the following frosting period, and dramatically reduce the performance.

For all-aluminum parallel multi-port heat exchangers, research on the air-side thermal performance, under wet and frosting/defrosting conditions, has been conducted by several researchers. Webb and Jung[25] investigated the application of brazed-aluminum heat exchangers in the residential air conditioner, and reported that the heat transfer rate of the brazed-aluminum heat exchangers was 50% higher than that of a conventional heat exchanger. Moreover, they observed that the condensate could be removed far from the heat exchanger surface, so it could be applied to the air conditioner system. Zhang et al.[26] studied the performances of three types of heat exchangers that use the louver-fin geometry. These were a parallel flow-extruded flat-tube heat exchanger with parallel fins (PF2), a parallel flow-extruded flat-tube heat exchanger with serpentine fin (PFSF), and a heat exchanger with round tubes and wave-plate fins (RTPF), each of which was studied experimentally under dry, wet, and frost conditions. Because the air-side pressure drop in the PF2 heat exchanger slowly increased under frost condition, it could be used for longer defrost cycles. Kim et al.[27] experimentally investigated the air-side thermal-hydraulic performance of 30 samples of louvered-fin brazed-aluminum heat exchangers under dehumidifying conditions. The test results were compared with those for dry surface heat exchangers, in terms of sensible j factor and friction factor f as functions of the Reynolds number based on louver pitch, and the correlations for j- and f-factors were developed. Furthermore, Kim et al.[28] studied the effect of inclination angles, θ, on the air-side performance of a brazed-aluminum heat exchanger under dry and wet conditions. They reported that the heat transfer performance for both dry and wet conditions was influenced insignificantly by the inclination angle ($-60° < \theta < 60°$), while the

pressure drops increased consistently with the inclination angle. In addition, Kim et al.[29] investigated the effect of air inlet humidity conditions on air-side heat transfer and pressure drop characteristics for an inclined brazed-aluminum heat exchanger, and reported that the heat transfer and pressure drop characteristics under wet conditions were not influenced substantially by the air inlet humidity for $\theta \leq 45$ °.

Wu et al.[30] experimentally studied the frosting process of a folded-louvered-fin, parallel-flow microchannel evaporator in a heat-pump central air-conditioning system. Mesoscale frost formation processes on its front surface were observed for three different test conditions, using a charge coupled device (CCD) camera, and the frost height correlation was provided. Moallem et al.[31] investigated the influence of surface temperature, water retention, and surface coating on the frosting performance of parallel microchannel heat exchangers. The results showed that temperature and air humidity were the primary parameters that influenced frost growth rates, whereas water retention and air velocity had a secondary impact on the frosting performance. Hydrophobic- and hydrophilic-coatings on microchannel coils slightly affected the heat transfer capacity in frosting conditions. Xia et al.[32] compared the thermal-hydraulic performance of four microchannel heat exchangers with various folded-louvered-fin geometries during the first frost growth period, and then, for analyzing the effects of retained liquid water after defrosting, the performance of two heat exchangers under defrosting and refrosting cycles was studied. They found that the air-side pressure drop and heat transfer in the refrosting period were significantly influenced by condensate droplets, and became periodic and repeatable after the third or fourth refrosting cycle. Xu et al.[33] studied the periodical frosting and defrosting performance of two types of microchannel heat exchangers, and all the processes were observed using a CCD camera. Ice blockage formed in the fin-root gaps of the horizontal-tube sample because of water retention. Cycle operation increased the blockage severity until the fin space was completely blocked. The amount of water retained, and its impact on frosting time, pressure drop, and capacity were further investigated. Moreover, Xu et al.[34] investigated the frost- and defrost-performance of microchannel heat exchangers for heat-pump systems, and found that the vertical-tube sample outperformed the horizontal-tube sample for a heat pump system, because water retention in the horizontal-tube sample rapidly increased as the cycle progressed.

Compared to the plain fin, slit- and louver-fins provided better heat transfer performance, by breaking boundary layers and mixing airflow. Dejong et al.[35] and Cowell et al.[36] visualized the flow pattern for louver and slit fins, respectively. The visualizations suggested that the louver fin may provide a better mixing of the airflow, which was further supported by Achaichia et al.[37]. However, the drainage performance, and the heat transfer and pressure drop performance need to be further compared under wet under frosting/defrosting conditions.

Modern techniques for manufacturing aluminum flat tubes are highly advanced, hence providing more design options for all-aluminum parallel heat exchangers. Considering the drainage problem of the fin-tube parallel heat exchangers described above, finless heat

exchangers may have the potential for application in air conditioning systems. As the name suggests, finless heat exchangers consist of only vertically set, thin flat-tubes without any fins that provide excellent drainage performance in wet and frosting/defrosting conditions. Not much research has been done in this area, until now. Shikazono et al.[38] numerically and experimentally investigated the heat transfer and pressure drop performance of two different types of finless heat exchangers that consisted of side-contacted and flat tubes. Based on the results, they proposed the empirical correlations for heat transfer coefficient and pressure drop for these two types of finless heat exchangers. Moreover, they claimed that even a small deviation in assembly could cause considerable deterioration in heat transfer performance. Nakano et al.[39] proposed a concept of a finless heat exchanger used in frozen cargo vehicles, and investigated the characteristics of frost formation on a tube surface using a numerical method. Following that, Onishi et al.[40] compared the heat transfer and pressure drop performance between the finless and conventional fin-tube heat exchanger, and they claimed that the finless heat exchanger provided better performance under both dry and frosting conditions. Kaneko et al.[41] proposed a concept of concavo-convex plate finless heat exchanger, and they found the optimal design of the concavo-convex geometry with numerical and experimental methods. For heat transfer enhancement, Onishi et al.[42] directly added a vortex generator on the flat tube surface. Using a numerical simulation, they finalized the optimal design of the vortex generator and the tube arrangement.

Although excellent drainage performance can be achieved by using the finless heat exchanger, their heat transfer performance in dry conditions is lower, when compared to that of the fin-tube parallel heat exchangers, for the following reasons. The first reason is that the smooth surface of the flat tube induces a thick flow boundary layer on it, which deteriorates its heat transfer performance. The second reason is that the total heat transfer area of the finless heat exchanger is lower as compared to the fin-tube parallel heat exchanger.

In recent years, the longitudinal vortex generators (LVG) applied in various heat exchangers have received considerable attentions for the advantages of remarkable heat transfer enhancement, accompanied by an acceptable pressure drop penalty. He and Zhang called the optimization studies of heat transfer enhancement applying longitudinal vortex generator as the “hot spots” for the future research[43]. In the conventional point of view, when the fluid flows through longitudinal vortex generators, streamwise vortices are generated due to flow separation on the leading edge of the LVG, causing disruption of boundary layer, as well as fluid swiring which enhancing the exchange of core and wall fluid, leading to the enhancement of heat transfer. On the other hand, this heat transfer enhancement can also be analyzed by the view of field synergy principle[44][45]. When the second flow generated by vortex generators results in the reduction of the intersection angle between the velocity and fluid temperature gradient, the heat transfer will be enhanced.

Figure 1.5 shows four types of common LVGs that include delta wing, rectangular wing, delta winglet and rectangular winglet. Recently, most research focus on the delta

winglet[46][47][48][49][50][51][52] and rectangular winglet LVGs[53][54][55][56][57]. Generally, there are two methods to add LVGs in the flow channel. The first method is directly bonded in the flow channel [51][52][53][54][55][57], as shown in figure 1.6a; the second method is punching LVGs on the fins[56][46][47][48][50][45], as shown in figure 1.6b. This method is relatively convenient and commonly used in the tube-fin heat exchanger. For optimal design for LVGs that increasing the heat transfer but decreasing the pressure drop, numerical simulation is a common way used by researchers[55][56][57][46][47][48][50][45]. Moreover, experimental investigations[53][54][55][49][52] and visualizations[55][51] are also applied for further study.

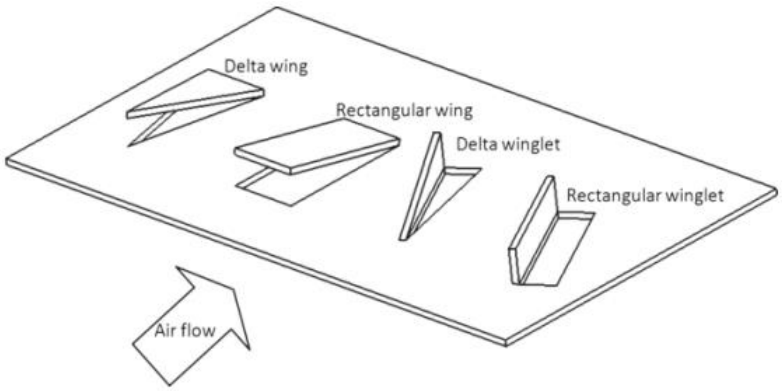

Figure 1.5 Four types of common LVGs[43]

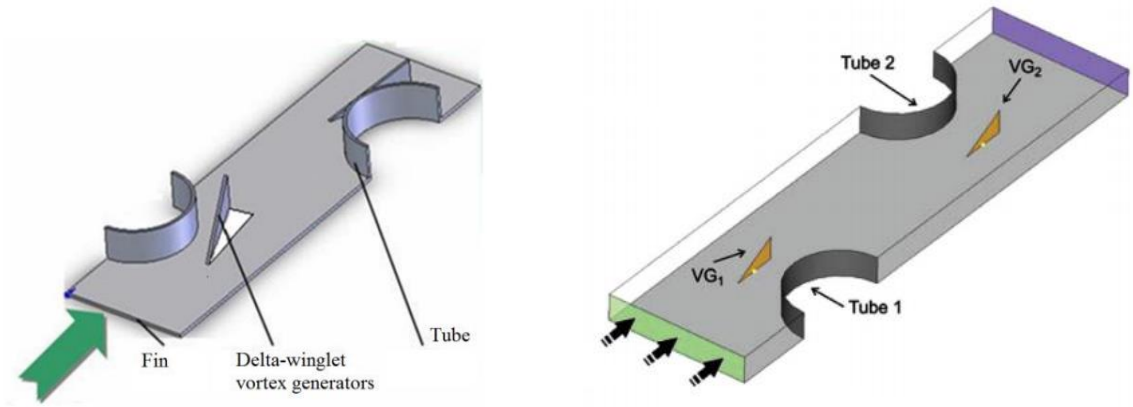

(a) **(b)**

Figure 1.6 Two types of common LVGs mounting methods[50][55]

1.3.3 Distribution of two phase flow in parallel tubes

The quality maidistribution of two-phase refrigerant in parallel tubes will cause early dry out in the tubes receiving lesser liquid mass flow rate, thus decrease the performance of parallel evaporators. There are two main reasons. The first one is that vapor and liquid refrigerant have different densities and therefor inertia force in two phase flow so that their tendencies to branch out of the manifold into parallel tubes are different. Secondly, the two phase flow tend to

separate from each other in the manifold because of gravity. Tuo[1] conducted a detailed review on this issue. Based on his review, I presented a brief introduction below.

In the past decades, Two-phase flow distribution in parallel tubes has been extensively studied by many scholars. Bowers et al.[58] presented two phase flow distribution in parallel microchannel tubes with rectangular and circle manifolds. The flow visualization shows that the shorter inlet length which results in more homogenous two phase flow in the manifold provides the most uniform distribution with an optimum protrusion depth near one half. Peng et al.[59] experimentally investigated the two phase R134a refrigerant distribution in a horizontal manifold with five vertical downward parallel tubes. The two-phase flow regimes in the manifold were visualized and mapped as a function of inlet refrigerant mass flux and quality. Cho and Cho[60] investigated the mass flow rate distribution and vapor-liquid phase separation of R-22 in parallel tubes under adiabatic condition. The effect of the orientation of the manifold on the mass flowrate distribution and phase separation was the largest among the test parameters. Horizontal manifold showed better mass flow rate distribution and phase separation characteristics than vertical manifold. Hwang et al.[61] investigated R410A refrigerant distribution in a horizontal manifold with total 30 upward branch microchannel tubes. Their results indicated that distribution of liquid was significantly affected by the manifold inlet location that the side-inlet location provides better results comparing to the end-inlet location in the range of operating conditions investigated. Moreover, the effect of the tube pitch was insignificant. Vist and Pettersen[62] reported two-phase distribution of R134a refrigerant in a horizontal circular manifold for both upward and downward set circular branch tubes. Compared to the inlet quality, little influence on the distribution results was observed when changing the total mass flux, or the heat load on the evaporator. Kim et al.[63] reported the refrigerant R-134a flow distributions in a round manifold with ten flat tubes, which simulating a brazed aluminum heat exchanger. Three different inlet orientations (parallel, normal, vertical) were investigated. Tests were conducted with downward flow for the mass flux from 70 to 130 kg/m^2s and quality from 0.2 to 0.6. At low mass flux or quality, vertical inlet yields the best flow distribution, followed by normal and then parallel inlet. As mass flux or quality increases, the optimum configuration switches to normal inlet configuration. The overall best configuration was the one with normal inlet.

As refrigerant maldistribution is appeared to be one of the major issues for degrading performance of microchannel evaporators, many researchers have contributed their efforts on the improvement of refrigerant distribution. The first method is preventing the separation of two phase flow in the manifold due to gravitational and inertial forces and creating a homogenous two phase flow. Peng and Hrnjak[64] used plain orifice and pressure swirl as expansion devices to create a homogeneous mist or quasi-mist flow. The atomized droplet size measured in their experiment was about 50 um~ 200 um as a function of inlet mass flow rate and quality. However, the plain orifice provided poorer distribution due to the dominance of

the front pooling effect; whereas the distribution results for the swirl atomizer inlet indicate somewhat a positive effect. Marchitto et al.[65] used orifices at the inlet of the multiple channels and nozzles at the distributor inlet to improve water-air two-phase distribution in 16 vertical upward channels with a cylindrical horizontal manifold. Their results indicated the orifice diameter, presence and geometry of an inlet nozzle and the specified range of gas and liquid inlet superficial velocities had significant influence on the distribution. Shi et al.[66] experimentally compared the performances of microchannel evaporators with different manifold structures. Among the eight sample evaporators tested, the maximum difference of the cooling capacity operating under the same condition was reported to be up to about 32%. Their results demonstrated the importance of design of manifold on the performance of parallel evaporators. Dshida and Hrnjak[67] also reported that maldistribution in a 4-pass MCHX caused up to about 25% COP reduction compared to the same residential mini-split type A/C and heat pump system using the baseline round tube plain fin heat exchanger. For improving the distribution, MCHX was modified into a single-pass design and refrigerant flow was divided into eight smaller flows with a conical distributor before entering the manifold. However, only 5% COP improvement was obtained upon the worst case. Besides the methods mentioned above, many other designs were patented by some companies. However, to our best knowledge, there is no perfect design which can provide uniform distribution of two phase refrigerant in a wide range of operating conditions.

Contrary to the method mentioned above which mixing the vapor-liquid refrigerant into a homogenous flow pattern, another approach is to feed only liquid refrigerant into microchannel evaporators. Figure 1.7 compares schematic system configurations of typical direct expansion (DX) and flash gas bypass (FGB) systems. Elbel and Hrnjak[68] claimed three major benefits of FGB approach: 1) reducing pressure drop across the microchannel evaporator; 2) increasing the local CO2 boiling heat transfer coefficient; 3) and improving the refrigerant distribution. Beaver et al.[69] reported up to 20% COP increment while maintaining the same capacity over the baseline DX system. Elbel and Hrnjak[70] applied FGB approach into transcritical CO2 Environmental Control Unit (ECU) using a step motor valve to control the pressure drop of the bypass line as well as the liquid level in the flash gas tank.

Although only liquid feeding the parallel tubes can be achieved by using FGB method, it is hard to obtain the uniform distribution and stable operation of parallel evaporator due to reversing flow. Tuo[1] detailed analyzed this problem in his doctor thesis. The diameter of microchannel used in A/C or refrigeration system evaporators is typically around 1 mm or less, which is much smaller that the ordinary tubes used in conventional tube-fin evaporators. In microchannel, nucleation bubble can easily grow up to a size comparable to the channel hydraulic diameter. Further bubble expand in a longitudinal direction along the channel in a

form of elongated bubble, as shown in figure 1.8.

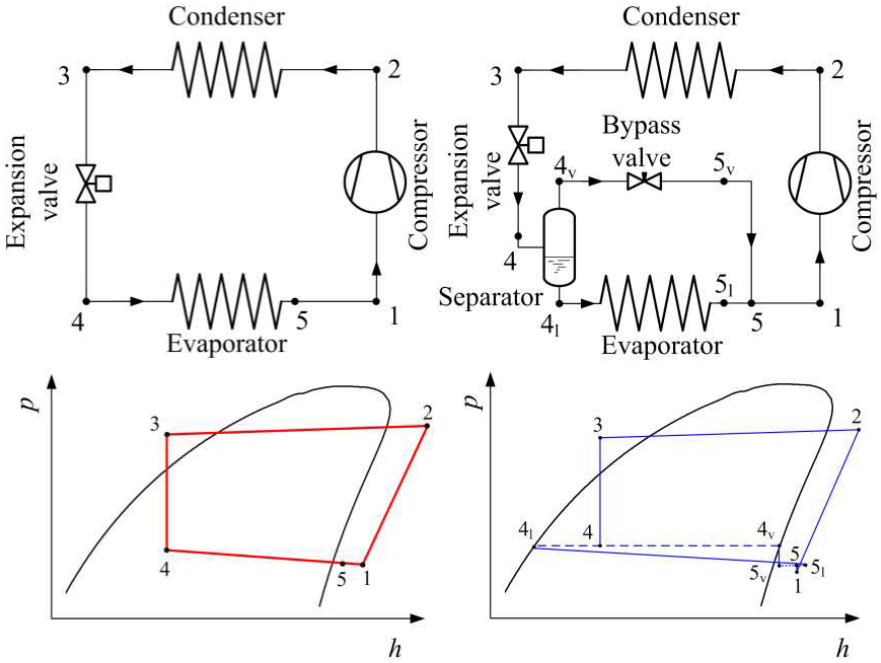

Figure 1.7 Schematic drawing of A/C systems: 1) DX system; 2) FGB system[1]

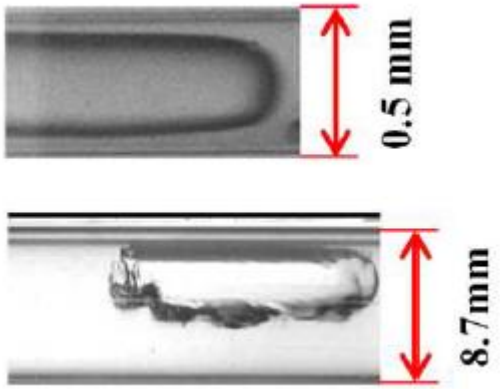

Figure 1.8 comparison of nucleation of bubbles in micro and conventional tubes[71][72]

The quick expansion of bubble will cause a pressure spike and push the incoming flow back to the inlet manifold, as shown in Figure 1.9. This phenomenon does not occur in the conventional tubes with a larger diameter. As shown in figure 1.8, since the local high pressure generated by a single bubble is confined to a small region of the channel and can hardly affect the global pressure distribution and the bulk flow dynamics[73]. Kew and Cornwell[74] proposed a threshold of the bubble growth confinement based on the dimensionless number called Confinement number Co (Eqn. 2-1), and set the threshold at Co = 0.5.

$$C_o = \frac{\sigma}{g(\rho_L - \rho_G)d_h^{\,2}} \tag{1.1}$$

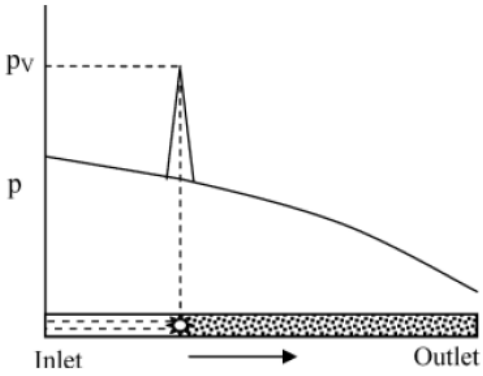

Figure 1.9 Schematic representation of pressure variation following nucleation during flow boiling in a microchannel[75]

Meanwhile, inlet manifold provides significant compressible volume for storing the reversed vapor, as shown in Figure 1.10. When forward flow is re-established, reverse vapor and liquid flow will be re-distributed among parallel microchannels. Very likely, liquid flow distribution with the presence of reverse vapor would be non-uniform[76][77].

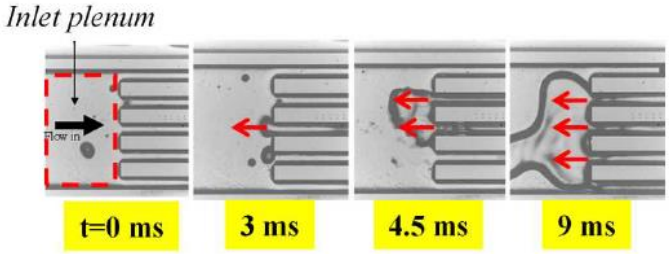

Figure 1.10 Transient flow oscillation in the inlet plenum of microchannels[78]

In addition, since the protrusion depth of flat tube, the backflow vapor will accumulate at the upper regime, and a gas-liquid interface be formed on the same level with the inlet of flat tubes. This interface fluctuates due to the inlet liquid flow, as shown in figure 1.11. The fluctuation of the interface will cause intermittent liquid inlet for each flat tubes, which causes intermittent dry-out. Considering this problem, Tuo[1] presented a revised flash gas bypass (FGBR) method to vent out the reverse vapor flow trapped in the inlet manifold. As shown in figure, two venting ports were set at the head and end of the manifold. With this method, the experimental comparison reveals that the vapor venting provided a 5% increase of cooling capacity and 3% of COP at the fixed compressor speed condition, while the maximum COP improvement was approximately 10% -12% when capacity is matched by reduction of compressor speed.

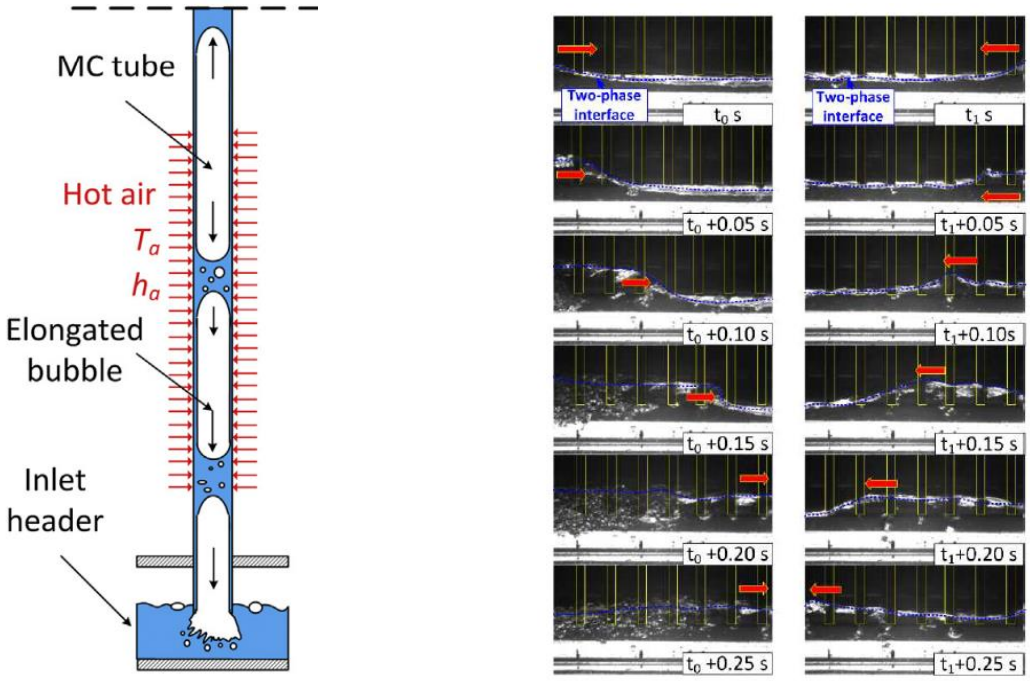

Figure 1.11 gas-liquid interface and its fluctuation in manifold[1]

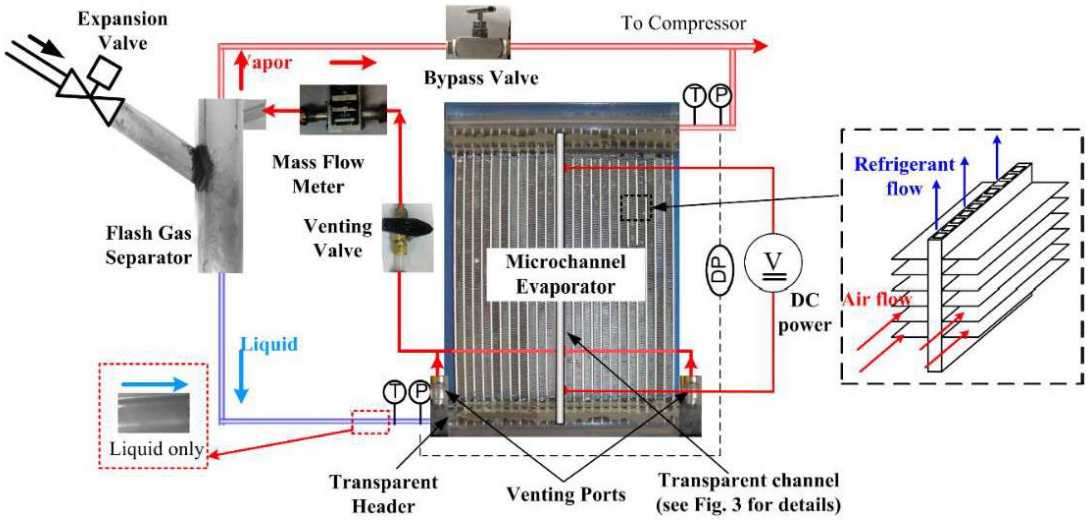

Figure 1.12 experimental setup of FGBR method[1]

However, the flash gas bypass method reported by the previous literature is not suitable for parallel heat exchangers which is supposed to reduce the refrigerant charge amount. Because using such method, a gas-liquid separator with a considerable volume is necessary, therefore the total inner system volume cannot be remarkably decreased. Therefore, a novel manifold need to be designed for achieving better liquid refrigerant distribution in parallel tubes without obvious inner volume increase.

Chapter 2. Refrigerant side performance of flat tubes with various cross sections

In this study, two types of rectangular aluminum multi-port extruded tubes (here called tubes A and B) were manufactured, and the local heat transfer coefficient and pressure drop were measured. Tube A had 16 channels with a cross-section of 0.91 ×0.21 mm while tube B had 40 channels with a cross-section of 0.34 × 0.21 mm. The tested results were compared to Tanaka's results[22], and a brief analysis of flow boiling pattern in each type of tube was presented. Furthermore, the comparison between the perdition results of several correlations and the experimental data was carried out.

2.1 Experimental setup and methodology

2.1.1 Experimental Setup

Figure 2.1 shows a schematic of the experimental setup. The liquid refrigerant was circulated using a gear pump, and the flow rate was measured with a Coriolis flow meter. The inlet vapor quality was controlled using a constant temperature bath and an electrically heated pre-heater. The test section was set vertically and heated by DC power. The flow patterns before and after the test section were observed by two sight glasses. After leaving the test section, the vaporized refrigerant flowed to a condenser and a sub-cooler before finally returning to the gear pump.

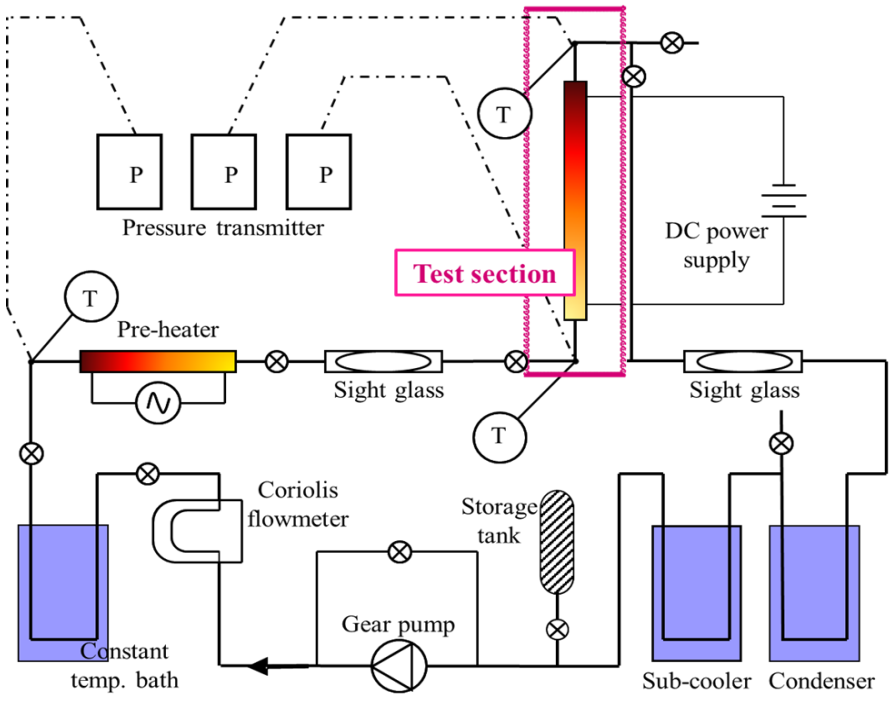

Figure 2.1: Schematic of experimental setup

2.1.2 Experimental methodology

Figure 2.2a shows the whole test section. There was a visualization section just before the aluminum tube, and an orifice plate with four holes of 1 mm diameter was mounted as shown in Figure 2.2b to enhance the mixing of vapor and liquid refrigerant. Figure 2.2c shows the mixture pattern of refrigerant after flowing through the orifice plate in experiments. The vapor and liquid were mixed intensively, which provided a more uniform distribution of liquid for each channel. The surfaces of the electrodes were coated with an electroless nickel plating to reduce the electric resistance. To minimize heat loss, the whole test section excluding the visualization section was covered with thermal insulation material. The test tubes were made of aluminum A1050. The cross-sections of tubes A and B are shown in Figure 2.3, and the detailed dimensions are listed in Table 2.1.

The pressures and temperatures of the refrigerant at the inlet and outlet of the test tube and at the inlet of the preheater were measured by a pressure sensors and a sheathed thermocouples, respectively. As shown in Figure 2.4, 24 0.1 mm OD T-type thermocouples were attached to the surface of the test tube along the tube length in eight groups. All the experimental data were collected under steady working conditions. The accuracy of the thermocouples and pressure sensors were ±0.1 K and ±0.1 kPa, respectively. The accuracy of the Coriolis flow meter was ±0.1%. The heat loss was confirmed to be less than 5%. The properties of the refrigerant R1234yf were determined by REFPROP version 9.1.

Table 2.1 Tube dimensions

Tube type	Type A	Type B
Number of channels	16	40
Tube width [mm]	16.6	16.6
Tube height [mm]	0.6	0.6
Wetted perimeter length [mm]	35.8	44
Cross-sectional area [mm^2]	3.06	2.86
Hydraulic diameter [mm]	0.34	0.26
Tube length [mm]	181, 266, 436	158, 220, 344
Heated length [mm]	85, 170, 340	62, 124, 248

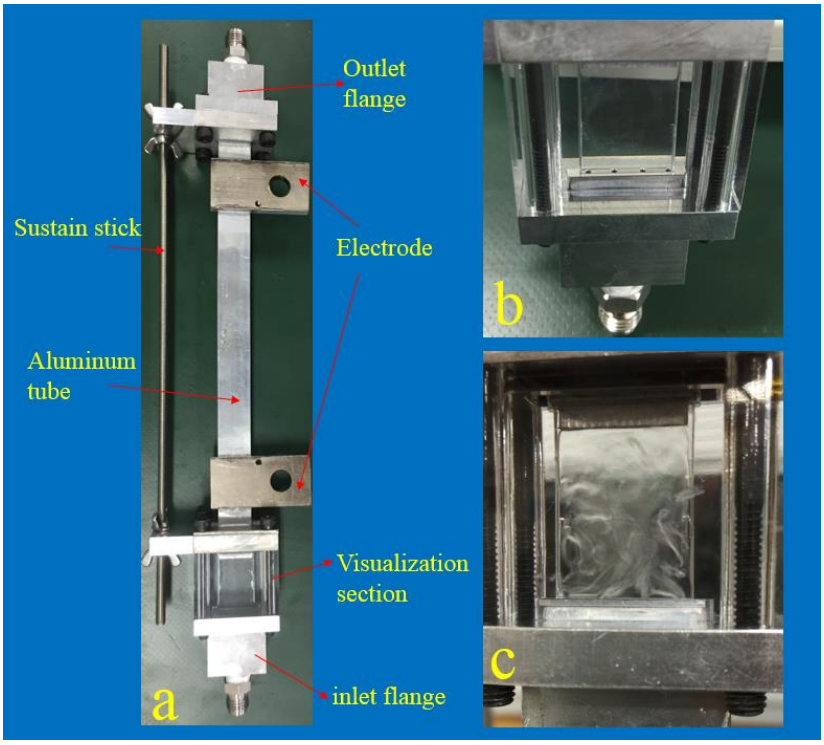

Figure 2.2 Test section

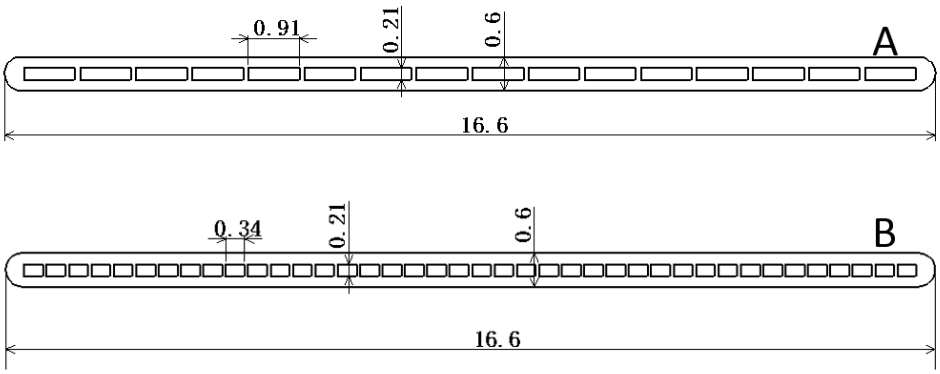

Figure 2.3: Tube dimensions

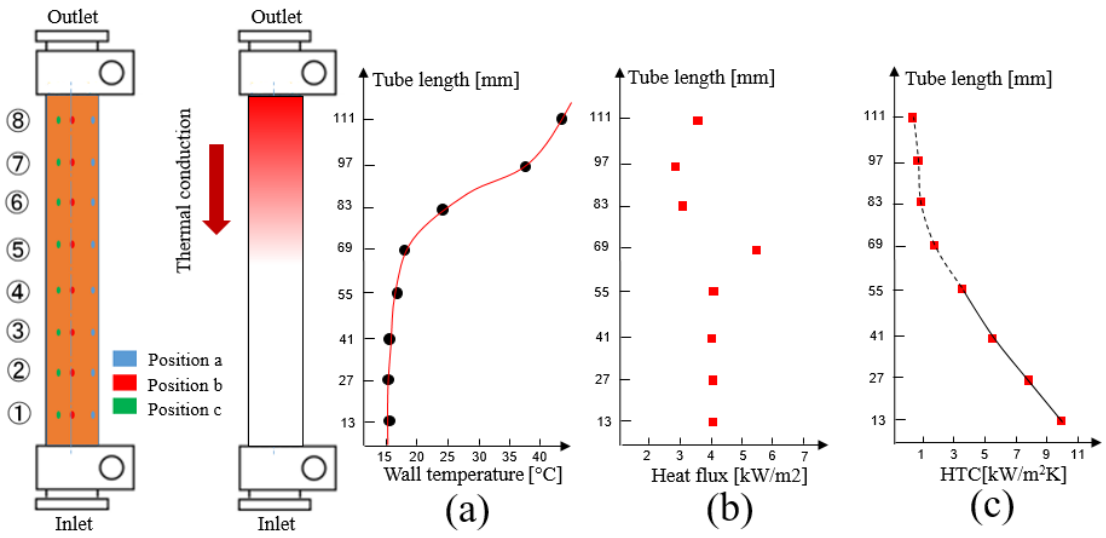

Figure 2.4: Tube temperature distribution

The heat flux and mass flux ranges were 3−16 kW/m^2 and 60−240 kg/m^{2}s, respectively. The heat flux was controlled by adjusting the output voltage of the DC power supply, and the mass flux was regulated by the speed of the gear pump. The boiling temperature was set to 15 ℃ at the inlet of test section. Before flowing into the test section, the vapor and liquid were required to achieve equilibrium, which was verified through temperature and pressure measurements. If the difference between the inlet temperature and the saturated temperature calculated from the inlet pressure was less than 0.1 K, it indicated that a state of equilibrium had been achieved. Because of this, the inlet vapor quality in all experiments was approximately 0.3, which is controlled by the preheater.

The assumptions made for the purpose of data reduction are listed below:

1. The pressure inside the tube was assumed to be linear along with the flow direction, so the local pressure was calculated from the inlet and outlet pressures. The local saturated temperature was calculated according to the estimated local pressure. The pressure drops in the flanges and visualization section were neglected.

2. The inner wall temperature was assumed to be equal to that of the outer wall. This assumption could be validated by numerical simulation, showing that for the low heat flux used in the experiments, the difference between the inner wall and outer wall was less than 0.03 K.

The local heat transfer coefficient h_{ref} [kW/m^{2}K], was calculated by

$$h_{ref} = \frac{q}{T_w - T_{ref}} \tag{2.1}$$

where T_w and T_{ref} are the average local wall temperature and saturated temperature determined by the local pressure, respectively. The average local wall temperature was defined as follows: where T_a, T_b, and T_c are outer wall temperatures at positions a, b and c shown in Figure 2.4.

Position b located on the symmetric axis of the flat tube, while position a was set nearby the edge and position c located in the middle between the symmetric axis and the edge. Assuming axial symmetry, the area-weighted average of the wall temperature is expressed by equation (2.2).

$$T_w = \frac{1}{5}(T_b + 2\,T_a + 2\,T_c \tag{2.2}$$

Although the tube was heated by electric resistance heating, the local heat flux q was not uniform at all locations because of two reasons. Firstly, due to the low mass flux and the rectangular channel geometry, dry patches occurred easily at high vapor quality region, which induced low heat transfer coefficient and high tube wall temperature. Hence, heat will be conducted from the high temperature part to the low temperature part in the aluminum tube material. Secondly, the electric resistance of aluminum tube along the tube length was uneven also because of the uneven temperature distribution in the tube. Since the identical current along the tube, the heat generated by electric was not uniform. In this paper, the method for determining the local heat flux is shown below.

The relation between the electric resistance of each tube and tube temperature ranged from 15 to 50 ℃ was measured first. Electricity was added on each tube while pure water with given inlet temperature was pumped to the tube to maintain the average tube temperature at the specific value. The water flow rate was adjusted large enough to keep the difference between the inlet and out water temperature less than 0.5 ℃. Then, the electrical resistance per tube length of each tube at the given temperature could be calculated by the recorded voltage, current and the tube length. By changing the water inlet temperature and repeating the procedure mentioned above, the temperature dependence of electrical resistance per length could be obtained by fitting the data points.

Figure 2.4 shows the tube temperature distribution of tube B when the mass flux was 60 kg/m^{2}s and the average heat flux was 4 kW/m^2. From the 6th position, the wall temperature increased dramatically. Based on the temperature at each measured position, the whole temperature distribution was fitted by a polynomial curve as shown in figure 2.4a. The tube was divided into many sections, and the heat flux of each section was calculated by equation (2.3). Since the wall temperature was usually higher on the downstream side, the heat flux in each section was calculated from the downstream side toward the upstream side.

$$q_{unit} = \frac{I^2 R(T_{unit}) L_{unit} + Q_{up} - Q_{down}}{A_{unit}} \tag{2.3}$$

where $R(T_{unit})$ is the electric resistance per length, T_{unit} is the wall temperature, Q_{up} is the heat conducted from the downstream section, and Q_{down} is the heat conducted to the upstream section, that are calculated from temperature gradient according to the polynomial curve. A_{unit} and L_{unit}

are the inner tube area and the length of the section, respectively. Figure 2.4b shows the heat flux calculated with the method mentioned above. The heat flux at the first four position were quite even because that the temperature distribution in this region was relatively uniform. Due to the sharp change of the tube wall temperature, the heat flux at the fifth measured position was much higher than the average heat flux while those at the last three positions were lower. The dryout occurred near the position where the heat flux took a local maximum value. Furthermore, the heat transfer coefficient at each measured position was determined and shown in Figure 2.4c.

The vapor quality x_p at the position p, which is counted from the entrance, was determined by equation (2.4).

$$x_p = \frac{\sum_{i=1}^{p} I^2 R(T_i) L_i}{G A_c h_{\mathrm{lg}}} + x_{in} \tag{2.4}$$

where G is the mass flux, A_c is the cross-sectional area of the flow, and h_{lg} is the heat of evaporation of R1234yf. x_{in} is the inlet vapor quality which is determined by the enthalpy of the refrigerant before the preheater and the heat input in the preheater.

Although the method described above is able to calculate the heat transfer coefficient with considering both the axial thermal conduction and the temperature influence of electric resistance, the uncertainty of the heat transfer coefficients from positions 5 to 8 which connected by dash line was hard to precisely evaluate. Because in these regions, Q_{up} and Q_{down} were calculated from the temperature gradient which might change dramatically. The number of measured points were not many enough to precisely establish the polynomial curve and express the temperature gradient. However, applying this method the heat transfer coefficient from position 1 to 4, where the vapor quality was low, could be accurately determined, and represented by solid line in Figure 2.4c. For the high vapor quality region, this method is also able to provide more reliable heat transfer coefficient than that with the uniform heat flux assumption, which represented by the dashed line in Figure 2.4c. The uncertainty related to the calculation of the local heat transfer in the low vapor quality region is estimated by the least square method of the measured quantities (saturation temperature, wall temperature, heated section, and power input). The largest uncertainty on the local heat transfer coefficient is 22.1% at the lowest heat flux of 3 kW/m^2.

2.2. Results and discussion

2.2.1 Heat transfer characteristics of tubes A and B

Figures 2.5 and 2.6 show the experimental heat transfer performance of tubes A and B while the mass flux varies from 60 to 240 kg/m^{2}s, and the heat flux varies from 3 to 16 kW/m^2. In order to facilitate visualization of trends, the experimental data points are connected by lines of

the same color for each condition. The data of both tubes clearly show that the heat transfer coefficient decreases as the vapor quality increases under current experimental conditions. For tube B, all data show an approximately linearly decreasing trend. For tube A, the heat transfer coefficient demonstrated similar trends for mass fluxes exceeding 120 kg/m^{2}s, while the heat transfer coefficient for a mass flux of 60 kg/m^{2}s linearly decreased from 7 to 1 kW/m^{2}K as the vapor quality increases from 0.3 to 0.7, and then leveled off at a low value. Similar trends were also presented by Tanaka et al.[22] and Enoki et al.[19]. In Tanaka's research, two types of rectangular multi-port tubes with hydraulic diameters of 1.5 mm and 0.9 mm were used, and the heat transfer coefficient decreased with the increasing vapor quality for a low mass flux of 15 kW/m^2. Enoki et al. reported similar results as flow boiling occurred in a rectangular tube for a low mass flux of 30 kW/m^2.

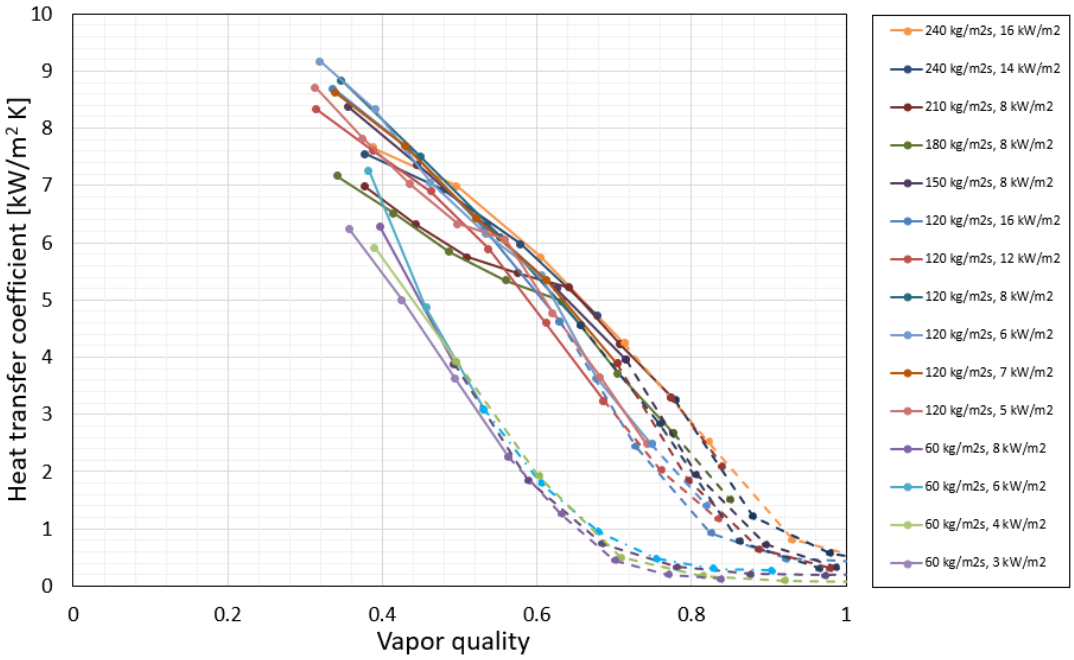

Figure 2.5: Heat transfer performance of tube A

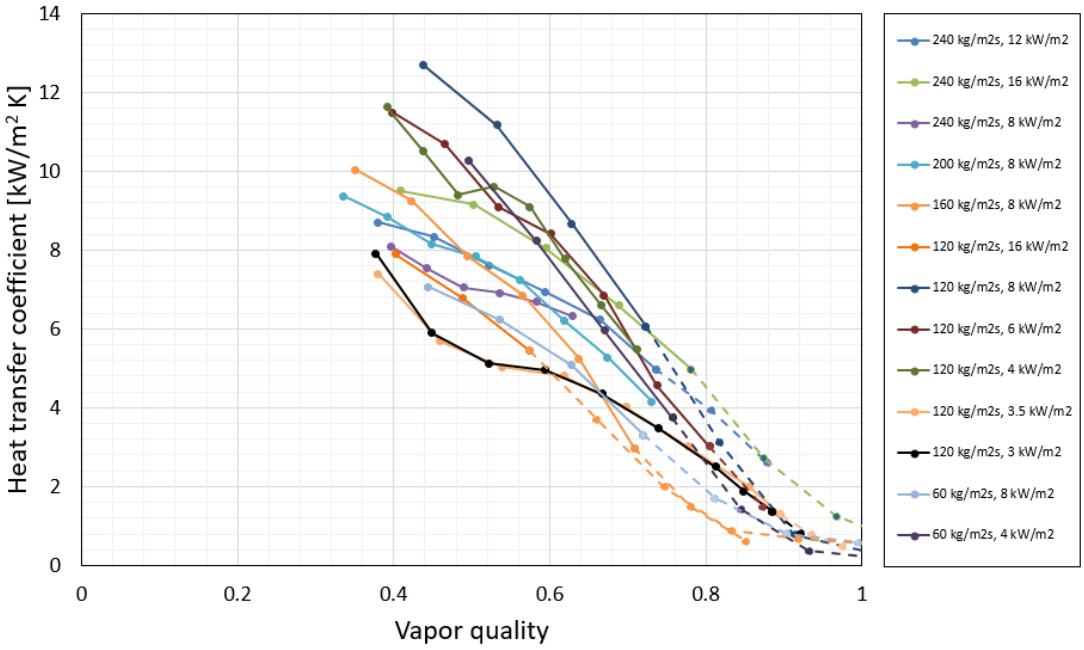

Figure 2.6: Heat transfer performance of tube B

It can be inferred that this trend is mainly induced by the typical flow pattern of a rectangular channel, in which most of the liquid refrigerant accumulates in the four corners. As shown in Figure 2.7C, for relatively higher mass fluxes, thin liquid films (blue region) cover all surfaces of the rectangular channel, which provides excellent heat transfer performance.[21] However, when the mass fluxes become lower, this liquid film shows reduced stability, which in turn induces intermittent dry patches and deteriorates the heat transfer performance. The channel shapes of tubes A and B are not square, thus the liquid accumulates in the four corners, which implies that dry patches will easily occur on the wider surfaces, as shown in Figure 2.7A and 2.7B. As the vapor quality increases, the mass of liquid decreases, thereby making it more difficult for the liquid film to be formed on the surface. Additionally, the increase in the vapor velocity may cause turbulence and disturb the formation of liquid film. Therefore, the dry patches will occupy increasingly more area of the tube surface, resulting in increasingly worse heat transfer performance.

Generally, the mass and heat fluxes strongly influence heat transfer performance through a complex mechanism while flow boiling occurs within a channel, which has been discussed in numerous research works. For tube B of the current study, although the mass and heat fluxes influence the heat transfer performance, their effects are substantially less dominant than that of vapor quality, thereby making it difficult to fully elucidate their mechanism of action. For tube A, when the mass flux was reduced to 60 kg/m^{2}s, a dramatic deterioration of heat transfer performance was clearly observed. The heat transfer coefficient decreases to a value of 2000

kW/m^{2}K at the vapor quality of 0.6, and it may be speculated that dry-out occurs everywhere except in the corners when the vapor quality reached 0.7. Although this phenomenon was not observed in tube A, it may be speculated that if the mass flux continued to decrease from 60 kW/m^2, a dramatic drop in heat transfer performance would occur.

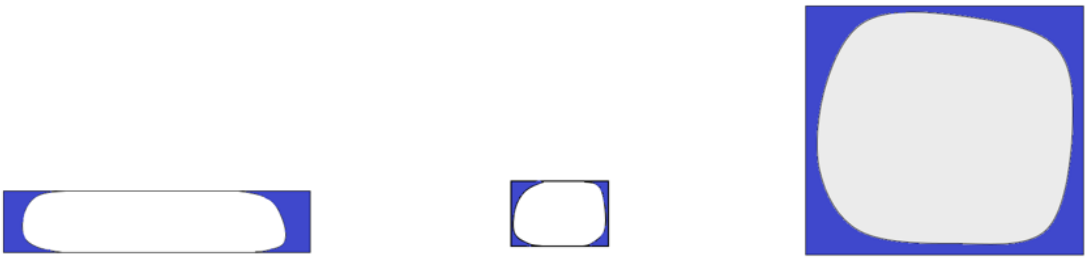

Figure 2.7: Flow patterns in three different tubes

2.2.2 Effect of cross section dimension on heat transfer

At the same heat and mass flux conditions, the heat transfer performances in tubes A and B were compared to that of Tanaka's tube with a cross-section of 0.9 × 0.9 mm, which is called tube C in this paper. Figure 2.8 shows the comparisons of heat transfer coefficients. It can be clearly seen that at the relatively lower mass flux of 60 kg/m^{2}s, tube C demonstrates the best performance over the entire measured vapor quality range, while tubes A and B demonstrate a substantially worse performance due to their structural limitations discussed in section 3.1. When the mass flux increases to 120 kg/m^{2}s, the dry patch is alleviated in tubes A and B. In the low vapor quality region, because of the smaller channel size, a thinner film is likely established in tubes A and B, which led to superior heat transfer performance over that of tube C. However, as the vapor quality increases, the dry patch occupies more of the tube surface, thereby the heat transfer performance drops dramatically. Figure 2.8 shows that for most cases, the heat transfer performance of tube B is better than that of tube A.

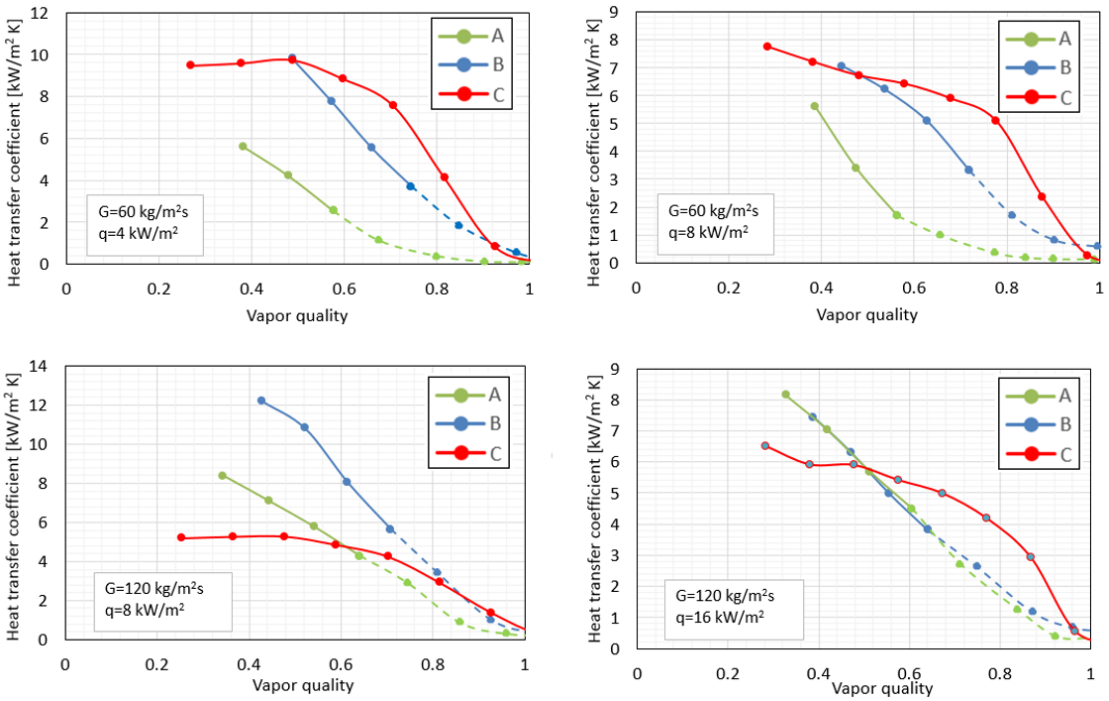

Figure 2.8: Comparisons of heat transfer performance in tubes A, B, and C

2.2.3 Pressure drop of tubes A and B

The two-phase pressure drop within the vertical tube can be expressed as the sum of frictional, gravitational, acceleration, inlet contraction, and outlet extraction components. The pressure drop in the visualization section is quite small compared to that within the tubes, so it may be neglected. The frictional pressure drop plays a dominant role among the five components; therefore, numerous researchers focus on it and many correlations are found in the literature. In this study, three correlations of Lee−Lee[79], Lockhart−Martinelli[80], and Mishima−Hibiki[81] were adopted for comparison with the experimental results of tubes A and B. The total pressure drop calculation method was the same as Anwar's[7]. Fifteen data points of tube A and 21 data points of tube B were compared with the calculation results, as shown in Figure 2.9. It can be seen that the historical Lockhart−Martinelli correlation shows the best agreement among the three correlations, in which 72.2% of the data were located in the ±30% range.

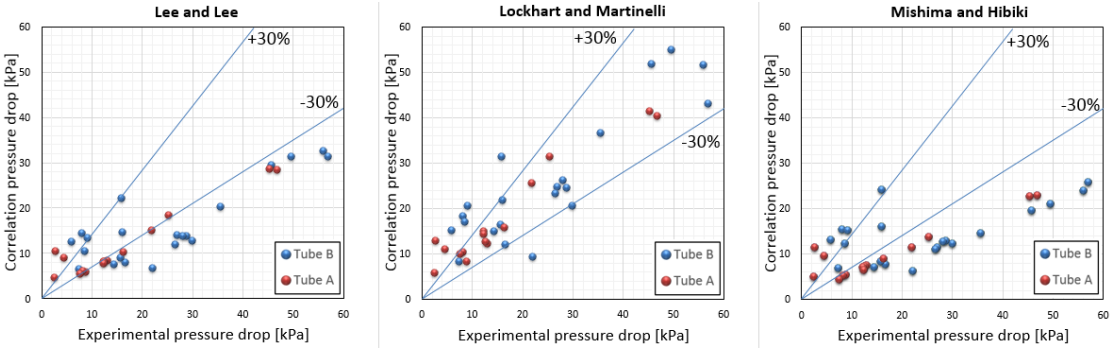

Figure 2.9: Comparison between experimental and correlation results of pressure drop

2.2.4 Assessment of predictive methods for heat transfer coefficient

In this section, the experimental heat transfer coefficients are compared to the results predicted by existing flow boiling heat transfer correlations. Kim et al.[18] summarized the present flow boiling heat transfer correlations and evaluated the performance of each correlation. According to the discussion of heat transfer performance, partial dry-out or dry-out played a crucial role on the heat transfer performance of tubes A and B. Hence, three correlations considering the dry-out are chosen for comparison: the Saitoh et al. correlation[82], the Agostini−Bontemps correlation[83], and the Bertsch et al. correlation[84]. The comparison results with vapor quality ranged from 0.4 to 0.95 of tubes A and B under various heat and mass flux conditions are shown in Figures 2.10 and 2.11.

The Saitoh et al. correlation was developed from the boiling heat transfer of R134a in horizontal small diameter tubes (0.51, 1.12, and 3.1 mm ID). It separates the flow boiling process in pre and post-dryout. The onset of dry-out is predicted by a simple annular flow model. For the pre-dryout region, a modified Chen-type correlation was developed with considering the influence of tube diameter using Weber number. For the post-dryout resion, the heat transfer coefficient is predicted as the summation of two terms: the heat transfer coefficient by the Dittus-Boelter's correlation in the vapor phase and the pre-dryout heat transfer coefficent in the liquid phase. The onset of dry-out of tubes A and B was 0.43 and 0.36 predicted by the correlation, following that the heat transfer coefficient decreased with the growth of vapor quality under all of the working conditions. This trend predicted by the correlation is acceptable, but the predicted heat transfer coefficients were lower than the experimental data. The main reason for this underestimation can be inferred that the Saitoh et al. correlation is developed form the data of circle tubes, in which the heat transfer mechanism is different from that in rectangular channels. In rectangular channels, most liquid accumulated in the four corners and thin liquid film generated which provide excellent heat transfer performance, though partial dry-out easily happens. Another reason is that this correlation is developed only form the data of R134a, thus it may be not suitable for R1234yf.

The Agostini−Bontemps correlation was established from the heat transfer data of R134a in multiport extruded tubes composed of 11 parallel channels (3.28×1.47 mm). It also separates the flow boiling process into two parts. When vapor quality x≤0.4, the heat transfer coefficient weakly depends on vapor quality. For vapor quality x ≥0.4, the heat transfer coefficient decreases with the increase of vapor quality, and simply correlated with vapor quality, heat flux and mass flux with a condition of boiling number $Bo \geq 4.3\times10^{-4}$. The comparison result is similar to that of Saitoh et al. correlation. The reducing trend of heat transfer coefficient with vapor quality was well predicted. However, for tube A the predicted heat transfer coefficients were much lower than the experimental result, whereas for tube B, mostly comparisons show that in low vapor quality region the predicted heat transfer coefficients are lower than the experimental data, but in high vapor quality region the contract results exist. The reasons for this unsatisfactory prediction is similar to that for the Saitoh et al. correlation. Firstly, all these data is predicted form the refrigerant of R134a. Secondly, the critical dry-out quality of 0.43 is speculated form the data in the rectangular multiport tubes with a channel dimension of 3.28×1.47 mm. However, our channel size is much less and the dry-out is much different. Particularly, for tube A, when the mass flux reduced to 60 kg/m^{2}s, the heat transfer coefficient decreased more sharply than that in high mass flux condition. This phenomenon is contract to the point in the Agostini−Bontemps correlation, which claim that the greater the mass flow rate, the more probable dry-out should be.

The Bertsch et al. correlation was also developed from Chen correlation based on 3899 experimental data points covering 12 different fluids with hydraulic diameter ranging from 0.16 to 2.92 mm. The heat transfer coefficient is a sum of weighed nucleate boiling and convective heat transfer terms. A suppression factor, *S*, is applied to the nucleate boiling term to account for dryout as the vapor quality increases, while the convective heat transfer term is multiplied by factor, *F*, to account for the enhanced convection due to higher flow velocities at increased vapor qualities. As shown in Figures 2.10 and 2.11, the Bertsch et al. correlation failed to predict the experimental data trends and values. The main reason is that the dry-out plays a dominant role in the heat transfer performance in our experiemnt, whereas in the correlation the convective heat transfer dominant the trend of total heat transfer coefficient.

Consequently, the three correlations mentioned above does not match the experimental data successfully, though the data trend is well predicted by the Saitoh et al. correlation and the Agostini−Bontemps correlation. The reason is that in all of these three correlations, the two-phase flow pattern in rectangular channel is not taken into account. From Tanaka's visualization[22] and the experimental data in this paper, it can be infer that in low-vapor quality region, most of the liquid refrigerant accumulates in the four corners of the rectangular channel, and nuclear boiling occurs there. On the four sides of the channel, thin liquid film forms and convective boiling happens. However, the liquid film is not stable, and the dry patch appears even in low vapor quality region. As the vapor quality increases, the dry patch occupies more

and more area, which leads to the decrease of heat transfer coefficient. Furthermore, the aspect ratio of the rectangular channel, which is important for the heat transfer performance as explained above, is not taken in to account in these three correlations.

As mentioned above, the heat transfer mechanism is quite complex that numerous research needs to be conducted to make it clear, if necessary. To our best knowledge, even for the adiabatic two phase flow in mini rectangular channels, the shape of liquid thus the thickness of liquid has not been clarified. The experimental data above shows that the dry-out is the dominant factor to the heat transfer performance. Thus, for determining the onset of the dry-out and the further partial dry-out area, as the first step, the model for determining the liquid film thickness on the rectangular channel faces in adiabatic and further boiling conditions need to be established. Now, some researchers focus on the liquid film thickness of adiabatic two phase annular flow in round mini tubes[85], which may offer some useful models of the fraction between gas and liquid, which should be the foundation for the research in rectangular channels. Besides that, for establishing a flow boiling model in multiport rectangular channel flat tubes, many other factors need to be taken into account. For instance, the mechanism of liquid film dry-out and rewetting, the instantaneous maldistribution in multiport channels which may affect the overall heat transfer performance of flat tube, and the disturbance to the liquid film from nuclear boiling.

Nevertheless, for the heat exchanger of air conditioner, especially for the finless heat exchanger, the air side heat resistance play a dominant role in the whole heat transfer process comparing to the refrigerant side. Otherwise, the inlet condition of two phase refrigerant is determined by the design of manifold. Thus, it is better to put the model establishment after the research on the air side performance and distributor design.

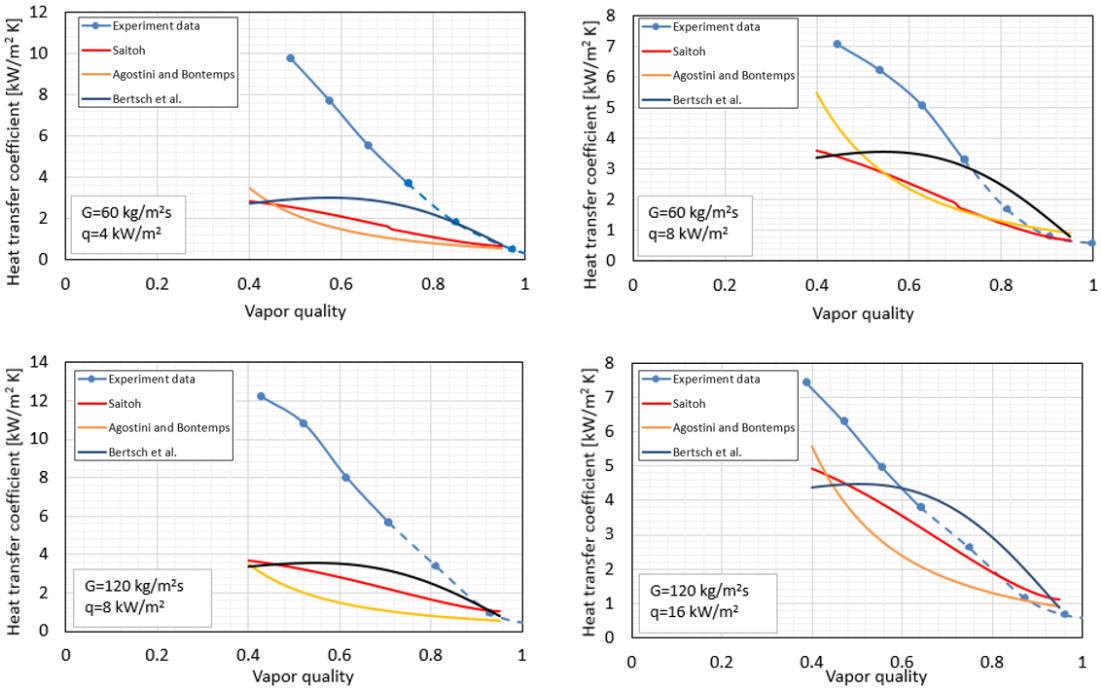

Figure 2.10: Comparison between experimental and correlation results of heat transfer coefficient of Tube A

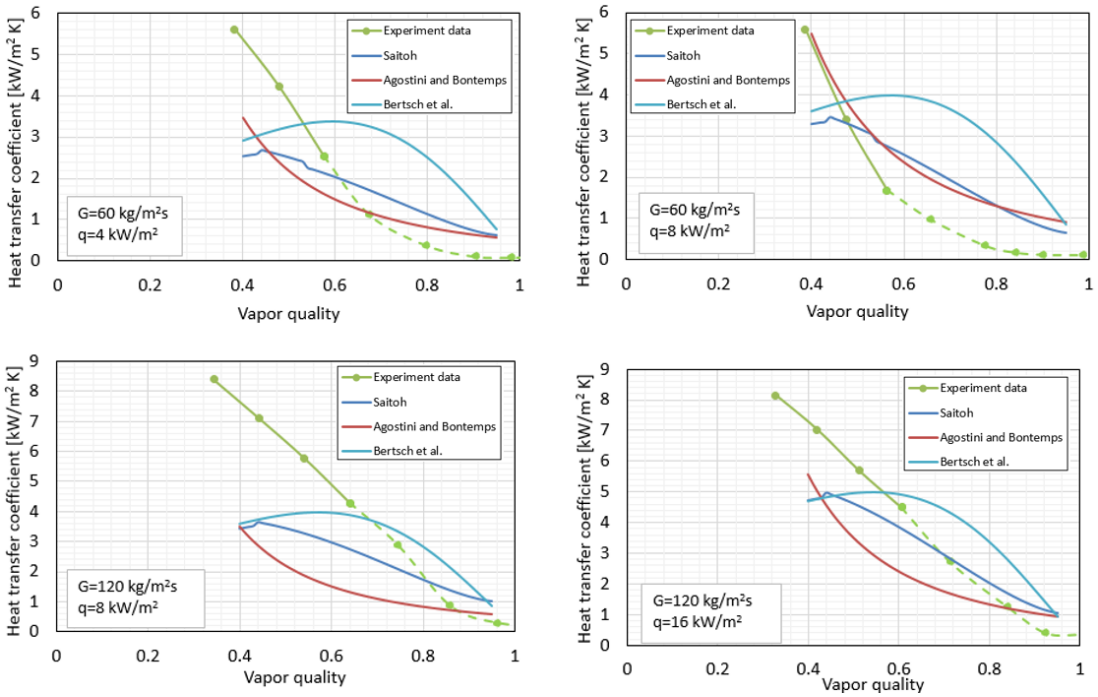

Figure 2.11: Comparison between experimental and correlation results of heat transfer coefficient of Tube B

2.3. Conclusions

The characteristics of local heat transfer and pressure drop were investigated experimentally for the vertical up-flow boiling of refrigerant R1234yf in two types of aluminum multi-port extruded tubes having 16 channels with a cross-section of 0.91 × 0.21 mm (tube A) and 40 channels with a cross-section of 0.34 × 0.21 mm (tube B). The heat transfer performance was compared with that of multi-port extruded tubes having 16 channels with a cross-section of 0.9 × 0.9 mm (tube C), and the pressure drop was compared with calculation results of three different correlations. From the results, the following conclusions can be drawn.

1. Under low heat and mass flux conditions, the heat transfer coefficient almost linearly decreased as a function of vapor quality in tubes A and B. As the vapor quality increased, the area of dry patches became lager within these rectangular channels, which deteriorated the heat transfer performance dramatically.

2. The channel dimensions significantly influenced the heat transfer performance. At a mass flux of 60 kg/m^{2}s, tube C showed better heat transfer performance than tubes A and B for all measured vapor quality regions because the shape of tubes A and B is not square, so the dry-out occurs more easily on the wider surfaces, thereby compromising the heat transfer performance. When the mass flux increased to 120 kg/m^{2}s, the dry-out was alleviated, enabling better performance in low vapor quality regions. In high vapor quality regions, the dry patches reoccupied the heat transfer area, leading to reduced heat transfer performance in tubes A and B. Moreover, tube A was worse than tube B because of its lower aspect ratio.

3. The correlations of Lee−Lee, Lockhart−Martinelli, and Mishima−Hibiki did not precisely predict the experimental pressure drops of tube A and B. Relatively, the Lockhart−Martinelli correlation showed better prediction. The data trend of decreasing heat transfer coefficient with increasing vapor quality was well predicted by the Saitoh et al. correlation and the Agostini−Bontemps correlation, but the value shows large deviation.

Chapter 3. Air side performance of fin-tube parallel heat exchangers

In this chapter, the heat transfer and pressure drop performance of five all-aluminum parallel multi-port heat exchangers, including three with slit fins with fin pitch of 1.2 mm, 1.4 mm and 1.6 mm, and the others with louver fins with the same fin pitches, were experimentally investigated under dry, wet and frosting/defrosting conditions.

3.1. Experimental setup and methodology

3.1.1 Experimental Setup

Figure 3.4 shows the experimental apparatus used for measuring the air-side heat transfer performance of the all-aluminum parallel multi-port heat exchangers. The heat exchanger under test was placed in a wind tunnel, where the temperature, humidity, and velocity of the air flow were precisely controlled. In the dry and wet conditions, water was circulated between the heat exchanger and the temperature-controlled baths as a heating or cooling source, while in the frosting/defrosting condition, water was replaced by brine. Air flowed from a hydrothermal chamber was by means of an inverter-controlled fan to the test section, through a rectifier. The flow rate of the air was controlled according to the pressure differential before, and after the nozzle set behind the test section, and the air velocity was calibrated by a venturimeter. The velocity of the air was calculated from the flow rate and the cross-sectional area of the channel. The temperature and humidity of the air were measured using calibrated thermocouples (±0.1 ℃), and dew point meters (±0.5 ℃). The uniformity of the air velocity over the cross section was confirmed using an anemometer probe. The distribution of the air temperature over the cross section was measured using 16 thermocouples (±0.1 ℃) just behind the heat exchanger. The air-side pressure drop was measured by a pressure difference sensor (±5 Pa). The flow rate of water or brine was measured by a Coriolis flow meter (±0.1%), and the inlet and outlet temperature were measure using platinum sensors PT100 (±0.01 ℃). The exchanged heat was calculated from the difference of the average temperatures between the incoming, and outgoing water or brine.

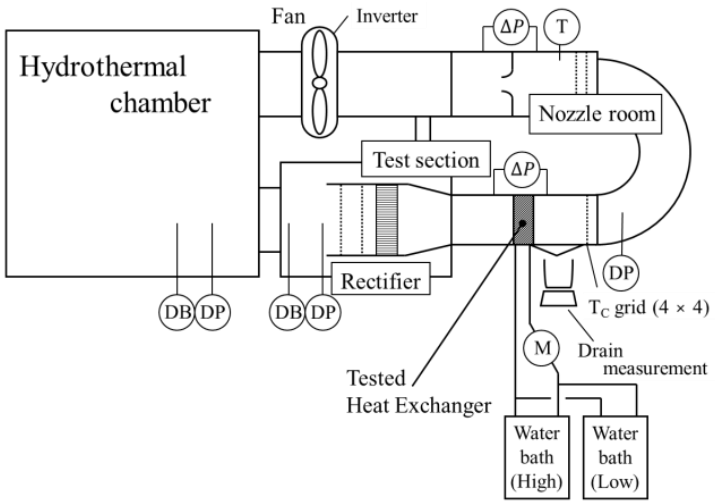

Figure 3.1 Experimental setup

3.1.2 Test sections and Experimental conditions

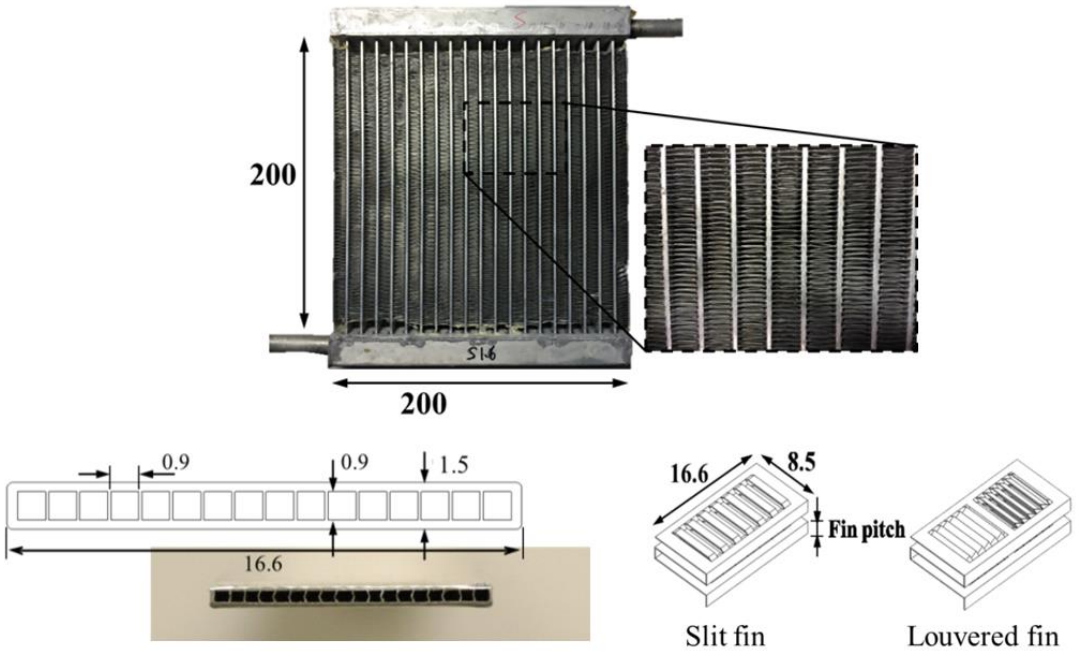

Figure 3.2 Tested heat exchangers and fin structures

The tested heat exchangers are shown in Figure 3.2, and their specifications are listed in Table 1. The front area of the heat exchangers is 200 × 200 mm, and the depth is 16.6 mm. Each heat exchanger was composed of 19 flat tubes with a tube-pitch of 10 mm. Each tube had 18 channels with a cross-section of 0.9 × 0.9 mm. The slit- and louvered-fins shown in Figure 3.2 were brazed on the flat tubes with various fin pitches. The heat exchangers of residential air conditioners alternately work as a condenser, or as an evaporator, depending on the season. When it functions as a condenser, the heat transfer surface is always dry, and only sensible heat is transferred. When it functions as an evaporator, the heat transfer surface is dry, wet, or frozen

depending on the air temperature and humidity, and the sensible- and latent-heats are simultaneously transferred. The air-side heat transfer characteristics under dry, wet, and frosting/defrosting conditions were measured. The experimental conditions are listed in Table 3.2. In the wet and frosting conditions the air was chilled by the water or brine, while in the dry condition the air was heated by the water. In the dry and wet conditions, the data was recorded for 10 min at an interval of 10 s in a stable working condition. In the frosting/defrosting test, the frosting and defrosting times were 30 and 5 min, respectively, and the frosting/defrosting operation was repeated six times. At the beginning of each frosting cycle, the flow rates of air and brine, and the inlet temperature of brine need time stabilize; thus, the data in the first 5 min was not recorded.

Table 3.1 Specifications of tested heat exchangers

Name	Fin type	Fin pitch (mm)	Heat transfer area	
			Tube area (m^2)	Fin area (m^2)
S1.2	Slit fin	1.2	0.126	0.775
S1.4	Slit fin	1.4	0.126	0.664
L1.2	Louvered fin	1.2	0.126	0.775
L1.4	Louvered fin	1.4	0.126	0.664
L1.6	Louvered fin	1.6	0.126	0.581

Table 3.2 Experimental conditions

Condition	Dry	Wet	Frosting/Defrosting
Water/brine temperature (℃)	40.0	10.0	-6.0/ 40.0
Water/brine flow rate (kg/min)	4.0	4.0	2.0/2.0
Air inlet temperature (℃)	27.0	27.0	2.0
Air inlet dew point temp. (℃)	14.6	20.0	-0.5
Air velocity (m/s)	0.5, 1.0, 1.5, 2.0, 2.5, 3.0,		2.0

3.1.3 Experimental data reduction

Under dry condition, the overall air-side heat transfer coefficients $\eta_a h_a A_a$ from the five heat exchangers were compared. Under wet and frosting/defrosting conditions, the air side transport coefficient based on enthalpy difference $b_a / \eta_a h_a A_a$ are compared. A brief description for the data reduction method is given below.

The total heat transfer rate is calculated by the data of the water side:

$$Q = c_w m_w (\mathrm{T}_{w,2} - \mathrm{T}_{w,1}) \tag{3.1}$$

The ε-NTU equation for both fluid unmixed conditions [14] is:

$$\varepsilon = 1 - \exp\left\{\frac{NTU^{0.22}}{C_r}\left[\exp(-C_r NTU^{0.78}) - 1\right]\right\} \tag{3.2}$$

The effectiveness and NTU under dry conditions are determined on the basis of logarithmic-mean temperature differences, whereas under wet and frosting/defrosting conditions they are based on the logarithmic-mean enthalpy differences. The thermal resistance of flat tube wall is negligible.

For a dry surface:

$$\varepsilon = \frac{Q}{m_a c_{p,a}(\mathrm{T}_{w,1} - \mathrm{T}_{a,1})} \tag{3.3}$$

$$C_r = \frac{\left(mc_p\right)_{\min}}{\left(mc_p\right)_{\max}} \tag{3.4}$$

NTU can be calculated by substituting Equations (1), (3) and (4) into Equation (2). Then, the total heat transfer coefficient, $U_o A_o$, can be obtained by:

$$NTU = \frac{U_o A_o}{\left(mc_p\right)_{\min}} \tag{3.5}$$

The overall air-side heat transfer coefficients, $\eta_a h_a A_a$, can be determined by the following equation. For the water/brine side heat transfer coefficient, the Nusselt number is fixed at 3.70[86].

$$\frac{1}{U_o A_o} = \frac{1}{h_w A_w} + \frac{1}{\eta_a h_a A_a} \tag{3.6}$$

For wet and frosting conditions:

$$\varepsilon = \frac{Q}{m_a(i_{a,1} - i_{w,1,s})} \tag{3.7}$$

$$NTU = \frac{U_{ow} A_{ow}}{C_{\min}} \tag{3.8}$$

$$C_o = m_a, \quad C_w = \frac{m_w c_{p,w}}{b_w}, \quad C_r = \frac{C_{\min}}{C_{\max}} \tag{3.9}$$

where C_{min} and C_{max} are the smaller and larger values of C_o and C_w, respectively. NTU can be calculated by substituting Equations (3.7) and (3.9) into Equation (3.2). Then, the total heat transfer coefficient $U_{ow}A_{ow}$ can be obtained by Equation (8), and the overall air-side heat transfer coefficients, $\eta_a h_a A_a$, can be determined by the following equation

$$\frac{1}{U_{ow} A_{ow}} = \frac{b_w}{h_w A_w} + \frac{b_a}{\eta_a h_a A_a} \tag{3.10}$$

where b_w and b_a are defined as follows:

$$b_w = \frac{i_{t,s} - i_{w,s}}{T_t - T_w}, b_a = \frac{\Delta i_t}{\Delta T_t} \tag{3.11}$$

where $i_{t,s}$ *and* $i_{w,s}$ are the enthalpy of the saturated moist air at the mean temperature of the flat tube, and water/brine, respectively, and b_a is the slope of the saturated moist air enthalpy curve at the mean flat tube temperature.

3.2. Results and discussion

3.2.1 Dry conditions

Figure 3.3 shows the air-side pressure drops of five heat exchangers at various air velocities, in dry conditions. As the air velocity increases from 1.5 m/s to 3 m/s, the pressure drop of each heat exchanger increases, as expected. For the same type of fins, the pressure drop of the heat exchanger with a smaller fin pitch, is larger than that with a larger fin pitch, at the same air velocity. Compared to the louvered-fin, the pressure drops of heat exchangers with slit fins are lower. In particularly, the pressure drops of L1.6 (see Table 1) are even higher than those of S1.4 when the air velocity increases from 2.5 m/s to 3 m/s.

Considering the overall heat transfer coefficients, the comparison between louvered- and slit-fins is similar to that for pressure drops. Figure 3.4 shows the overall air-side heat transfer coefficients of five heat exchangers as dry air velocity ranged from 1.5 m/s to 3 m/s. As expected, the overall heat transfer coefficients of each heat exchanger increased with the increase in air velocity, and for each type of fin the overall heat transfer coefficient increased with a decrease in fin pitch. L1.2 showed the largest overall heat transfer coefficient, followed by L1.4 and S1.2. S1.4 showed the smallest overall heat transfer coefficient, although it had more heat transfer area than L1.6. The comparison of the air-side pressure drops and the overall heat transfer coefficients between louvered- and slit-fins showed that louvered fins had higher heat transfer coefficients than slit fins, but induced more pressure drop under dry air conditions. This conclusion agreed with the findings by Dejong et al. [35], Cowell et al. [36] and Achaichia et al. [37].

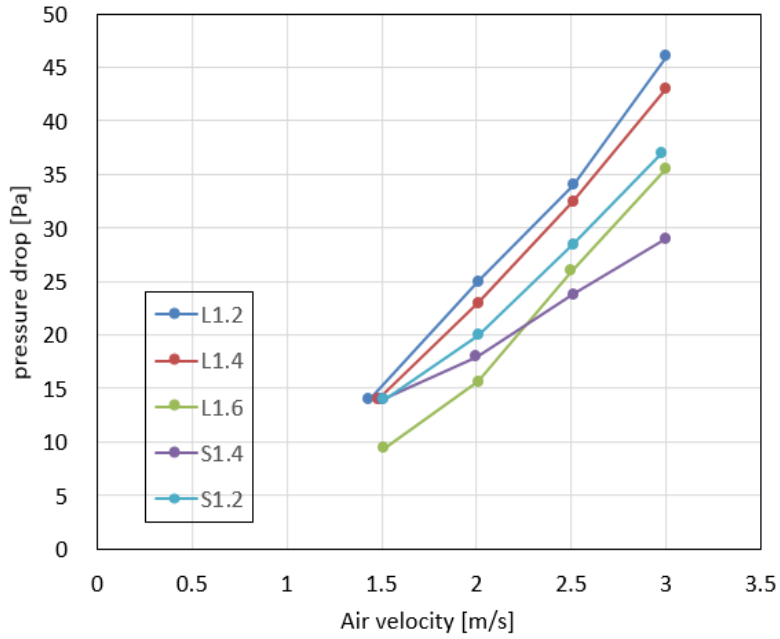

Figure 3.3 Air-side pressure drops of five heat exchangers at various air velocities in dry conditions

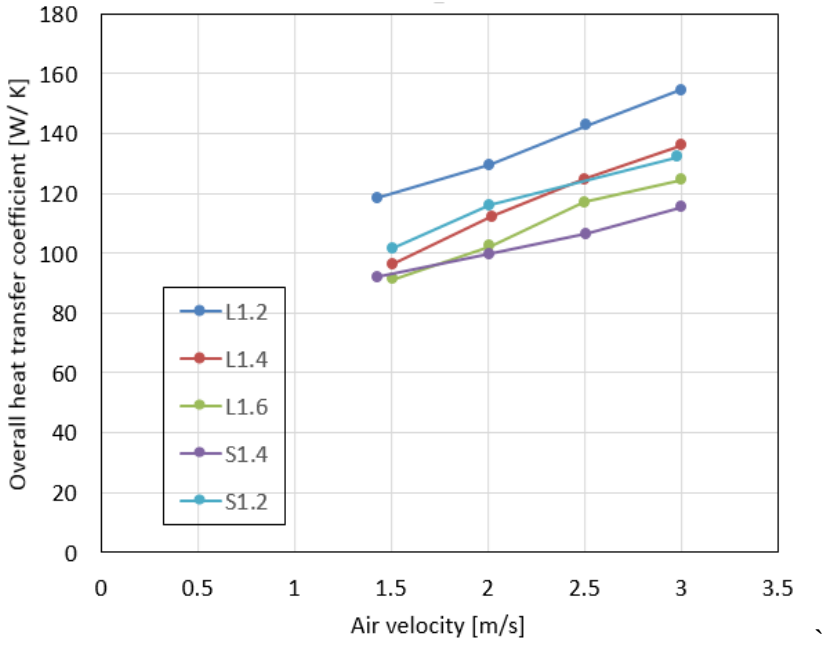

Figure 3.4 Overall air-side heat exchanger coefficients of five heat exchangers at various air velocities in dry conditions

3.2.2 Wet conditions

Under the wet condition, the water vapor in the air will condense on the cold fins and flat tubes. Because the fins are horizontally arranged, the condensate will accumulate on the fins and drop down gradually, under gravity. The condensate on the fins reduces the flow area of

the heat exchangers, which causes a greater pressure drop than in the dry condition. On the other hand, the condensate will induce two effects on heat transfer. Firstly, the condensate on the fins acts another thermal resistance of the whole heat transfer, and, secondly, the irregularly distributed water droplets will promote turbulence in the airflow, which is beneficial for heat transfer.

Figures 3.5 and 3.6 show the pressure drops and overall transport coefficients of the five heat exchangers under wet conditions. Compared to dry conditions, the pressure drop of each heat exchanger is higher at the same air velocity, due to the condensate. This differs from the results in dry conditions. L1.6 clearly shows the smallest pressure drop, while the pressure drops of the other four heat exchangers have similar curves. Under wet conditions, the condensate covers the fins with a high density, which alleviates the effect of fin structure on pressure drop. Hence, the pressure drops of the heat exchangers with the same pitch slit- and louvered-fins, are similar. Furthermore, the condensate water creates an irregular block of the flow area of the heat exchangers, which plays a role comparable to the fins in causing pressure drops. Thus, the effect of fin pitch is also reduced. However, as the fin pitch increased to 1.6 mm, the flow area increased significantly, and the drainage ability was also increased, which caused much smaller pressure drops.

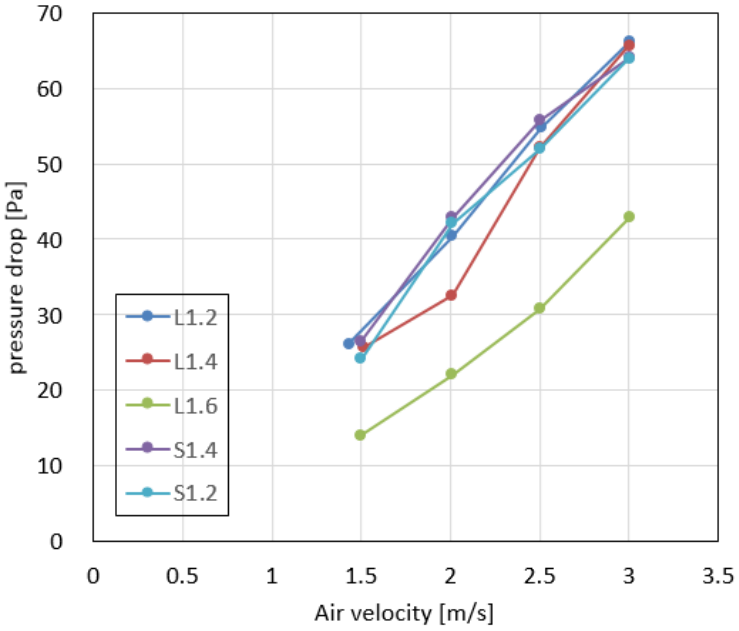

Figure 3.5 Air-side pressure drops of five heat exchangers at various air velocities in wet conditions

The comparison of overall transport coefficients of the five heat exchangers also shows a difference from those under the dry conditions. As with the pressure drops, L1.6 showed the smallest overall transport coefficients. Of the other four heat exchangers, S1.4, which has bigger fin pitch and smaller heat transfer surface areas, surprisingly showed larger overall transport

coefficients than L1.2 and S1.2. The result can be inferred that, S1.4 has better drainage performance than the others, so that the thermal resistance of condensate on S1.4 is the smallest. The better drainage performance of S1.4 also can be observed under the frosting/defrosting condition. For the other three, the heat transfer performance is similar.

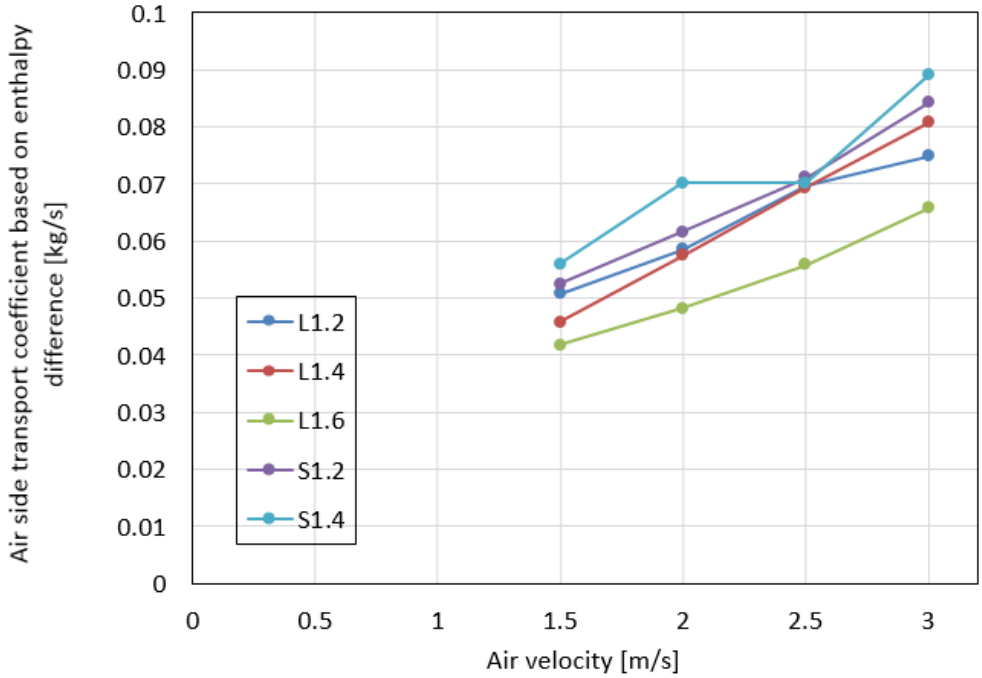

Figure 3.6 Overall air-side overall transport coefficients of five heat exchangers under various air velocities in wet conditions

3.2.3 Frosting/defrosting condition

Under the frosting/defrosting condition, the frost formation on a heat exchanger was different for each cycle. During each defrosting period, some of the water remained on the horizontally arranged fins, then frosted quickly on the fins as the following frosting period began. This had a significant influence on the pressure drop and heat transfer performance of the following frosting period.

Figures 3.7 and 3.8 show the pressure drops and overall transport coefficients of the five heat exchangers, for 6 cycles of frosting/defrosting. As expected, the pressure drops of all heat exchangers dramatically increased with time in each frosting period, owing to the growth of the frost layer. It is worth noting that the pressure increase rate was different in each of the six cycles, especially for L1.2. This phenomenon was also reported in the research of Xia et al. [32]. The reason can be inferred as follows. At the beginning of each defrosting period, the frost defrosts quickly and drains down due to gravity. The drainage velocity decreases sharply with time because of the horizontally arranged fins, which block the water. At the end of the five

minute defrosting period, a considerable amount of water was still on the fins. When the following frosting period began, the water froze quickly and created an initial condition for the frosting period. However, the defrosting process of six defrosting periods was not identical, and the retention of water at the end of each defrosting period was irregular, which provided different initial conditions for the following frosting period. Thus, the pressure drops of the six cycles differed from each other for each heat exchanger. The effects of fin-type and -pitch on the pressure drops were not completely evident. L1.2, which showed the greatest pressure drop in dry and wet conditions, showed much lower pressure drops compared to S1.2 and L1.4, except in the last cycle when it increased to the largest. Overall, S1.2 showed the largest pressure drop of all the heat exchangers, followed by L1.4, and S1.4 showed the smallest pressure drop.

In each frosting cycle, the overall transport coefficients of all five heat exchangers decreased with time because of the growth of the frost layer. Differing from the pressure drops, the overall transport coefficients of a single heat exchanger exhibit similarity in all the six cycles. The fin pitch shows significant impact on the overall transport coefficients. L1.2 and S1.2 which have lower fin pitch and higher heat transfer areas exhibits higher overall transport coefficients, and followed by L1.4 and S1.4, while L1.6 shows the smallest values. However, the effect of fin type was not significant, because that under frost condition the fins are covered by the frost.

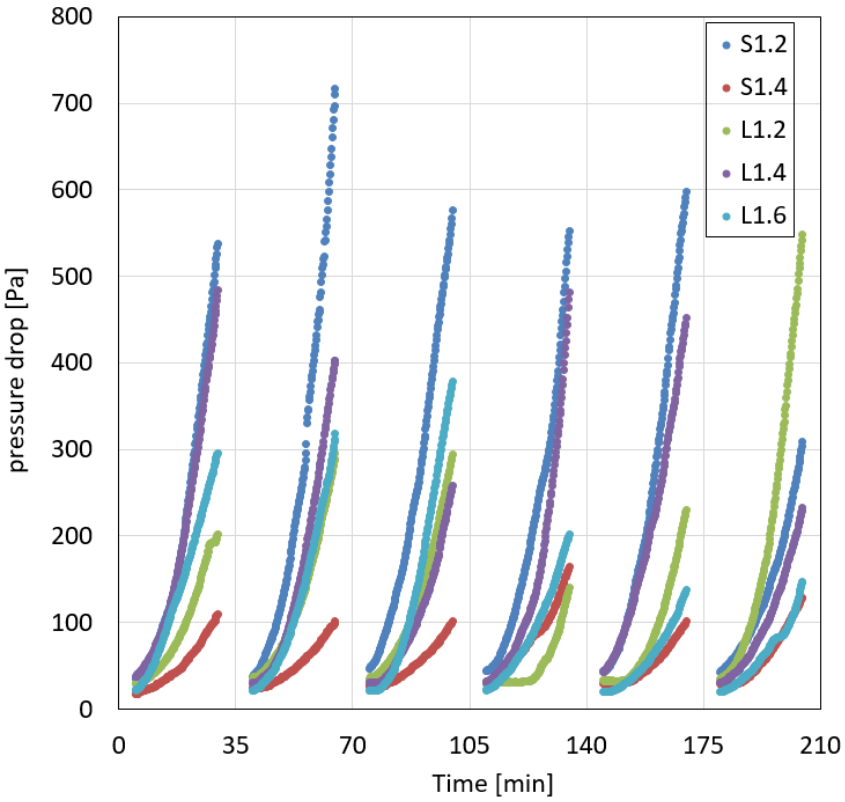

Figure 3.7 Air-side pressure drops of five heat exchangers at an air velocity of 2 m/s in the frosting/defrosting condition

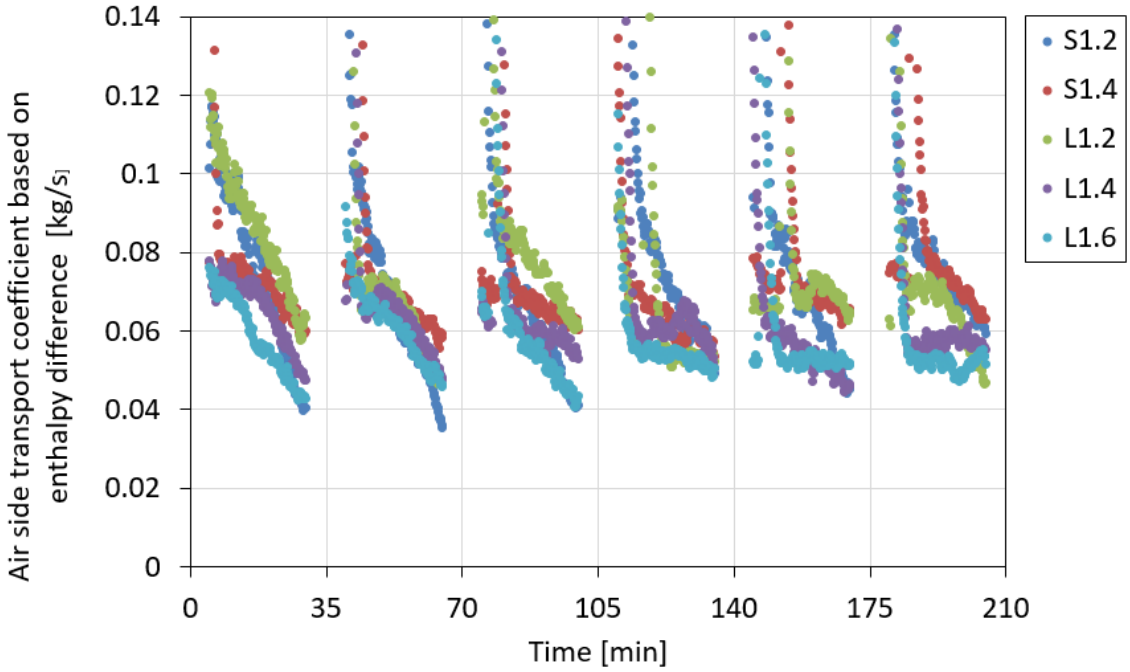

Figure 3.8 Overall air-side overall transport coefficients of five heat exchangers at an air velocity of 2 m/s in the frosting/defrosting condition

3.3. Conclusions

In this study, the air-side pressure drops and overall transport coefficients of three louvered-fin all-aluminum parallel multi-port heat exchangers with a fin pitch of 1.2 mm, 1.4 mm and 1.6 mm, and two with slit-fins with a pitch of 1.2 mm and 1.4 mm were experimentally measured under dry, wet and frosting/defrosting conditions. The effects of fin pitch and type on the pressure drop and heat transfer performance were discussed.

1. In the dry condition, as the air velocity increased from 1.5 m/s to 3 m/s, the pressure drops and overall heat transfer coefficients of each heat exchanger increased. At the same air velocity, the pressure drops and overall heat transfer coefficients of louvered-fin heat exchangers were higher than those of slit-fin heat exchangers with same fin pitch.

2. In the wet condition, louvered- and slit-heat exchangers with fin pitch of 1.2 mm and 1.4 mm showed similar pressure drops and overall transport coefficients, which reflected that the effects of fin type and pitch were alleviated by the condensate on the fins. However, when the louvered-fin pitch increased to 1.6 mm, it showed lower pressure drops and overall transport coefficients.

3. In the frosting/defrosting condition, the pressure drop of a single heat exchanger was not identical in each frosting cycle, because of the different initial conditions due to the irregular retention distribution, whereas the overall heat transfer coefficients were relatively stable. The

heat exchangers with a lower fin pitch showed higher overall transport coefficients. Nonetheless, the effect of fin type was not obvious on the overall transport coefficients.

4. For the heat exchangers of indoor units, which operate under dry and wet conditions, the louvered-fin with a fin pitch of 1.2 mm is recommended. However for the heat exchangers of outdoor units, which may operates under the frosting/defrosting condition, the slit-fin with a fin pitch of 1.4 mm is suggested.

Chapter 4. Air side performance of a finless heat exchanger

In this dissertation, for enhancing the heat transfer performance of the finless heat exchanger, a longitudinal vortex generator was installed in front of the finless heat exchanger with a narrow gap, which ensured that under wet and frosting/defrosting conditions, the condensed or defrosted water would not fall on the LVG, ensuring that the drain and defrosting performance was not affected by the LVG. As shown in figure 4.1, when air flow through the LVG, longitudinal vortexes will generate and further flow into the heat transfer area. The mixing of hot and cold air will be enhanced by longitudinal vortexes, therefore the air side heat transfer performance will increase with a penalty of additional pressure drop caused by LVG. Using numerical simulation, comparing to triangle winglet (TLVG) and rectangular winglet LVG (RLVG), a double triangle LVG (DTLVG) with better heat transfer enhancement ability was developed. Furthermore, parameter analysis was conducted for optimal design of DTLVG. Then, the DTLVG was manufactured by 3D printing method. The heat transfer performance and pressure drop of the finless heat exchanger with and without the DTLVG were experimentally measured and compared under dry, wet, and frosting/defrosting conditions. Otherwise, these results also be compared to the fin-tube parallel heat exchangers.

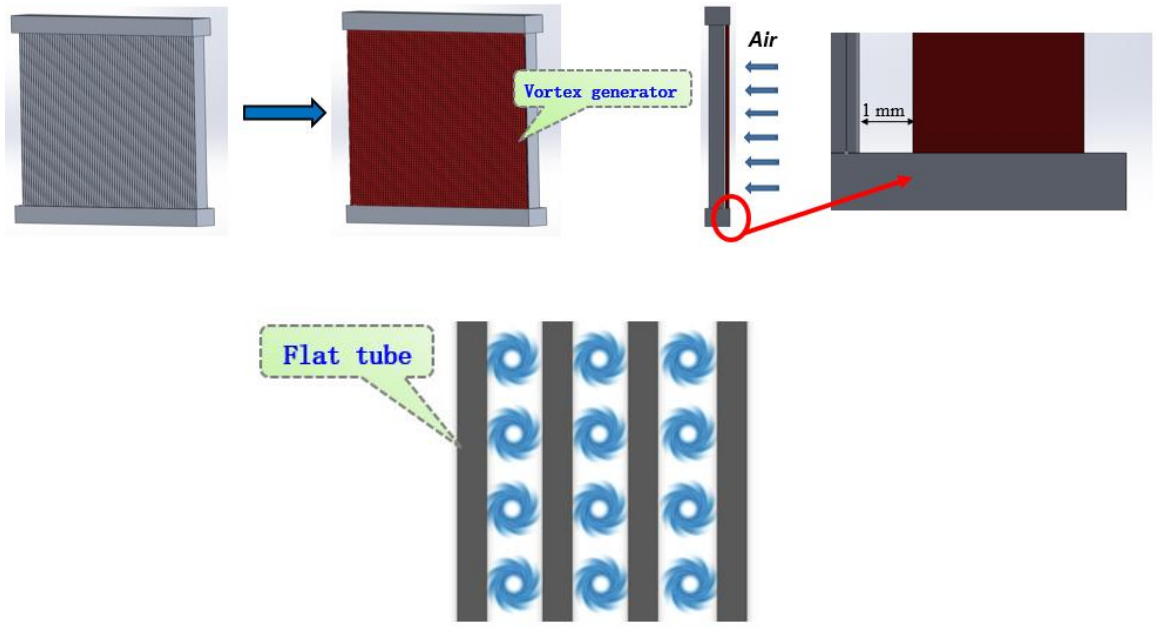

Figure 4.1 Concept of finless heat exchanger with LVG

4.1 Numerical model

The finless heat exchanger shown in Figure 4.2 consists of 80 vertically set, parallel aluminum multiport flat-tubes with a tube pitch of 2.5 mm. Each tube with a thickness of 0.6 mm, a width of 16.6 mm and a length of 200 mm, had 16 rectangular channels with a section of 0.9 mm × 0.2 mm, as shown in figure 4.3.

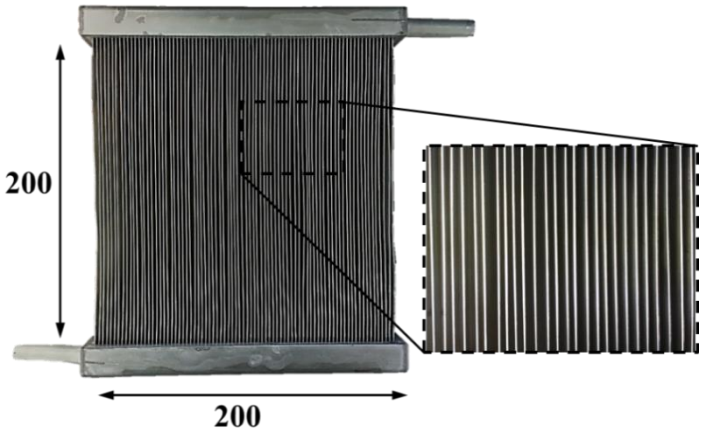

Figure 4.2 The finless heat exchanger

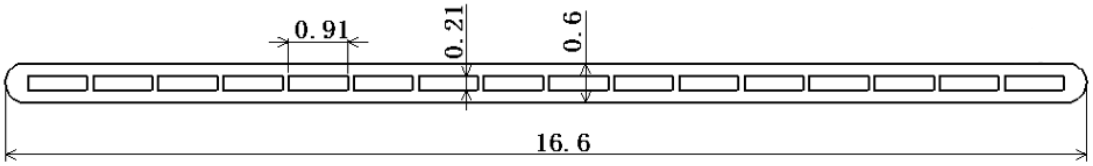

Figure 4.3 the flat tube in the finless heat exchanger

The LVG plate consisted of thousands of small LVG units was installed in front of the finless heat exchanger with a small gap of 0.5 mm, and each unit faced the gaps between flat tubes. The TLVG, RLVG and DTLVG unit and its computational domain are shown in Figure 4.4, 4.5 and 4.6. The depth of all the units is 2.5 mm, and the height of TLVG and RLVG is 3.1 mm while that of DTLVG is 3.6 mm. the computational domain is extended upstream 5 mm and downstream 41.5 mm so that the uniform inlet boundary condition and fully developed outlet boundary condition can be used reasonably. The gap between the computational boundary and the unit is 0.2 mm.

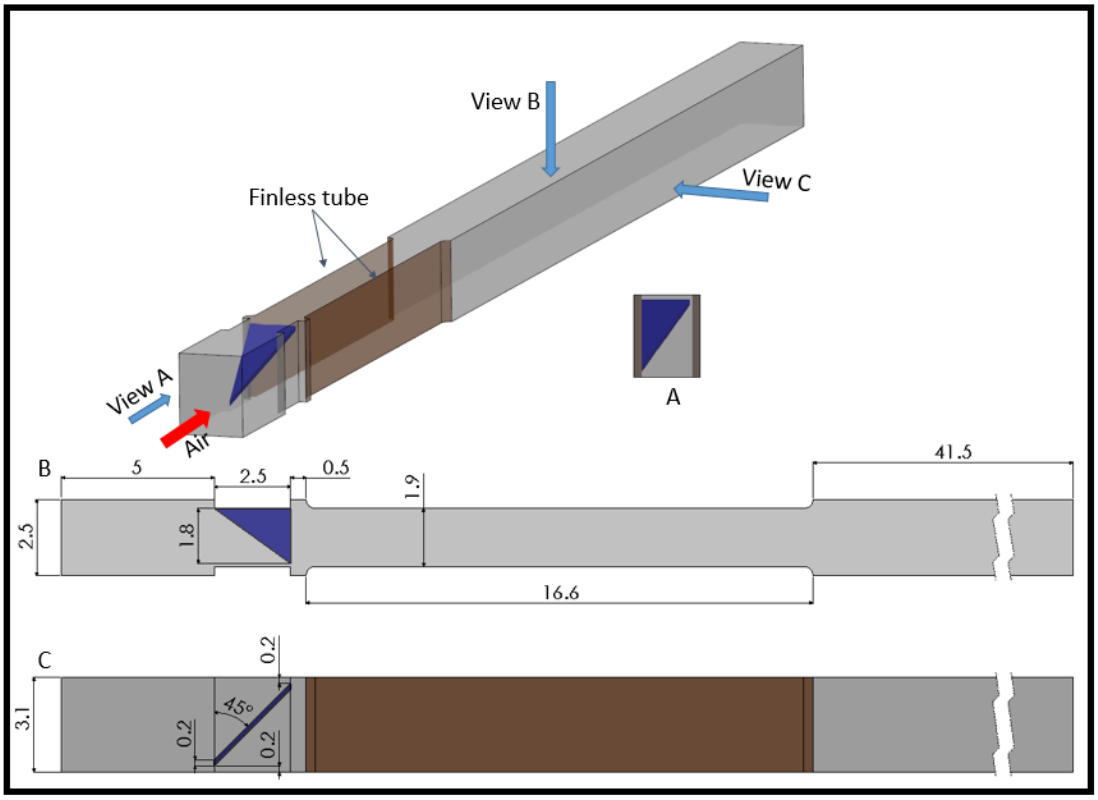

Figure 4.4 Computational region of TLVG

The governing equations for the laminar convection heat transfer include continuity, momentary and energy equations as following.

Continuity equation:

$$\frac{\partial(\rho u_i)}{\partial x_i} = 0 \tag{4.1}$$

Momentum equation

$$\frac{\partial(\rho u_i u_k)}{\partial x_i} = \frac{\partial}{\partial x_i}(\eta \frac{\partial(u_k)}{\partial x_i}) - \frac{\partial p}{\partial x_k} \tag{4.2}$$

Energy equation

$$\frac{\partial(\rho u_i T)}{\partial x_i} = \frac{\partial}{\partial x_i}(\frac{\lambda}{c_p}\frac{\partial T}{\partial x_i}) \tag{4.3}$$

The governing equations were solved using the finite volume method. The differencing scheme was QUICK, and the pressure field solution method was SIMPLE. The laminar model was adopted for the viscous model because of the low Reynolds number in the computational domain. In calculation, the air inlet temperature and velocity was 300 K and 2 m/s, respectively, and the tube surface was set at a constant temperature of 313.15 K. Suitable boundary conditions were attributed to each boundary. The calculation was stopped when a steady or periodical flow temperature field was achieved.

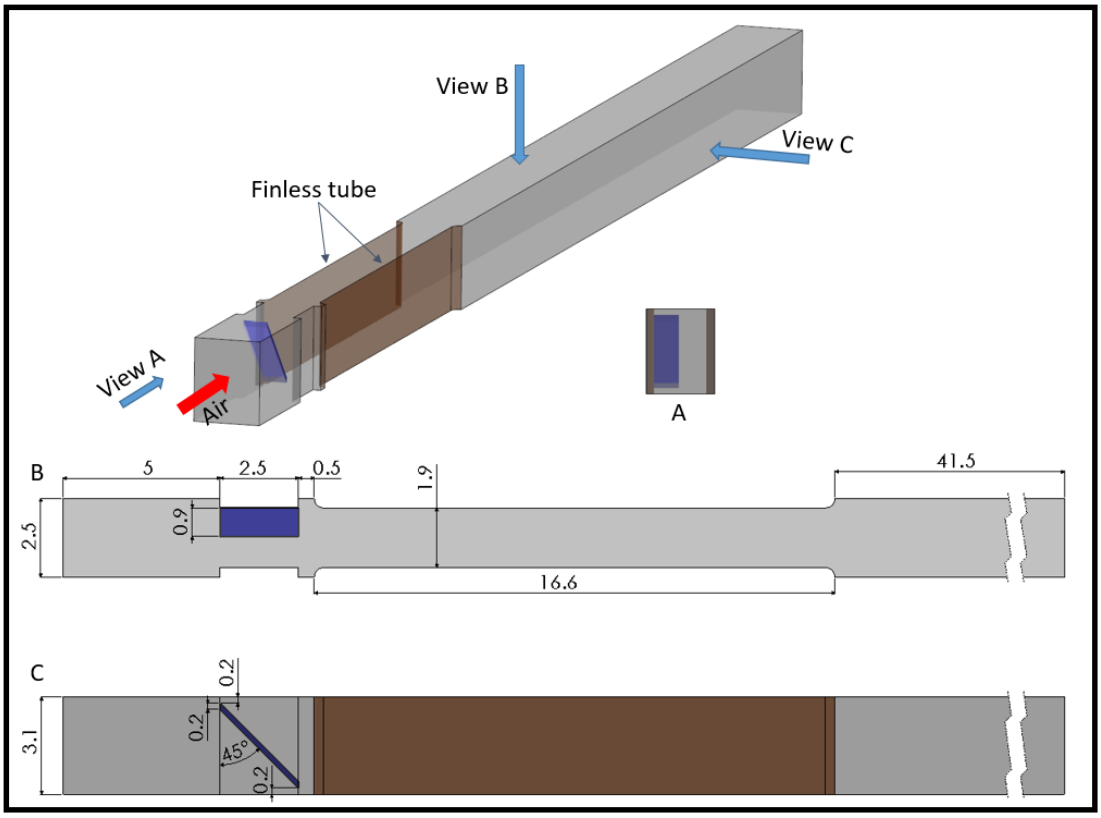

Figure 4.5 Computational region of RLVG

The heat transfer coefficient is defined as

$$h = \frac{Q}{A\Delta T_{\ln}} \tag{4.4}$$

Where Q is the exchanged heat, A is the tube face area in the computational filed, and $\Delta T_{\ln}$ is the logarithmic mean temperature difference which defined by

$$T_{\ln} = \frac{(T_w - T_{in}) - (T_w - T_{out})}{\ln(\frac{T_w - T_{in}}{T_w - T_{out}})} \tag{4.5}$$

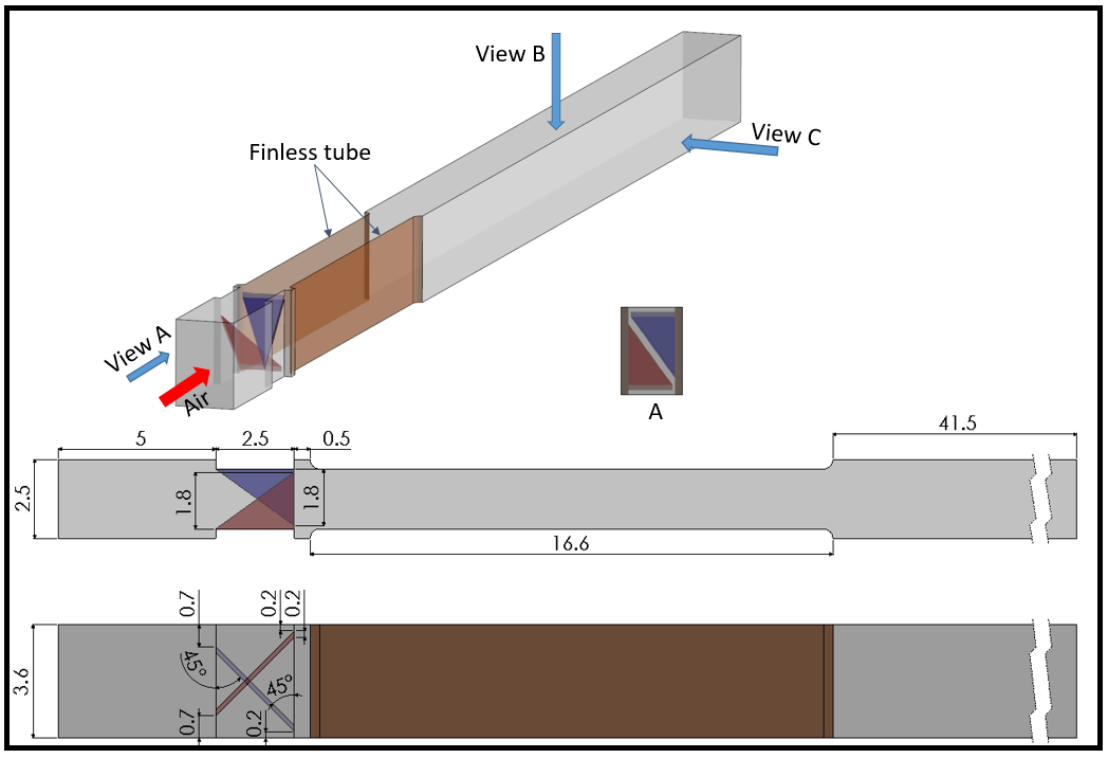

Figure 4.6 Computational region of DTLVG

Non-uniform mesh with tetrahedron cells is used for the computational domain. For achieving mesh independency, the maximum element size for the whole domain, the heat transfer domain and the LVG is tested and listed in table 4.1. Since the error of Mesh 1 is 3.4% comparing to Mesh 2, we used Mesh 1 for the further calculations.

Table 4.1 mesh independence

Mesh	Maximum element size [mm] (whole domain)	Maximum element size [mm] (heat transfer domain)	Maximum element size [mm] (LVG)	Number of element	Heat transfer coefficient (w/m^2k)	Error (%)
1	0.2	0.1	0.05	4654099	133.9	3.4
2	0.15	0.1	0.04	17270578	129.5	-
3	0.2	0.08	0.05	13526145	132.2	2.1

The validation for the numerical simulation is presented below. Based on CFD results, N. Shikazono et al[38] presented a correlation for calculating the heat transfer coefficient and pressure drop of flat tubes under low air velocity conditions. They compared the correlation results to their experiment results and good agreement was achieved. For verifying of the numerical calculation used in this paper, the heat transfer coefficients of the finless flat tube without the LVG was calculated when the air velocity varied form 1.5 m/s to 3 m/s. The results were compared to the correlation results and a maximum deviation of 9.9% for heat transfer

coefficient and 5.4% for pressure drop was found, which proved that the numerical calculation in this paper is reliable.

4.2. Comparison between TLVG, RLVG and DTLVG

Figure 4.7, 4.8 and 4.9 show the tangent vectors vertical to the air flow direction and air temperature on four section surfaces with a distance of 0 mm, 16/3 mm, 32/3 mm and 16 mm from the head of flat tube. After the air flowed through the LVG, vortexes were obviously created, and kept following towards the outlet. The vortexes enhanced the exchange of hot and cold air as well as broke the thermal boundaries, thus the heat transfer was enhanced. It can be observed that along the flow direction, the intensity of vortexes decreased because of friction, so that exchange between hot and cold air was sharply weakened, and the heat transfer enhancement also be reduced. Particularly, for TLVG, the main vortex generated in the upper region while much lower tangent velocity of air was observed in the lower region. Thus, strong heat transfer enhancement only achieved in the upper region. Similar phenomenon is also observed for RLVG, but the main vortex existed in the lower region. However, for the DTLVG, the vortexes are axisymmetric that the heat transfer in both lower and upper regions were enhanced identically. Figure 4.10 shows the heat transfer coefficients for the finless heat exchanger with TLVG, RLVG and DTLVG. The heat transfer coefficient of the finless heat exchanger without LVG is 70 W/m^2k. DTLVG created an enhancement rate of 92.3% and made the heat transfer coefficient increasing to 133.9 W/m^2k, leading that of TLVG with 52.9% and of RLVG with 52.1%, but also induced a pressure drop of 34 Pa which is higher than that of TLVG with 16 Pa and of RLVG with 15 Pa. For the finless heat exchanger, the air side pressure drop is much lower comparing to the fin-tube parallel heat exchanger. Hence, we can using more pressure drop penalty to trade for more heat transfer enhancement.

As introduced by Torri et al.[87], there are three types of vortexes created by vortex generator: the main vortex, the induced vortex and the corner vortex. Figure 4.11 shows the tangent vectors created by TLVG and RLVG on the section surfaces with a distance of 2 mm and 2.5 mm from the head of flat tube, respectively. For these two types of LVG, three types of vortexes were clearly generated. However, for DTLVG, we cannot see the induced vortex clearly. Figure 4.12 shows the tangent vectors on the section surfaces from the inlet region to the heat transfer region. When the air flowed through the DTLVG, two main vortexes were clearly created. However, the direction of the two main vortexes is opposite, thus the fraction between them is quite strong, which making them degrading to one vortex quickly. Form figure 4.12, we can see that two main vortexes only lasted to 4 mm. Although the two main vortexes degraded quickly, DTLVG still offer more heat transfer enhancement comparing to the other two types of LVG.

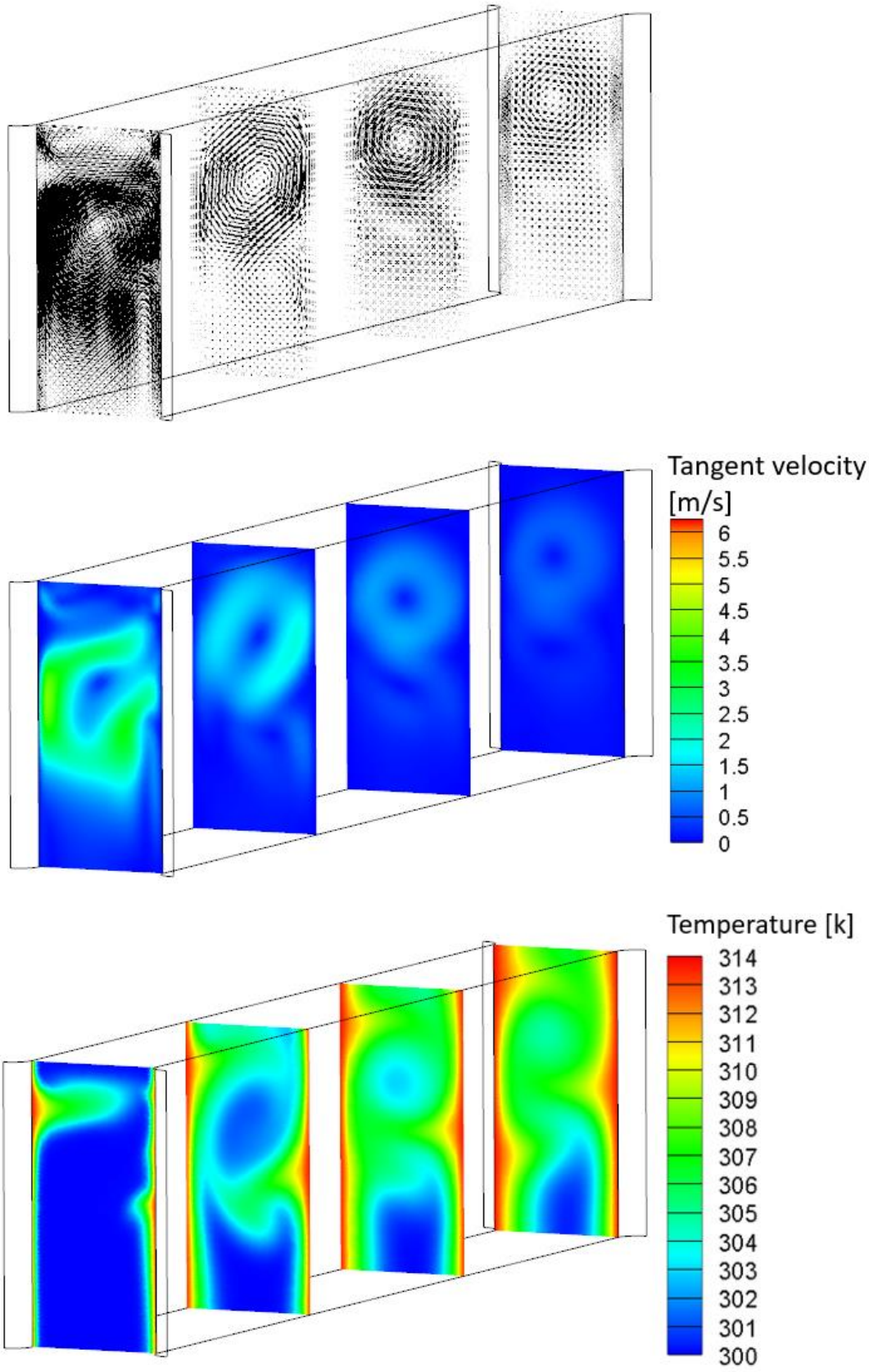

Figure 4.7 Vectors and temperature contours of TLVG

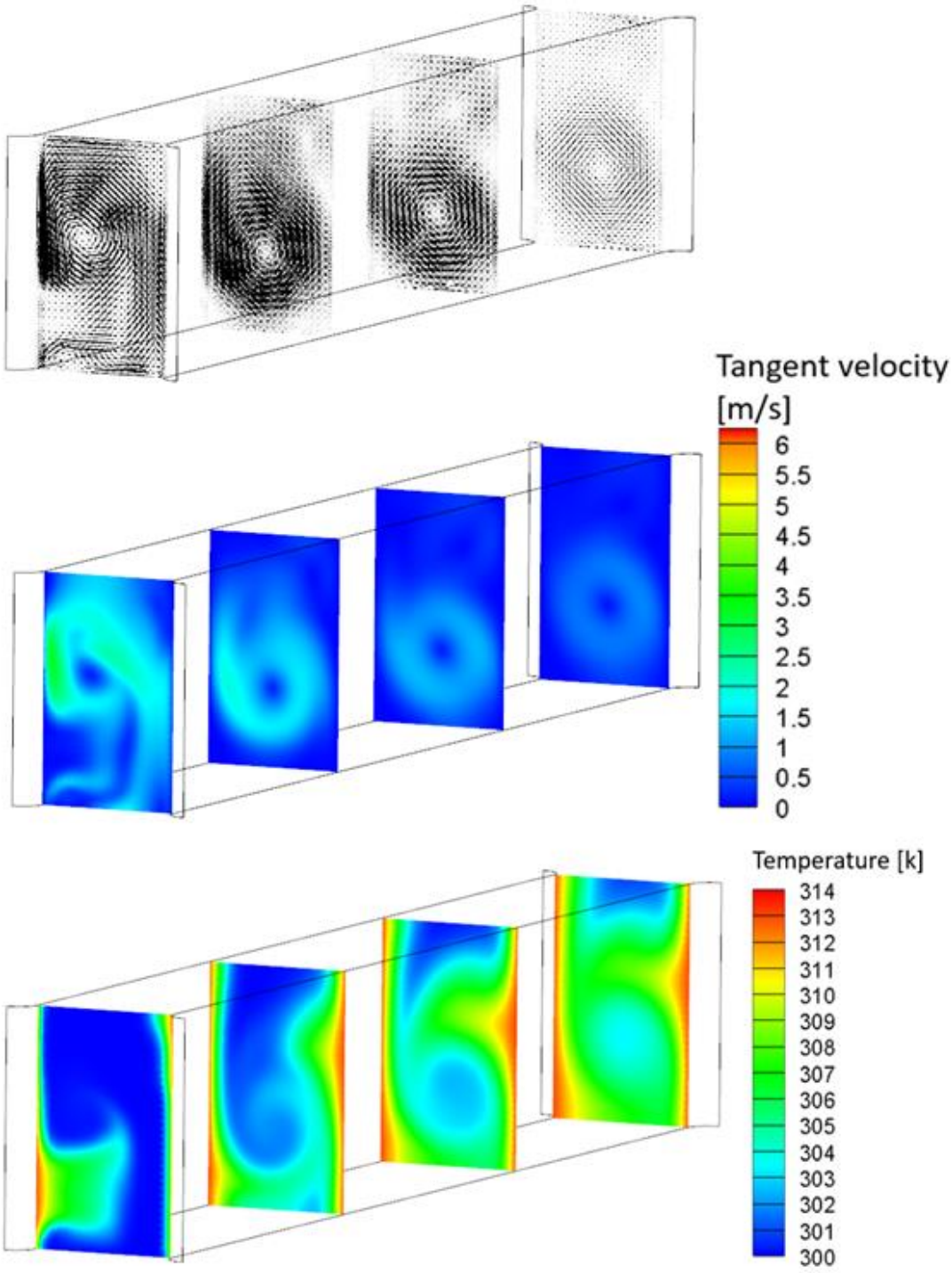

Figure 4.8 Vectors and temperature contours of RLVG

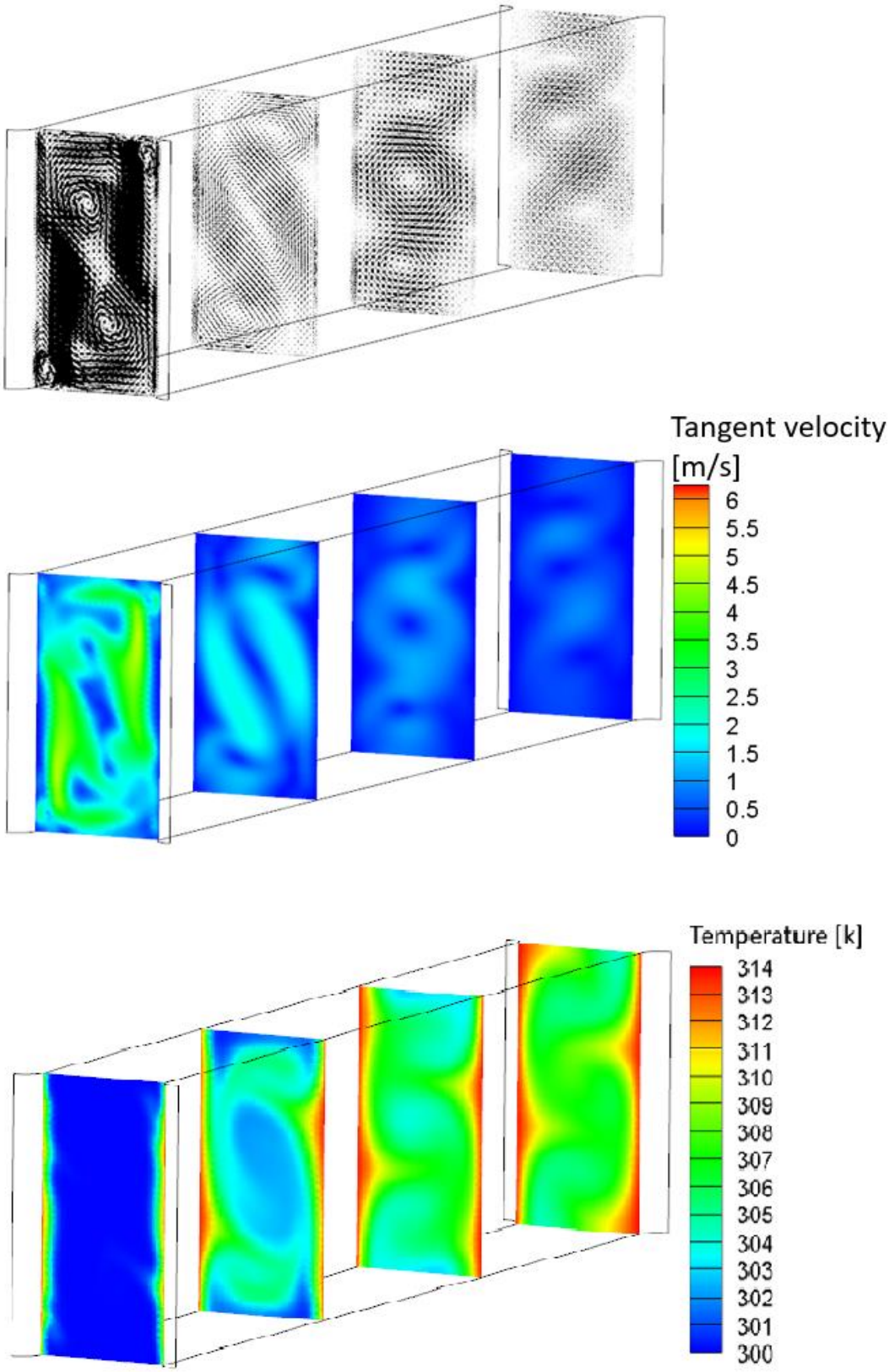

Figure 4.9 Vectors and temperature contours of DTLVG

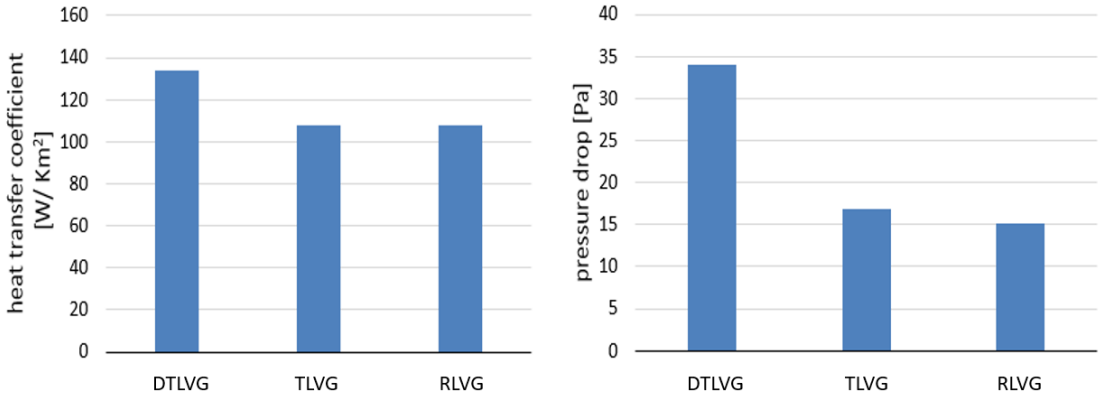

Figure 4.10 heat transfer coefficient and pressure drop of the finless heat exchanger with TLVG, RLVG and DTLVG

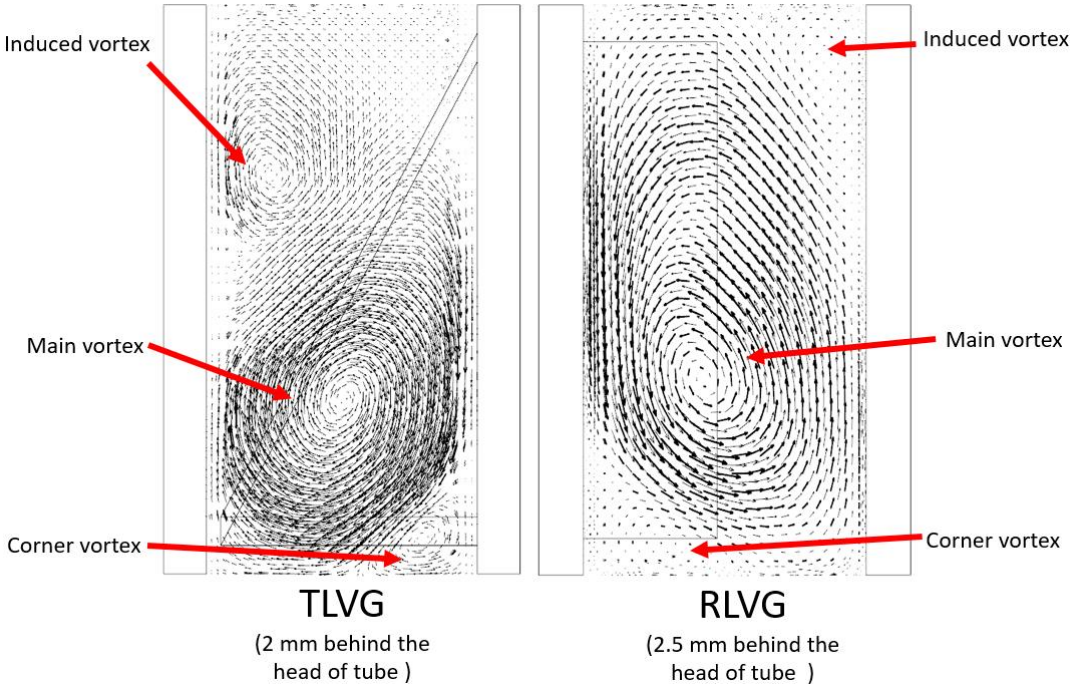

Figure 4.11 Comparison of Vectors on the section surfaces with a distance of 2 mm from the head

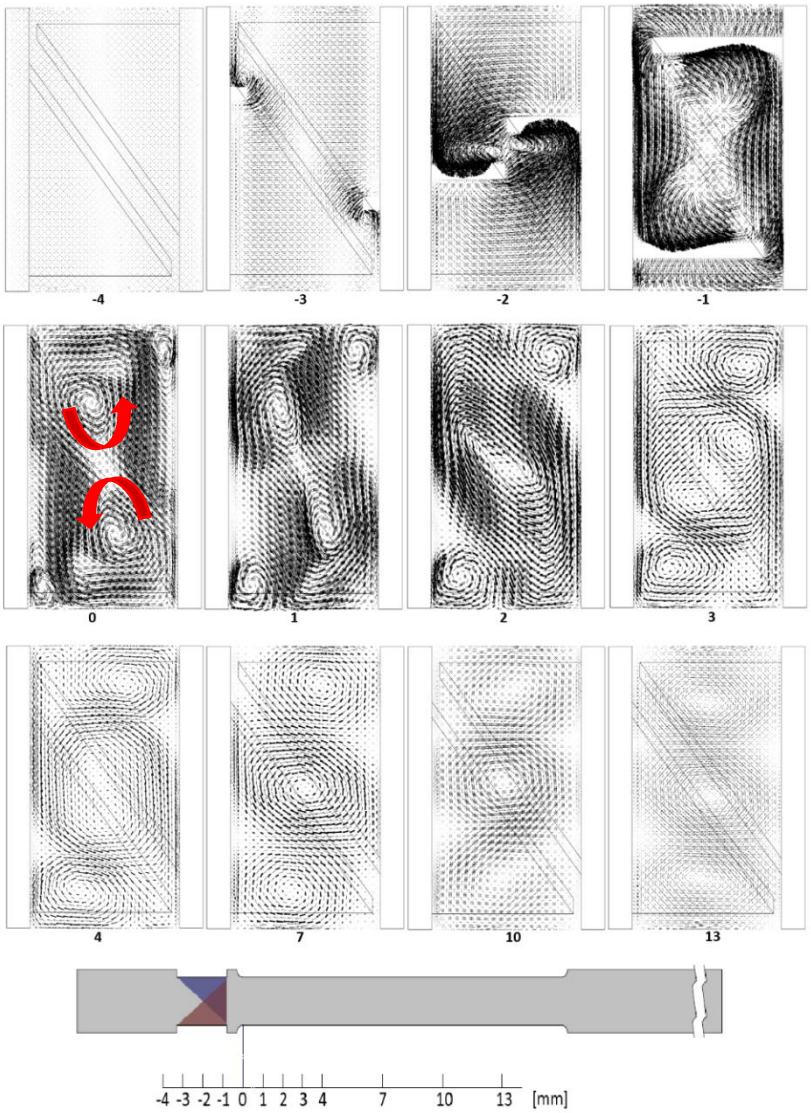

Figure 4.12 development of air tangent vectors for DTLVG

4.3 Parameter analysis of DTLVG

For optimal design of DTLVG, there are many parameters which influence the performance of DTLVG deserved to analysis. It can be easily inferred that the geometry of the DTLVG itself determines its performance. However, there are too many geometric parameters which has significant influence, such as the attach angle, the width, the height and thickness of each winglet, the distance between two winglets and so on. Moreover, these parameters may have joint influence on its performance. Hence, the analysis on the geometric parameters of DTLVG is difficult and may be conducted in the future. In this section, except for the geometric parameters of the DTLVG, several other parameters were analyzed below.

4.3.1 Gap between the DTLVG and finless heat exchanger

The gap between the DTLVG and finless heat exchanger plays an important role on the performance of DTLVG. As the vortex intensity decreases along the flow direction because of friction, a large gap will reduce the performance of DTLVG. However, if gap is very small, under the defrosting condition, the drainage water may be drop on the DTLVG and frost again. The DTLVG does not have the ability to defrost the ice, thus air block may be happen. For analysis, gap was set as 0.5 mm, 1 mm, 1.5 mm and 2 mm. the heat transfer coefficient and pressure drop for each a is shown in figure 4.13. As gap decrease from 0.5 mm to 1 mm, the heat transfer coefficient decreased from 133.9 W/m^{2}k to 129 W/m^{2}k. When gap kept decreasing to 2 mm, only 117.1 W/m^{2}k remained. The pressure drop almost kept constant. The result shows that the gap between the DTLVG and finless heat exchanger influence the heat transfer performance, which need to be carefully considered combining the drainage performance.

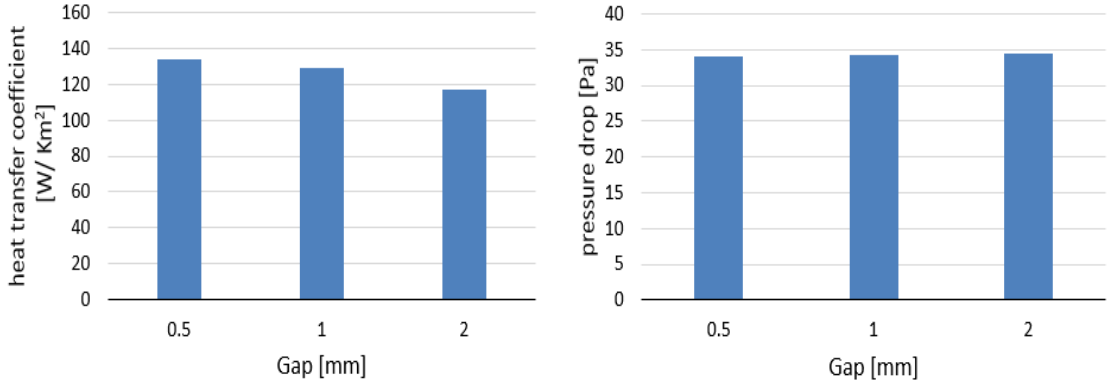

Figure 4.13 heat transfer coefficient and pressure drop of the finless heat exchanger with DTLVG with various

4.3.2 Tube width

As shown in figures 4.12, along the flow direction the intensity of vortex will keep decreasing thus the heat transfer decreases. If the width of tube become larger, the total heat transfer enhancement will decrease. For analysis, tube width was set as 12 mm, 16.6 mm and 20 mm. the heat transfer coefficient and pressure drop for each tube width is shown in figure 4.14. The result shows that when b increased to 20 mm, the heat transfer coefficient decreased from 133.9 W/m^{2}k to 110.1 W/m^{2}k. However, if b reduced to 12 mm, the heat transfer coefficient sharply grew to 186.3 W/m^{2}k. The pressure drop is similar, because that most of the pressure drop was caused by the DTLVG. In conclusion, DTLVG contributes more heat transfer enhancement for

narrow finless tube heat exchanger.

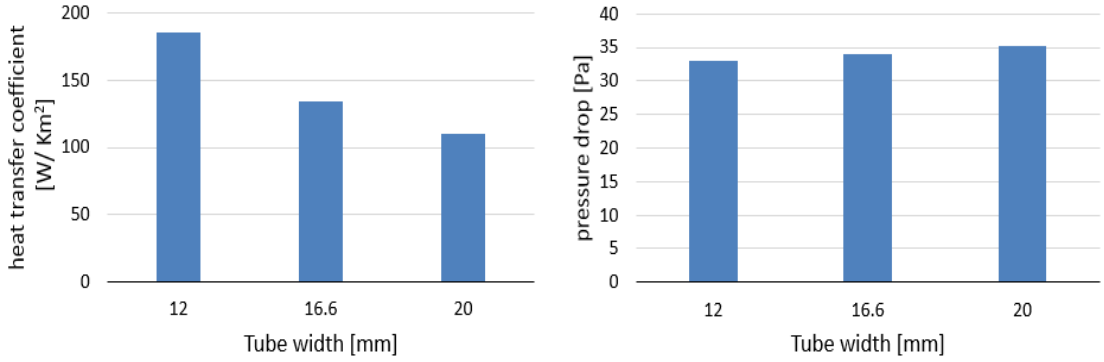

Figure 4.14 heat transfer coefficient and pressure drop of the finless heat exchanger with DTLVG with various tube width

4.3.3 Air velocity

Figure 4.15 shows the heat transfer coefficient and pressure drop for the finless heat exchanger with and without DTLVG as the air velocity various from 1.5 m/s to 3 m/s. As the air velocity increases, the heat transfer coefficient and pressure drop increases. With DTLVG, the increase rate at the air velocity of 1.5 m/s is 72%. While the air velocity grows to 3 m/s, the increase rate sharply increases to 120%. The reason is that the vortex intensity is strongly influenced by the air velocity that the large velocity provides stronger vortexes. However, the pressure drop also sharply increased by the growth of air velocity.

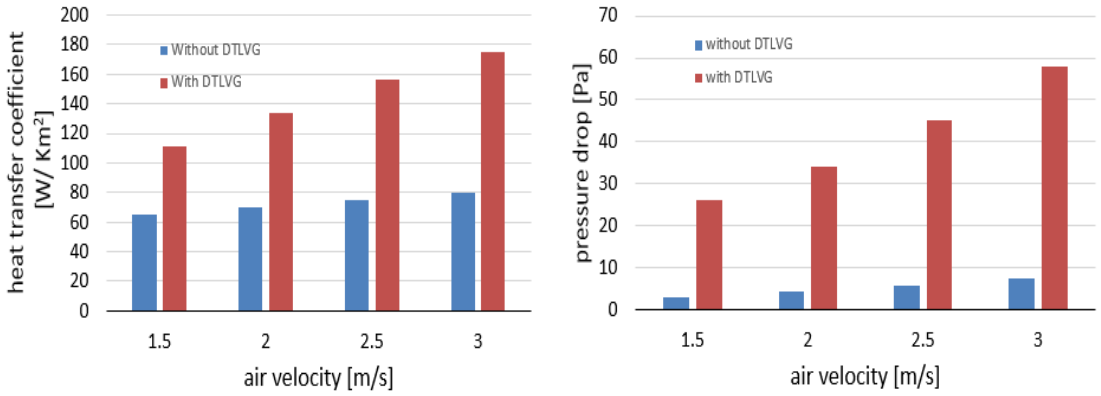

Figure 4.15 heat transfer coefficient and pressure drop of the finless heat exchanger with and without DTLVG at various air velocities

4.3.4 Robustness analysis

The finless heat exchanger is consisted only by the flexible flat tubes. Because there is no fins between these flat tubes, the tube pitches may be deviated from the designed tube pitch. Figure 4.16 shows the practical finless heat exchanger. The deviation of tube pitches is obvious, which causes that the vortexes created by the DTLVG could not directly transfer to the heat transfer region. Thus the vortexes will be destroyed by the flat tube and the heat transfer

enhancement will be reduced. As shown in figure 4.17, parameter (*e*-*d*)/2 representing the deviation of tube pitch. In this parameter analysis, the deviation of tube pitch is set as 0.4 mm and 0.8 mm. The heat transfer coefficient and pressure drop for each case is shown in figure 4.18. The result shows that when the deviation increased form 0 mm to 0.8 mm, the heat transfer coefficient decreased from 133.9 W/m^{2}k to 108 W/m^{2}k with a decreasing rate of 19.3%. Thus, the manufacture quality has considerable influence on the performance of DTLVG.

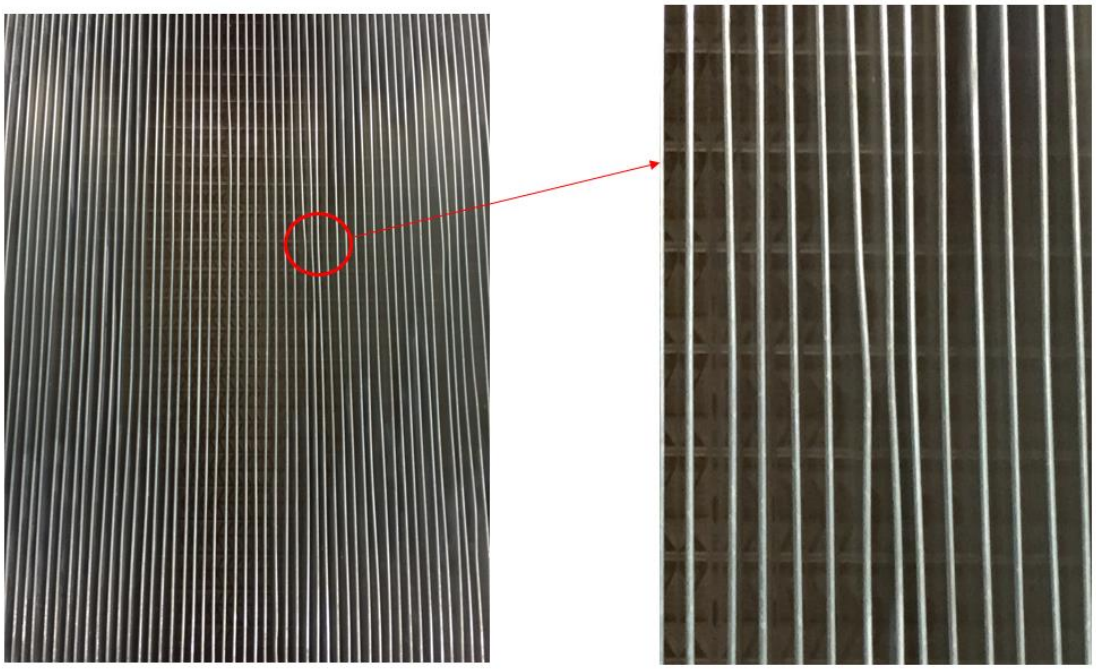

Figure 4.16 deviation of tube pitch in practical finless heat exchanger

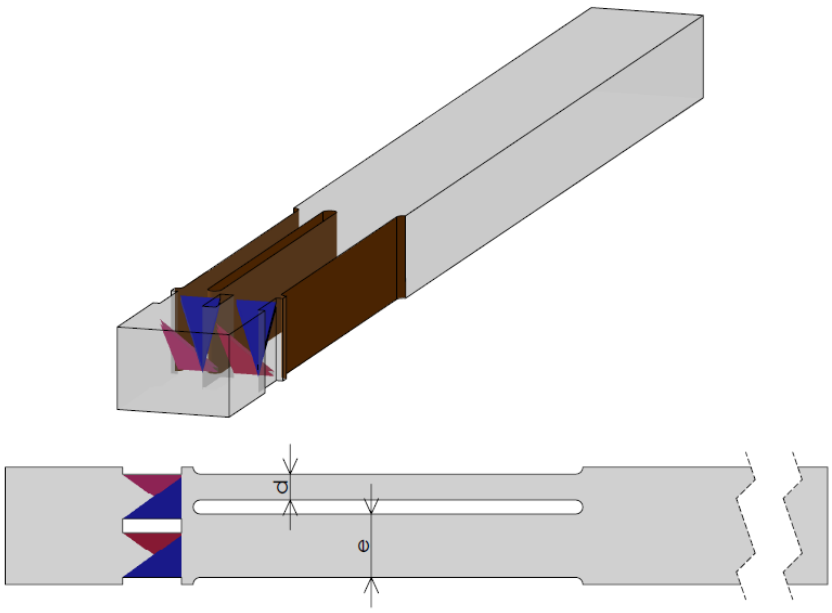

Figure 4.17 computational domain for pitch deviation analysis

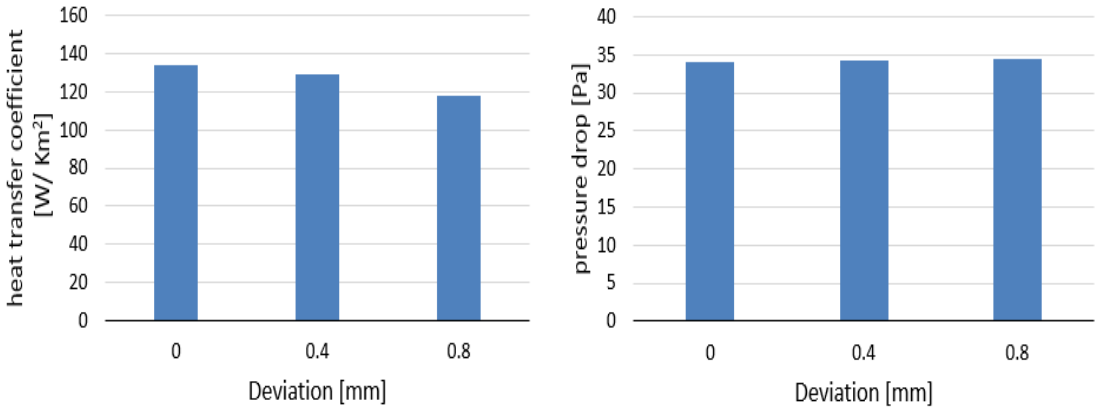

Figure 4.18 heat transfer coefficient and pressure drop of the finless heat exchanger with various tube pitch deviation

4.4. Experimental investigation on the performance of finless heat exchanger with DTLVG

The finless heat exchanger shown in Figure 4.19 consists of 80 vertically set, parallel aluminum multiport flat-tubes with a tube pitch of 2.5 mm. Each tube with a thickness of 0.6 mm, a width of 16.6 mm and a length of 200 mm, had 16 rectangular channels with a section of 0.9 mm × 0.2 mm. For the air-side heat transfer improvement, a DTLVG shown in Figure 4.19 was developed using numerical methods and manufactured using 3D printing technology. The LVG was installed in front of the finless heat exchanger with a gap of 1 mm, and the double triangles directly faced the gaps between flat tubes. The heat transfer performance and pressure drop of the finless heat exchanger with and without the DTLVG were experimentally measured under dry, wet, and frosting/defrosting conditions in a temperature- and humidity-controlled air tunnel. The experimental setup and test conditions are same to those for the fin-tube parallel heat exchanger introduced in section.

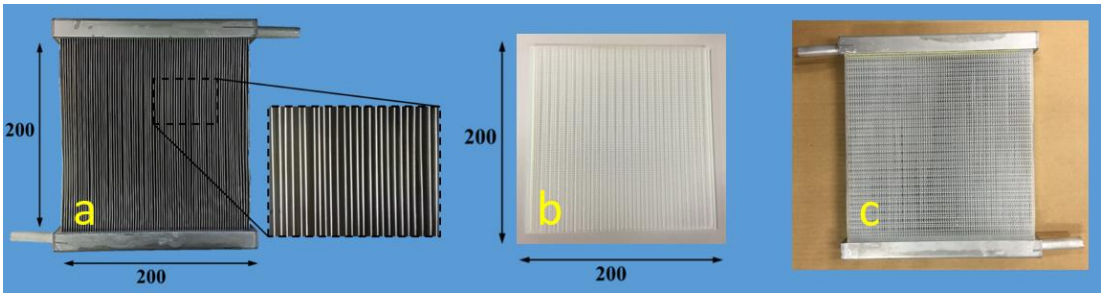

Figure 4.19 The tested finless heat exchanger and LVG

4.4.1 Dry conditions

Figure 4.20 shows the air-side pressure drops of the finless heat exchanger with and without DTLVG, as well as five fin-tube parallel heat exchangers at various air velocities, in dry conditions. As the air velocity increases from 1.5 m/s to 3 m/s, the pressure drop of each heat exchanger increases, as expected. Because of the DTLVG, the pressure drop of the finless heat exchanger dramatically increased which already surpassed the value of the fin-tube parallel heat exchanger S1.4, L1.4 and L1.6, and got close to L1.2 and S1.2. As shown in figure 4.21, though the heat transfer coefficient of the finless heat exchanger sharply enhanced by the DTLVG, comparing to fin-tube heat exchanger there was still a big gap. At the air velocity of 2 m/s, DTLVG dragged the heat transfer coefficient from 43.7 W/m^2k to 67.8 W/m^2k with an enhancement rate of 50.6%. For the fin-tube heat exchanger, all the value is beyond 100 W/m^2k. Therefore, under dry condition, the performance of finless heat exchanger is much lower than the fin-tube parallel heat exchangers which have more heat transfer surface area, even with the enhancement by DTLVG.

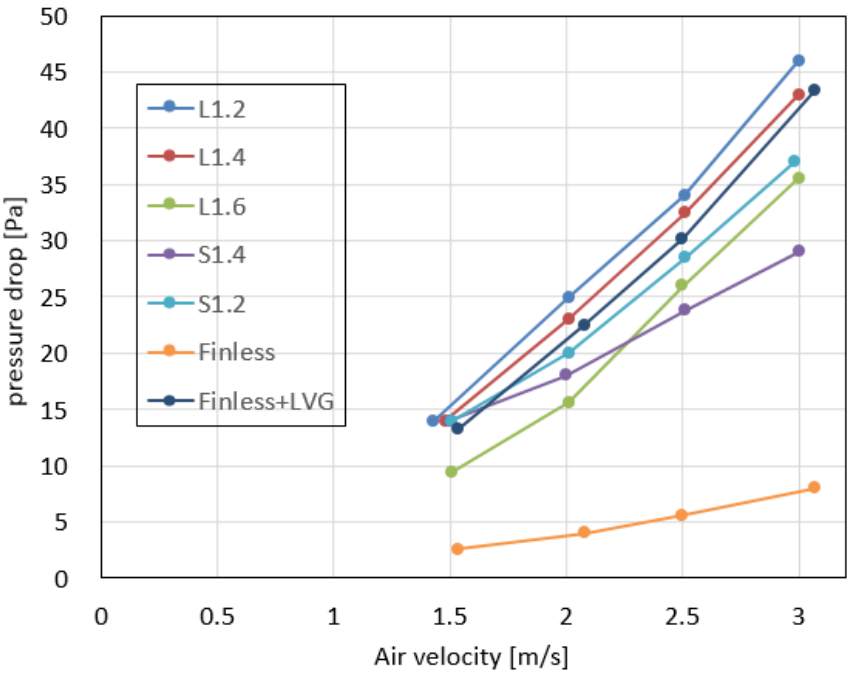

Figure 4.20 Air-side pressure drops of five heat exchangers at various air velocities in dry conditions

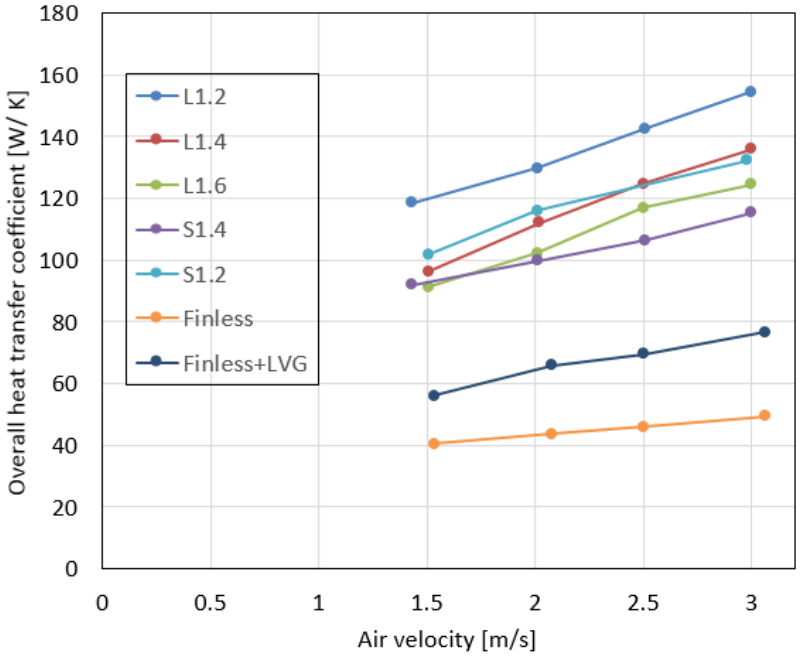

Figure 4.21 Overall air-side heat exchanger coefficients of five heat exchangers at various air velocities in dry conditions

4.4.2 Wet conditions

Under the wet condition, because of the better drainage performance, the performance gap

between the finless and fin-tube heat exchanger became smaller. Figure 4.22 shows the air-side pressure drops of the finless heat exchanger with and without DTLVG, as well as five fin-tube parallel heat exchangers at various air velocities, in wet conditions. For the finless heat exchanger, the condensate can be dropped down easily by gravity, while for the fin-tube heat exchanger, the condensate will stay on the horizontal set fins. Thus between the air and heat exchanger, there is water film contributing an additional thermal resistance. Without DTLVG, the air side transport coefficient of finless heat exchanger was still lower than that of fin-tube ones. Nevertheless, as shown in figure 4.23, with the enhancement by DTLVG, we can see that they are comparable. Under an air velocity of 2 m/s, the transport coefficient of the finless heat exchanger was dragged from 0.040 kg/s to 0.060 kg/s by DTLVG, which already surpassed the value of L1.6 and be comparable to L1.4, L1.2 and S1.2. Considering the pressure drop, though DTLVG induced a sharp increase for the finless heat exchanger, it is still much lower than S1.2, S1.4, L1.2 and L1.4.

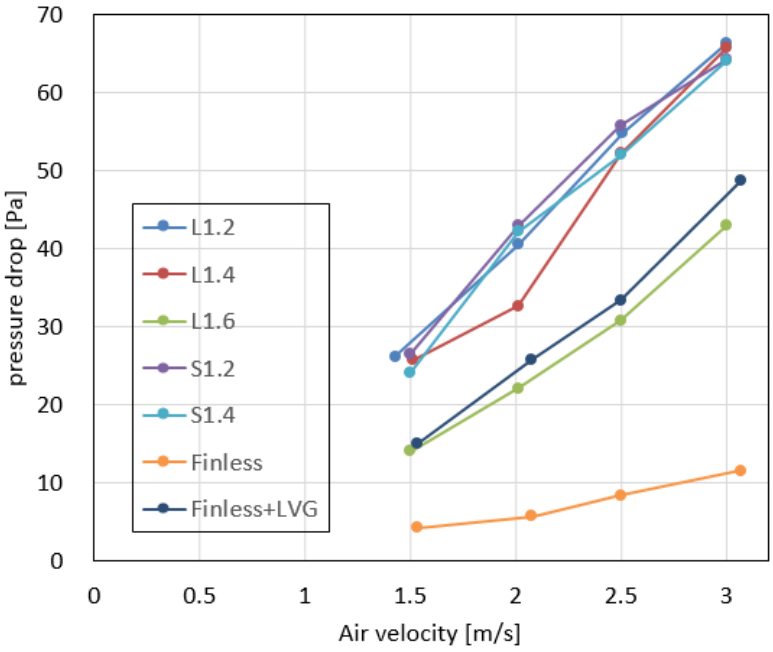

Figure 4.22 Air-side pressure drops of five heat exchangers at various air velocities in wet conditions

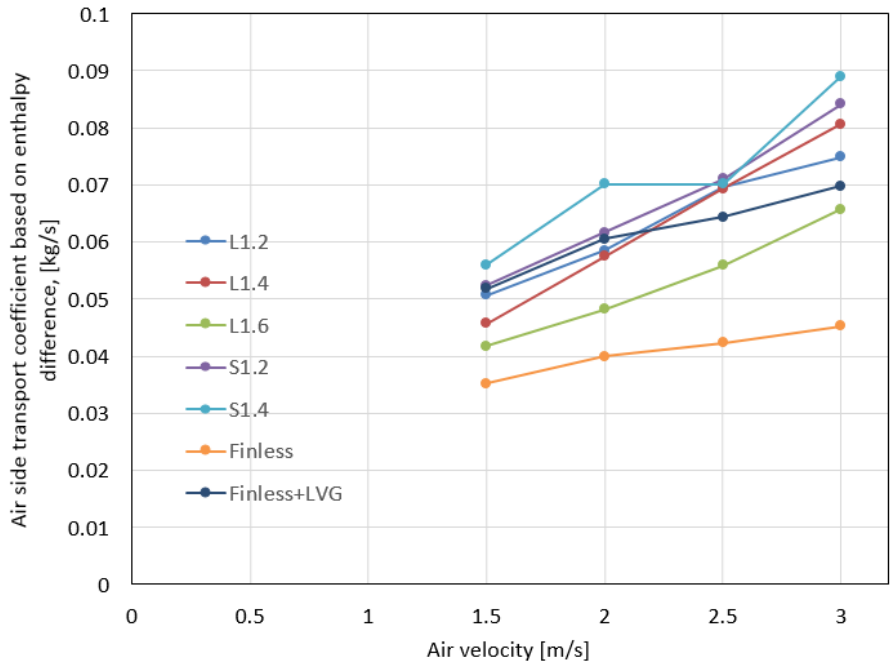

Figure 4.23 Overall air-side heat transfer coefficients of five heat exchangers under various air velocities in wet conditions

4.4.3 Frosting/defrosting conditions

Under the frosting/defrosting condition, the frost formation on fin-tube heat exchanger and finless heat exchanger is totally different. During each defrosting period, some of the water remained on the horizontally arranged fins for the fin-tube heat exchanger, then frosted quickly on the fins as the following frosting period began. This had a significant influence on the pressure drop and heat transfer performance of the following frosting period. However, for the finless heat exchanger, the water can be quickly be dropped down by gravity, which preventing the problem on the fin-tube heat exchangers.

Figures 4.24 and 4.25 show the pressure drops and overall heat transfer coefficients of the finless and fin-tube parallel exchangers, for 6 cycles of frosting/defrosting. As expected, the pressure drops of all heat exchangers dramatically increased with time in each frosting period, owing to the growth of the frost layer. Comparing to the fin-tube heat exchangers, the pressure drop of finless heat exchanger is much lower. At the end of each frosting period, the value with and without DTLVG just achieved 25 Pa and 50 Pa, while that of fin-tube heat exchangers all surpassed 100 Pa, especially in several cycle it surpassed 500 Pa. Moreover, it is worth noting that the pressure increase of finless heat exchanger for each cycle is almost similar. The reason is that after defrosting, there is almost no water remain on the heat exchanger, so each frosting period began with a similar initial condition.

In each frosting cycle, the overall heat transfer coefficients of finless heat exchanger slightly decreased with some fluctuation. With the enhancement by DTLVG, the transport coefficient

of finless heat exchanger increased around 50%, which prevailed over the fin-tube heat exchangers in most of the cycles. Another phenomenon needed to point out is that the decreasing rate of finless heat exchanger is much slower than that of fin-tube heat exchangers. The reason can be concluded to the formation of the remained water on the fin-tube heat exchanger, which provided a thermal resistance of ice quickly.

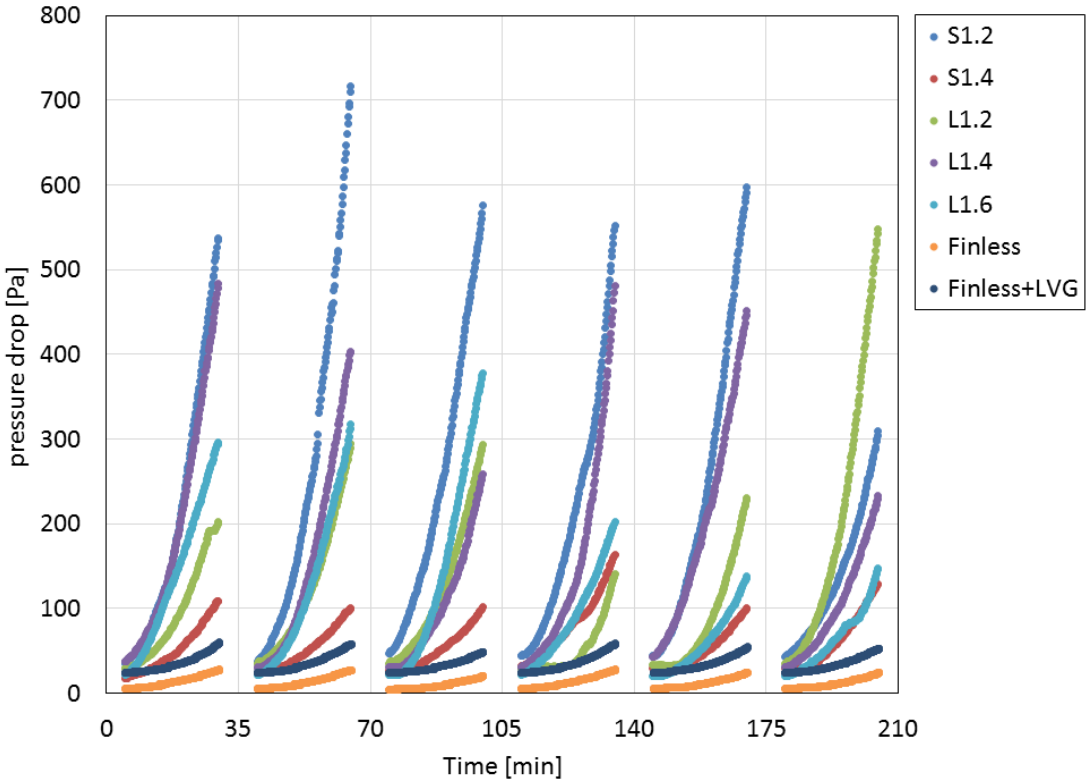

Figure 4.24 Air-side pressure drops of five heat exchangers at an air velocity of 2 m/s in the frosting/defrosting condition

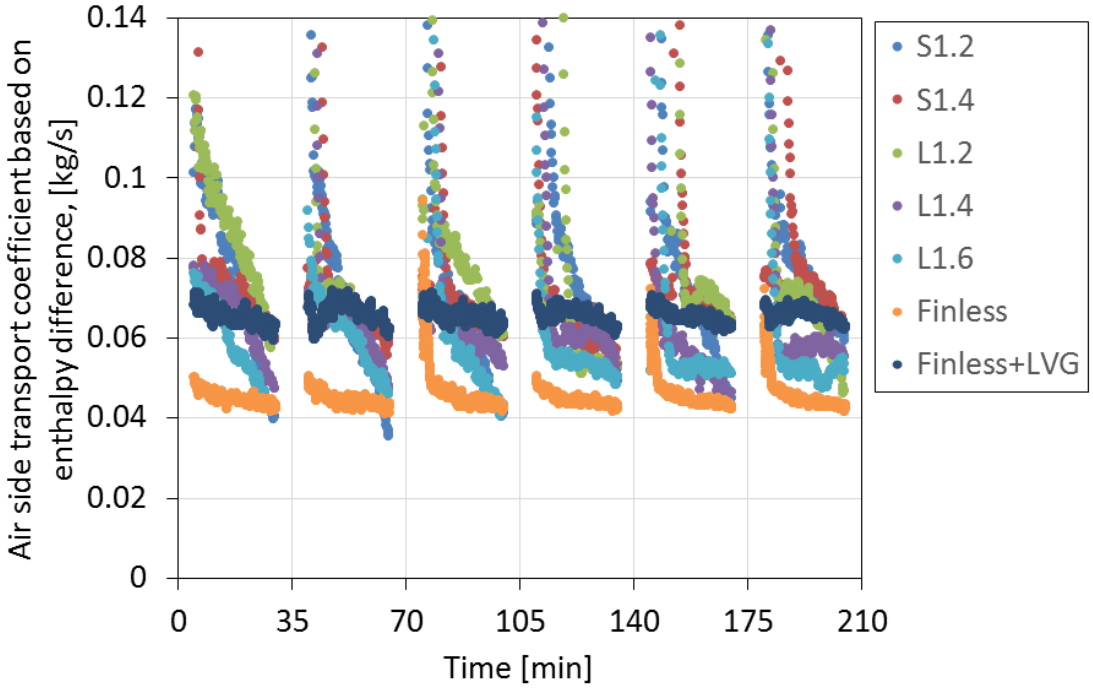

Figure 4.25 Overall air-side heat transfer coefficients of five heat exchangers at an air velocity of 2 m/s in the frosting/defrosting condition

4.5 Conclusions

Considering the poor drainage performance of fin-tube parallel heat exchangers, we proposed the finless heat exchangers with excellent drainage performance. However, the heat transfer performance of the finless heat exchanger is much lower than the fin-tube ones, due to the less heat transfer area and lower heat transfer coefficient. Hence, we proposed a method for the heat transfer enhancement of the finless heat exchanger, that in front of which a vortex generator is set. In the heat transfer domain between the flat tubes, the longitudinal vortex can disrupt the thermal boundary, as well as enhance the mixing of hot and cold air, thus the heat transfer performance can be sharply enhanced. With numerical simulation, a double triangle vortex generator is designed, which can offer more heat transfer enhancement comparing to conventional triangle and rectangular vortex generators. Moreover, some parameters analysis which affect the performance of vortex generator is conducted using numerical simulation. Finally, the heat transfer performance and pressure drops of finless heat exchangers with and without vortex generator were experimentally measured under dry, wet and frosting/defrosting conditions while the air velocity varied from 1.5 m/s to 3 m/s, and compared with the fin-tube parallel heat exchangers. Some conclusions are summarized below.

1. The heat transfer coefficient enhancement brought by the double triangle vortex generator is 92.3% when the air velocity is 2 m/s. Comparing with the triangle and rectangular vortex generator, the double triangle vortex generator bought 20% higher heat transfer coefficient, but also doubled the pressure drop, which achieved 34 Pa. However, the pressure drop is still acceptable.

2. Some parameters can significantly influence the performance of vortex generator. The smaller gap between the finless heat exchanger and the vortex generator, the shorter flat tube width, and the higher air velocity can offer higher heat transfer performance. The tube pitch deviation can sharply decrease the performance of vortex generator, a deviation of 0.8 mm can bring a decrease of 19.4% on heat transfer coefficient.

3. The heat transfer performance enhancement by the vortex generator is verified by experiments. Under the dry condition, comparing to the fin-tube heat exchangers, the heat transfer performance of finless heat exchanger is still about 40% less, while the pressure drop is similar. Under the wet condition, due to the excellent drainage performance, the heat transfer coefficient reached the same level with the fin-tube heat exchanger, while the pressure drop is lower. Under the frosting/defrosting condition, the heat transfer coefficient is similar, but the pressure drop is much lower, which only reach 50 Pa at each end of frosting period. Totally, comparing to the fin-tube heat exchanger, the performance of finless heat exchanger with vortex generator is still lower under dry condition, but it shows superiority under wet and frosting/defrosting conditions.

Chapter 5. Design of a novel manifold for parallel heat exchangers

5.1 Design of manifold

As mentioned in section 1.3.3, the gas and liquid tend to separate from each other in the manifold because of their different densities and initial force. These phenomenon inspire an idea to achieve using FBG without additional inner volume. That is, using the manifold as separator. The detail design of manifold is shown in figure 5.1. After two phase flow enter the inlet which set on one side of the manifold, because of lower density, gas changes its flow direction to the manifold length direction immediately, while the liquid impact on the manifold wall and accumulated at the bottom because of gravity. Since the inlets of flat tubes are set at the bottom of manifold, they will only receive liquid but not two phase flow. Moreover, the part of manifold, which combines the flat tubes, is inclined to ensure the reverse bubble converging to the main gas flow due to buoyance. Therefore, the bubbles will not accumulate in the bottom. The gas flow will be discharged out and converging to the evaporated gas at the out let of heat exchanger.

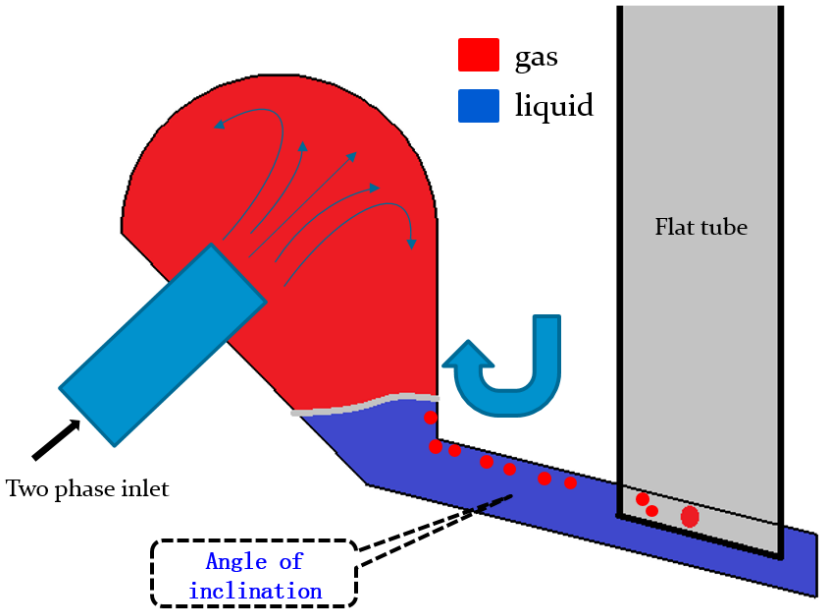

Figure 5.1 design of manifold

Figure 5.2 shows the working process of this new design. The two phase flow enter the inlet and separated in the header. The liquid enter the flat tubes for evaporating, while the gas flow through the whole header and then vent to the outlet of header. Meanwhile, the reverse bubbles converge to the main gas flow and vent out together. A valve is set in the gas flow path for regulating the pressure drop to achieve that the liquid flow to the flat tubes while most of gas vent out by the gas flow path. This design may be able to provide uninterrupted liquid inlet condition for each flat tube.

In addition, for each tube, the pressure drop ΔP_i which includes three parts: the pressure drop in the inlet header $\Delta P_{header,in}$, in the flat tube $\Delta P_{tube,i}$ and in the outlet header $\Delta P_{header,out}$, is equal to each other. If the diameter of header is large enough to decrease $\Delta P_{header,in}$ and $\Delta P_{header,out}$, $\Delta P_{tube,i}$ in each tube is almost equal. Because that $\Delta P_{tube,i}$ was mainly determined by the mass flux of inlet liquid, more uniform distribution of liquid in the heat exchanger may be achieved.

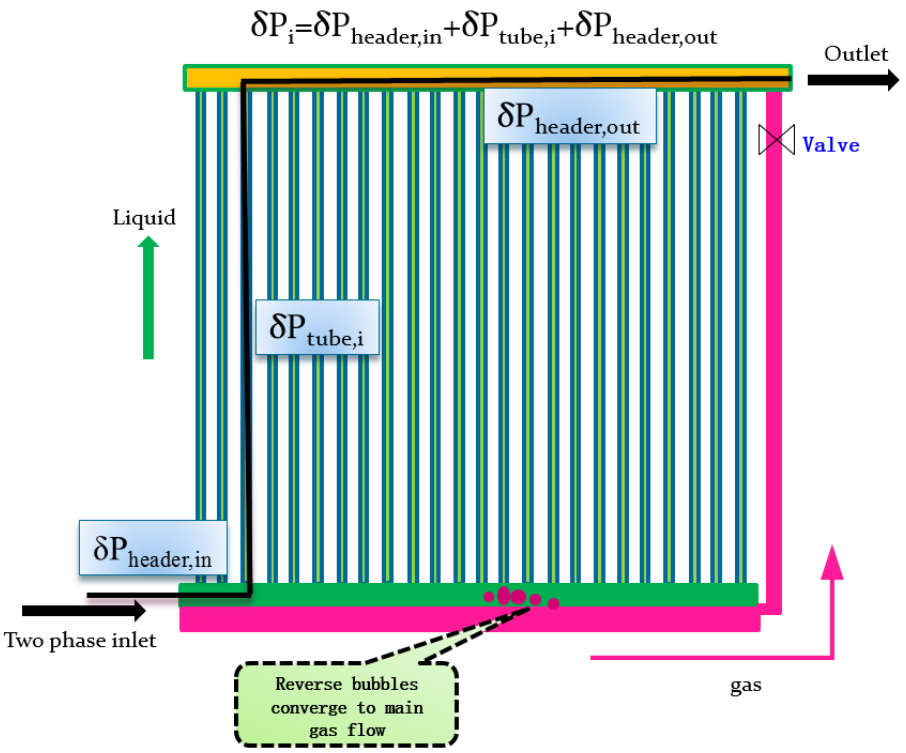

Figure 5.2 working process of the novel manifold

5.2 experimental verification

5.2.1 Design of experiment

According to the research presented in chapter 4, finless heat exchanger has potential to be used in the air conditioner system. For enhancing the air side heat transfer performance and reducing material, a new "finless tube" is proposed and shown in figure 5.3. Actually, there is a fin welding on the shorter flat tube, but the fin has the same orientation to the flat tube, making it similar to the previous one. For testing in a practical air conditioner system, a new heat exchanger composed of 209 pieces of this new finless tube is planned to be manufactured and tested in the outdoor unit. The length of each tube is 464 mm and the tube pitch is 2.2 mm. The test condition is listed in table 5.1.

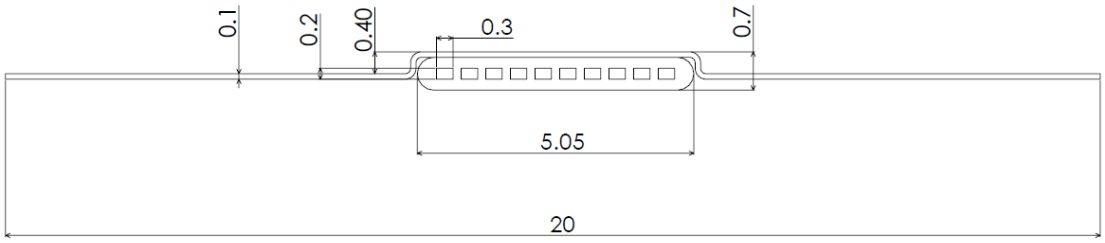

Figure 5.3 dimension of new "finless tube"

Table 5.1 test condition for the new "finless" heat exchanger

Refrigerant	R290
Evaporating temperature	-5 ℃ (superheated temperature: 0℃)
air temperature	5 ℃
air velocity	2 m/s
Air side heat transfer coefficient (with LVG)	108.1 W/m^{2}k
Mean refrigerant side heat transfer coefficient	4 kW/m^{2}k
Heat capacity	2.5 kW
Pressure drop (Lee-Lee correlation[79])	7.2 kPa

The experiment method is shown in figure 5.4. The heat provided to the heat exchanger is from the electric heating taps which can offer constant heat flux. If maldistribution happens, dry-out appears earlier in the tube receiving less liquid, thus in the dry-out region the temperature dramatically increases, which can be observed by the thermal camera. The heating tap is adhered on one side of the tubes, while the thermal camera monitors the opposite face. Hence, the width direction of the tube should be perpendicular to the manifold direction, as shown in figure 5.5.

R245fa which has a low saturated pressure under room temperature is chosen as the working fluid. Some properties of R245fa and R290 which may take significant influence on the distribution performance are listed in table 5.2. Because of the difference between refrigerant properties and heat exchanger structures, we cannot adopt the same working condition of the test heat exchanger for the experimental heat exchanger. However, we can choose several crucial parameters to be same to the test working condition.

In this new design of manifold, the reversed bubbles and their further movement, as well as the separation of two phase flow in the manifold, and finally the distribution performance need to be carefully observed. Thus, three working conditions are set and shown in table 5.3. In the first condition, the evaporated bubble volume, which may determine the quantity of reversed bubbles, is set to be same to the test condition. In the second condition, the heat flux, which may also be another influence factor for the reversed bubbles, is set be equal. In the third condition, for

investigating the separation of two phase flow in the manifold, the gas and liquid volume flow rate is set to be same. The detail design of the experimental heat exchanger is also listed in table 5.3.

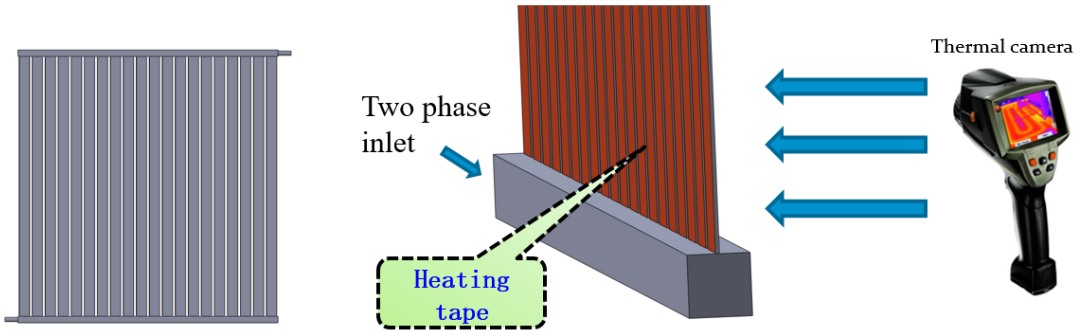

Figure 5.4 Experimental method

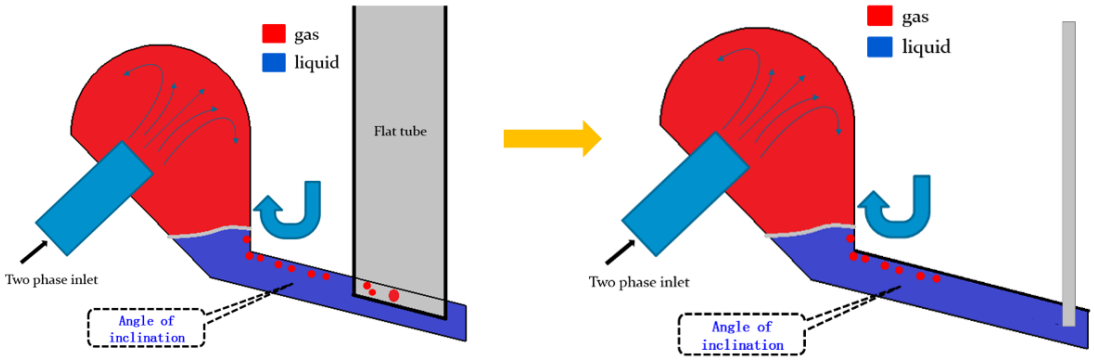

Figure 5.5 Arrangement of flat tubes

Table 5.2 Properties of R290 and R245fa

	R290 (propane)	R245fa
Saturated temperature (°C)	-5.0000	25.000
Saturated pressure (MPa)	0.40604	0.14825
Liquid density (kg/m^3)	535.27	1338.5
Vapor density (kg/m^3)	8.9103	8.5531
Latent heat (kJ/kg)	381.72	190.32
Liquid viscosity (mPa-s)	0.13223	0. 40725
vapor viscosity (Pa-s)	0.0073019	0.010256
Surface tension (mN/m)	10.786	14.045

Table 5.3 Experiment conditions

	Heat flux (kW/m^2)	Liquid volume flow rate (mL/s)	Gas volume flow rate (mL/s)	Liquid mass flow rate (g/s)	Gas mass flow rate (g/s)	Cooling capacity (W)
Test heat exchanger	2.7	15.1	389	8.1	3.5	2500
①	1.35	3.2	83	4.4	0.74	428
②	2.7	3.2	83	4.4	0.74	855
③	7.1	15.1	389	20.5	3.5	3290

①: Same volume of bubble evaporated, and Same ratio of gas to liquid volume flow rate

tube number: 20, tube length: 400 mm, tube channel number: 40, channel dimension: 0.21*0.34 mm

②: Same heat flux and Same ratio of gas to liquid volume flow rate

tube number: 20, tube length: 400 mm, tube channel number: 40, channel dimension: 0.21*0.34 mm

③: Same gas and liquid volume flow rate

tube number: 20, tube length: 400 mm, tube channel number: 16, channel dimension: 0.9*0.9 mm

The experimental setup is shown in figure 5.6. A gear pump is used for circulation, and the mass flow rate is measured by a Coriolis flowmeter. The pre-heater heated by electric is used to control the vapor quality at the inlet of test section, thus to control the gas and liquid volume flow rate. After the test section, the fluid flow to the first and second condenser for condensation. On one side of the test section, as shown in figure 5.7, a heating tape is adhered to each flat tube surface for evaporating the refrigerant. On the other side, black Aluminum tapes are adhered on the surfaces to prevent the influence of reflection of infrared ray from the environment, as shown in figure 5.8. For convenience, The shape of the manufactured manifold is shown in figure 5.9.

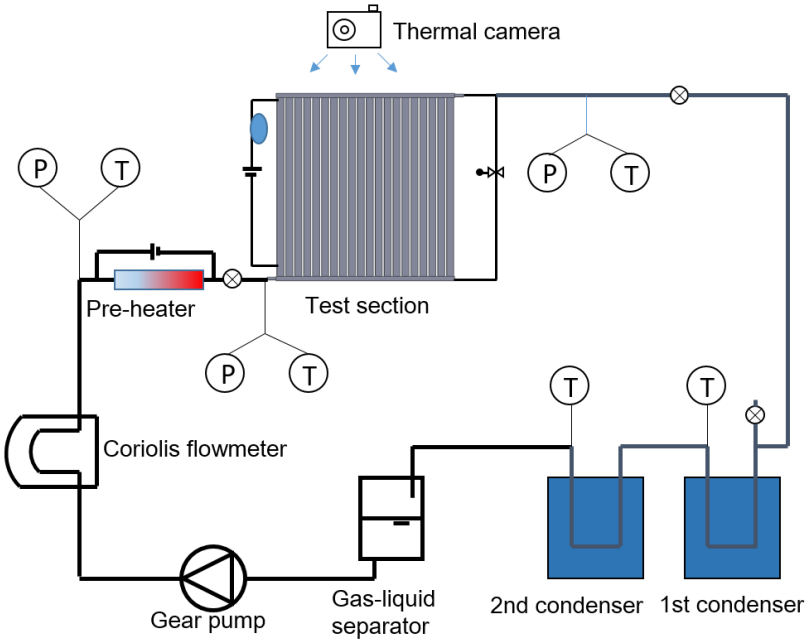

Figure 5.6 experimental setup of verification for the design of novel manifold

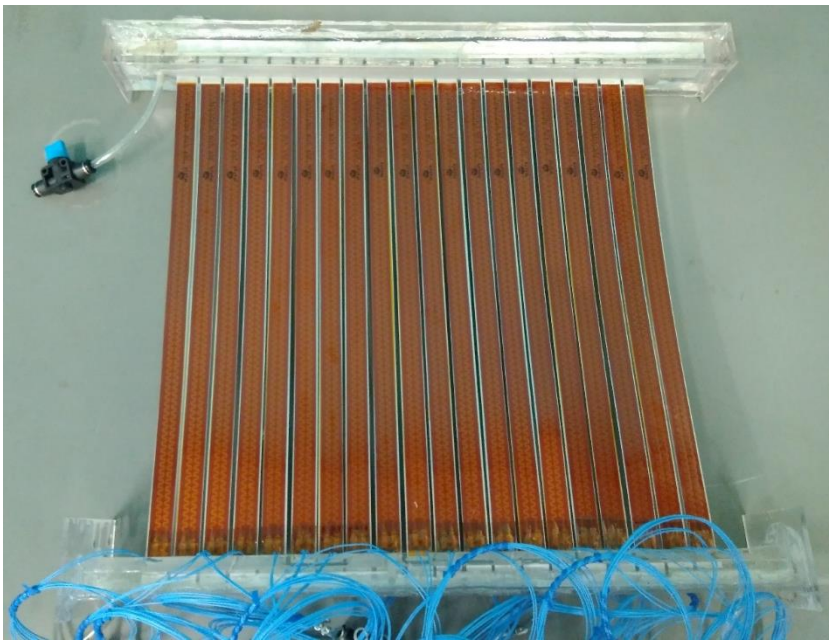

Figure 5.7 heating tapes on the flat tubes

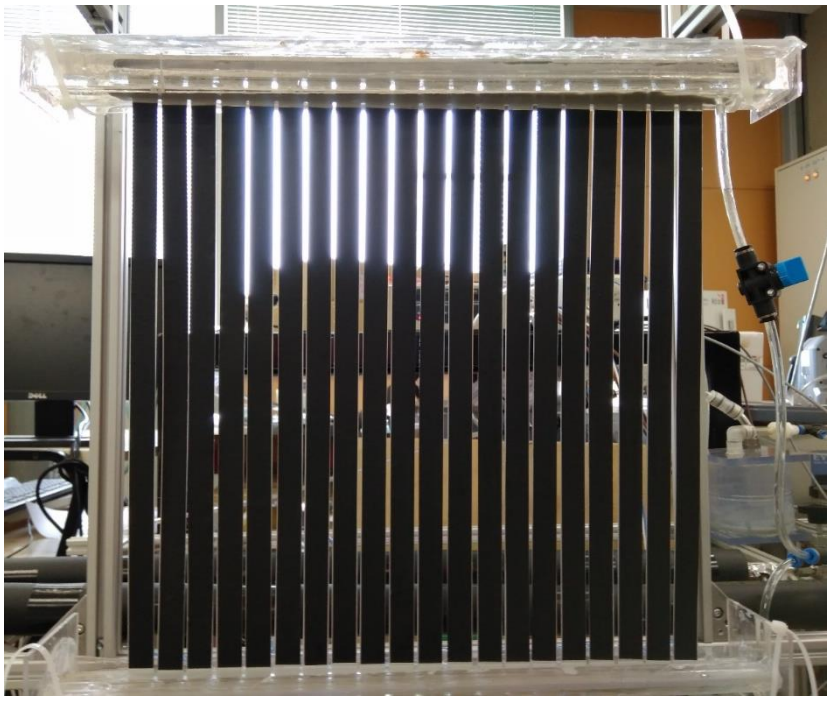

Figure 5.8 black Aluminum tapes on flat tubes for preventing reflection

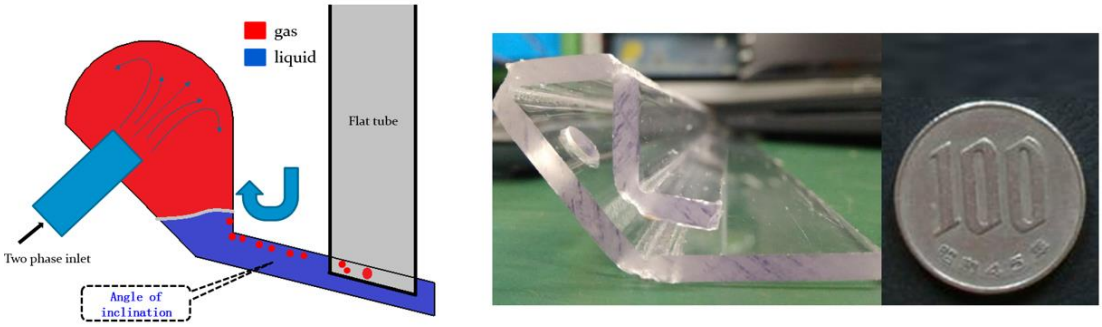

Figure 5.9 shape of manufactured manifold

5.2.2 Experiment results

For verifying the manufacture quality of the experimental heat exchanger, as well as the uniformity of heating, the heat exchanger is heated without any fluid inside. As shown in figure 5.10, the uniformity of heating is good, while the white color represent higher temperature than the red color. Then, subcooling liquid was pumped into the heat exchanger. It was found that the heat exchanger is uniformly cooled down, which validated the good quality of this heat exchanger and not tubes were blocked.

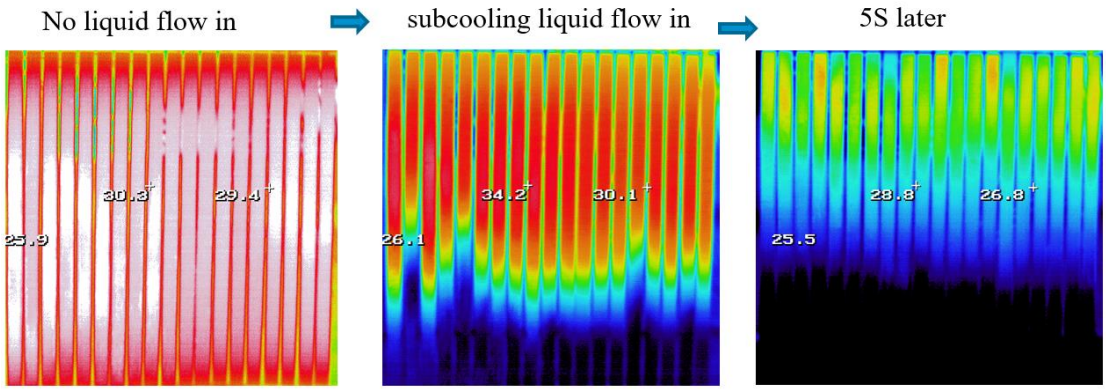

Figure 5.10 verification of manufacture quality of experimental heat exchanger

With a well manufactured heat exchanger, the experiment under the first condition listed in table 5.3 was conducted. Firstly, the two phase flow entered the heat exchanger without heating. As shown in figure 5.11, the separation between gas and liquid is clear. While the control valve is closed, liquid flowed through the tubes close to the inlet, while gas flowed to the further tubes as expected. By enlarging the control valve opening, more and more gas was piped to the outlet while more tubes received liquid. Figure 5.12 shows this adjusting process.

Then the heat was uniformly added on the tubes. For the tubes which received liquid, the reversed bubbles were clearly observed in a high frequency. As shown figure 5.13, the bubbles converged to the main gas flow quickly, which validated that the angle of inclination is effective. By adjusting the control valve, we achieved a state that all liquid flowed to the tubes while all

the gas was piped to the outlet. In such state, as shown in Figure 5.14 consisting of four randomly chosen thermal figures, the dry-out onset point of each tube is quite close, which meant that this new design of manifold has potential to offer acceptable distribution of refrigerant, while the control valve opening is well adjusted. However, the four figures also shows that the dry-out onset point of each tube somehow fluctuated. The reason may be attributed to the system pressure fluctuation and the reversed bubbles which caused pressure fluctuation.

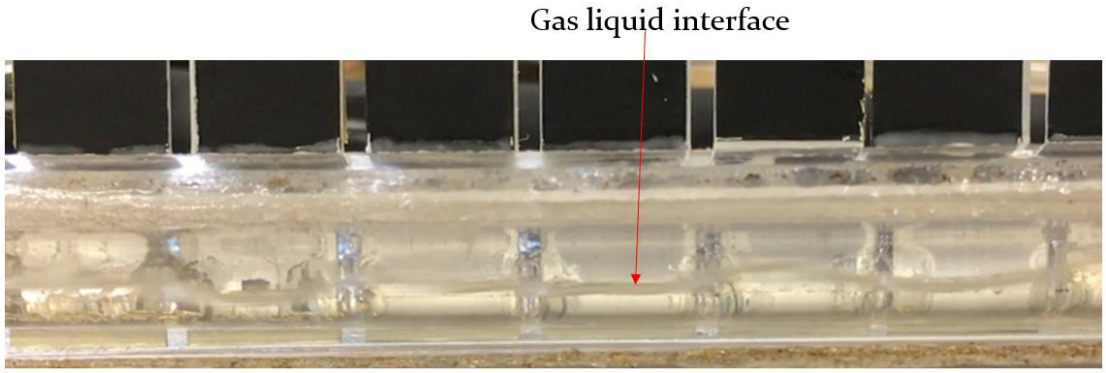

Figure 5.11 gas-liquid interface in the manifold

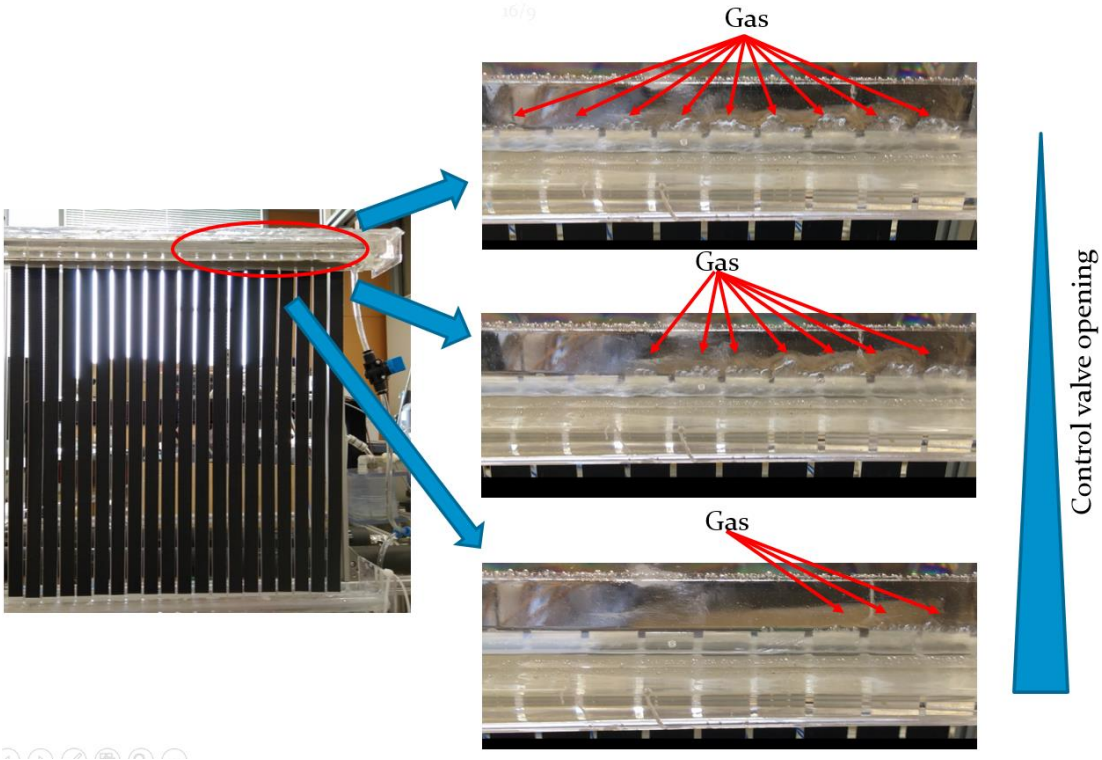

Figure 5.12 By-pass of gas

However, the control valve cannot be easily adjusted perfectly. If the valve opening is smaller than the perfect value, a part of gas will flow through the last several tubes, leading which lose their heat transfer ability as shown in figure 5.15. On the contrary, if the opening is larger than the perfect value, the liquid will gradually accumulate in the manifold. As the thickness of

liquid layer increasing, the wave on the gas-liquid interface tended to be stronger, as shown in figure 5.16. When the wave peak reach the inlet of by-pass tube, liquid instantaneously blocks the by-pass tube, leading an instantaneous pressure peak in the manifold. The instantaneous pressure peak causes a sudden mass flux increase of liquid in the heat transfer tubes and rewets the dry-out region. After the pressure peak, the liquid accumulates again. Figure 5.17 shows the thermal figures in such a cycle.

The experiment under the second and third conditions will be done in the future.

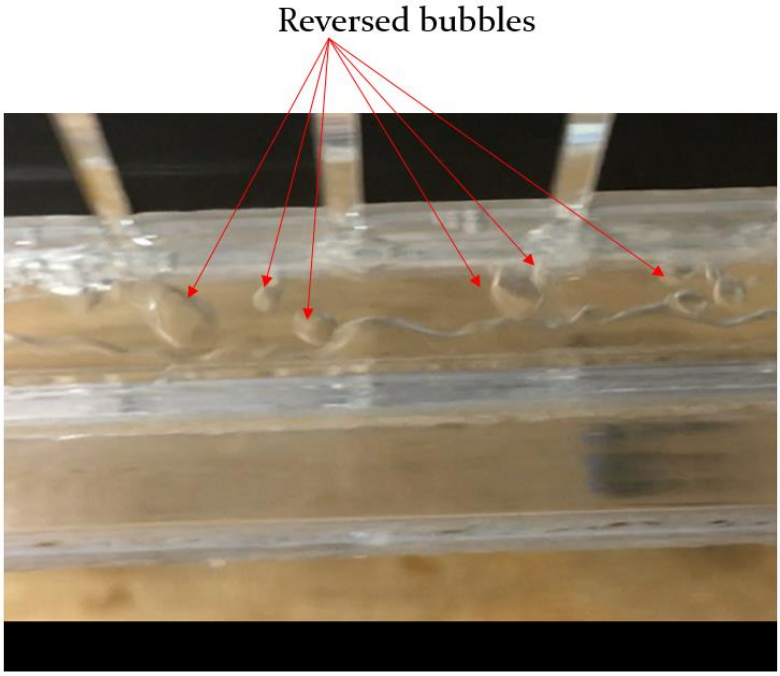

Figure 5.13 Reversed bubbles

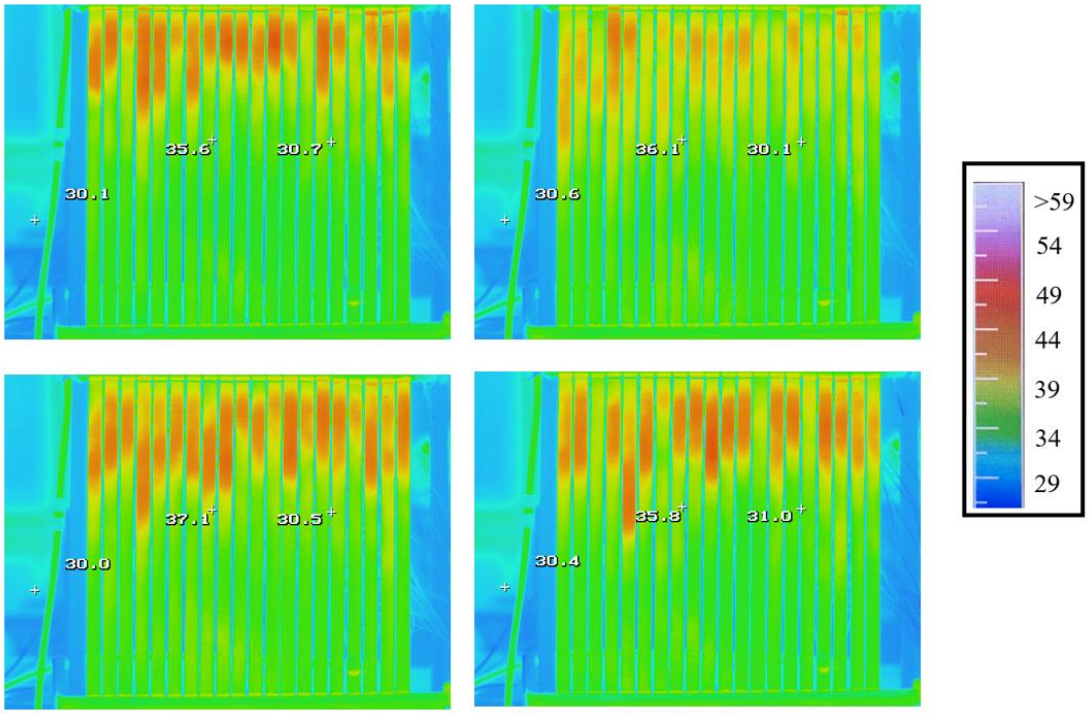

Figure 5.14 four randomly chosen thermal figures while the control valve was perfectly adjusted

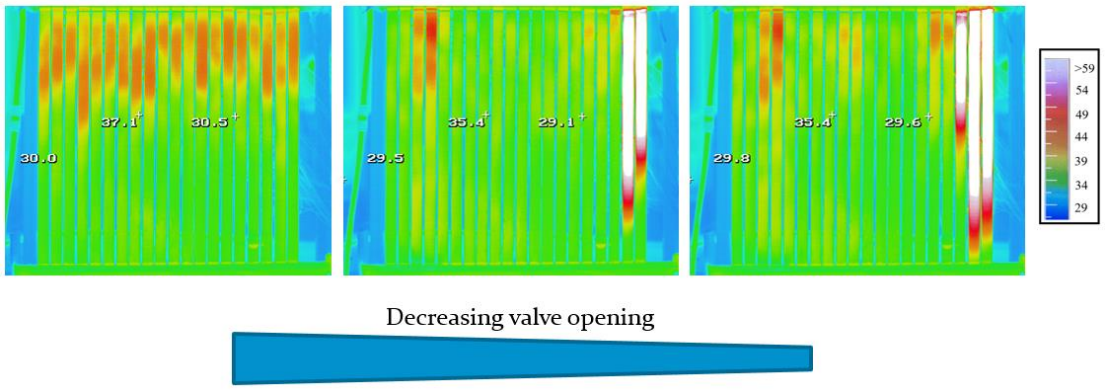

Figure 5.15 thermal figures while the control valve opening decreasing

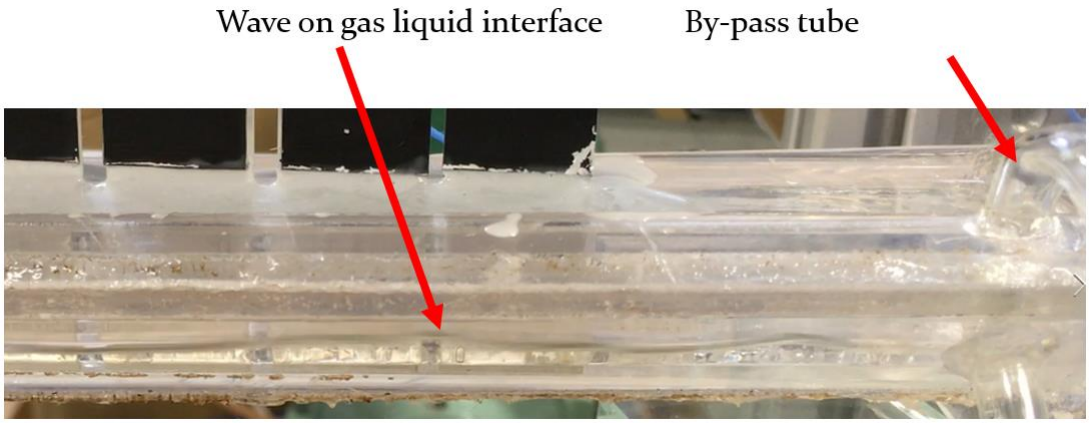

Figure 5.16 wave on gas liquid interface

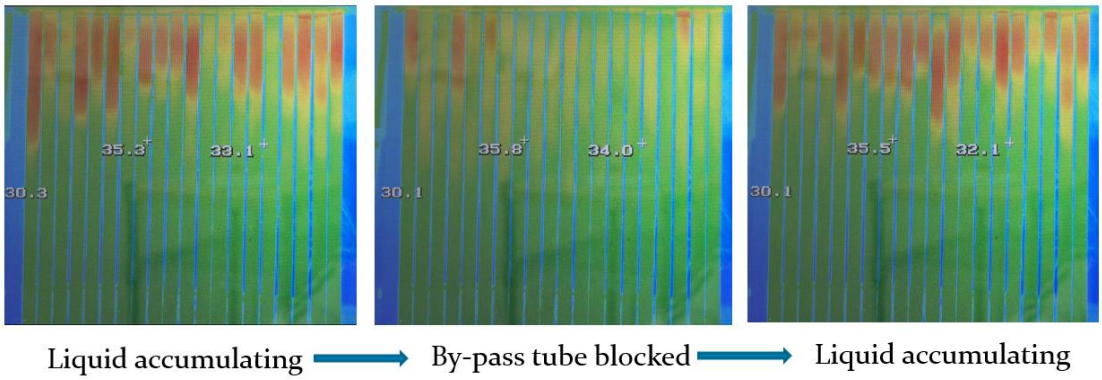

Figure 5.17 periodic thermal figures while the control valve was over opened

5.3 Conclusions and future work

The present experiment showed that utilizing the new manifold as a separator, a uniform liquid refrigerant distribution in each tube can be achieved by well adjusting the control valve. The reversed bubbles generated, converged to the main gas flow and flowed out rapidly, however they may cause slight pressure vibration in the manifold. The valve opening is important to the manifold performance. If it is too small, some heat transfer tubes may lose their heat transfer ability. On the contrary, an over opened control valve will cause a periodic pressure fluctuation in the manifold, which may lead to unstable operation.

In the future, the second and third working conditions listed in table 5.3 will be conducted to confirm the performance of manifold under larger two phase mass flow rate condition. The mechanism of pressure fluctuation in the manifold need to be further studied.

Chapter 6. Conclusions

For reducing the refrigerant charge amount in residential air conditioner system, therefor the low GWP but flammable refrigerant can be used safely, the aluminum parallel heat exchangers are supposed to be adopted instead of the conventional tube-fin ones. In this dissertation, the research focus on three aspects of the parallel aluminum heat exchanger. The first part is the up-flow boiling performance including heat transfer coefficient and pressure drop in aluminum flat tubes with various cross sections. The second part is the air side heat transfer coefficient and pressure drop under dry, wet and frosting/defrosting conditions. The fin-tube parallel heat exchanger may has deficiency on drainage, therefore we proposed the finless heat exchanger, whose heat transfer performance was further enhanced by a vortex generator. And the third part is a new design of manifold for parallel heat exchangers, which is expected to enhance the distribution uniformity of two phase flow among parallel flat tubes. The conclusions of each part is shown below.

1. Refrigerant side

The characteristics of local heat transfer and pressure drop were investigated experimentally for the vertical up-flow boiling of refrigerant R1234yf in two types of aluminum multi-port extruded tubes having 16 channels with a cross-section of 0.91 × 0.21 mm (tube A) and 40 channels with a cross-section of 0.34 × 0.21 mm (tube B). The heat transfer performance was compared with that of multi-port extruded tubes having 16 channels with a cross-section of 0.9 × 0.9 mm (tube C), and the pressure drop was compared with calculation results of three different correlations. From the results, the following conclusions can be drawn.

Under low heat and mass flux conditions, the heat transfer coefficient almost linearly decreased as a function of vapor quality in tubes A and B. As the vapor quality increased, the area of dry patches became lager within these rectangular channels, which deteriorated the heat transfer performance dramatically.

The channel dimensions significantly influenced the heat transfer performance. At a mass flux of 60 kg/m^{2}s, tube C showed better heat transfer performance than tubes A and B for all measured vapor quality regions because the shape of tubes A and B is not square, so the dry-out occurs more easily on the wider surfaces, thereby compromising the heat transfer performance. When the mass flux increased to 120 kg/m^{2}s, the dry-out was alleviated, enabling better performance in low vapor quality regions. In high vapor quality regions, the dry patches reoccupied the heat transfer area, leading to reduced heat transfer performance in tubes A and B. Moreover, tube A was worse than tube B because of its lower aspect ratio.

The correlations of Lee−Lee, Lockhart−Martinelli, and Mishima−Hibiki did not precisely predict the experimental pressure drops of tube A and B. Relatively, the Lockhart−Martinelli correlation showed better prediction. The data trend of decreasing heat transfer coefficient with increasing vapor quality was well predicted by the Saitoh et al. correlation and the

Agostini−Bontemps correlation, but the value shows large deviation.

2. Air side

Firstly, the research focuses on the performance of fin-tube parallel heat exchangers. The air-side pressure drops and overall transport coefficients of three louvered-fin all-aluminum parallel multi-port heat exchangers with a fin pitch of 1.2 mm, 1.4 mm and 1.6 mm, and two with slit-fins with a pitch of 1.2 mm and 1.4 mm were experimentally measured under dry, wet and frosting/defrosting conditions. The effects of fin pitch and type on the pressure drop and heat transfer performance were discussed.

In the dry condition, as the air velocity increased from 1.5 m/s to 3 m/s, the pressure drops and overall heat transfer coefficients of each heat exchanger increased. At the same air velocity, the pressure drops and overall heat transfer coefficients of louvered-fin heat exchangers were higher than those of slit-fin heat exchangers with same fin pitch.

In the wet condition, louvered- and slit-heat exchangers with fin pitch of 1.2 mm and 1.4 mm showed similar pressure drops and overall transport coefficients, which reflected that the effects of fin type and pitch were alleviated by the condensate on the fins. However, when the louvered-fin pitch increased to 1.6 mm, it showed lower pressure drops and overall transport coefficients.

In the frosting/defrosting condition, the pressure drop of a single heat exchanger was not identical in each frosting cycle, because of the different initial conditions due to the irregular retention distribution, whereas the overall heat transfer coefficients were relatively stable. The heat exchangers with a lower fin pitch showed higher overall transport coefficients. Nonetheless, the effect of fin type was not obvious on the overall transport coefficients.

For the heat exchangers of indoor units, which operate under dry and wet conditions, the louvered-fin with a fin pitch of 1.2 mm is recommended. However for the heat exchangers of outdoor units, which may operates under the frosting/defrosting condition, the slit-fin with a fin pitch of 1.4 mm is suggested.

Considering the poor drainage performance of fin-tube parallel heat exchangers, we proposed the finless heat exchangers with excellent drainage performance. However, the heat transfer performance of the finless heat exchanger is much lower than the fin-tube ones, due to the less heat transfer area and lower heat transfer coefficient. Hence, we proposed a method for the heat transfer enhancement of the finless heat exchanger, that in front of which a vortex generator is set. In the heat transfer domain between the flat tubes, the longitudinal vortex can disrupt the thermal boundary, as well as enhance the mixing of hot and cold air, thus the heat transfer performance can be sharply enhanced. With numerical simulation, a double triangle vortex generator is designed, which can offer more heat transfer enhancement comparing to conventional triangle and rectangular vortex generators. Moreover, some parameters analysis which affect the performance of vortex generator is conducted using numerical simulation. Finally, the heat transfer performance and pressure drops of finless heat exchangers with and without vortex generator were experimentally measured under dry, wet and frosting/defrosting

conditions while the air velocity varied from 1.5 m/s to 3 m/s, and compared with the fin-tube parallel heat exchangers. Some conclusions are summarized below.

The heat transfer coefficient enhancement brought by the double triangle vortex generator is 92.3% when the air velocity is 2 m/s. Comparing with the triangle and rectangular vortex generator, the double triangle vortex generator bought 20% higher heat transfer coefficient, but also doubled the pressure drop, which achieved 34 Pa. However, the pressure drop is still acceptable.

Some parameters can significantly influence the performance of vortex generator. The smaller gap between the finless heat exchanger and the vortex generator, the shorter flat tube width, and the higher air velocity can offer higher heat transfer performance. The tube pitch deviation can sharply decrease the performance of vortex generator, a deviation of 0.8 mm can bring a decrease of 19.4% on heat transfer coefficient.

The heat transfer performance enhancement by the vortex generator is verified by experiments. Under the dry condition, comparing to the fin-tube heat exchangers, the heat transfer performance of finless heat exchanger is still about 40% less, while the pressure drop is similar. Under the wet condition, due to the excellent drainage performance, the heat transfer coefficient reached the same level with the fin-tube heat exchanger, while the pressure drop is lower. Under the frosting/defrosting condition, the heat transfer coefficient is similar, but the pressure drop is much lower, which only reach 50 Pa at each end of frosting period. Totally, comparing to the fin-tube heat exchanger, the performance of finless heat exchanger with vortex generator is still lower under dry condition, but it shows superiority under wet and frosting/defrosting conditions.

3. Distribution of two phase flow in parallel tubes

Utilizing the new manifold as a separator, a uniform liquid refrigerant distribution in each tube can be achieved by well adjusting the control valve. The reversed bubbles generated, converged to the main gas flow and flowed out rapidly, however they may cause slight pressure vibration in the manifold. The valve opening is important to the manifold performance. If it is too small, some heat transfer tubes may lose their heat transfer ability. On the contrary, an over opened control valve will cause a periodic pressure fluctuation in the manifold, which may lead to unstable operation.

Acknowledgement

Time flies. I am going to finish my three years' abroad life in Japan, and return back to China. Fortunately, I get a doctoral degree, which would not have been possible without the contributions of several people.

First of all, I would like to show my gratitude to my supervisor, Professor Hihara Eiji. At the beginning of this research, he encouraged me to create new ideas, which made me feeling excited and optimistic for the future. In the first year, I almost got nothing in the research, but he never blamed on me and kept encouraging me. When I proposed something, he always supported and trusted on me, this gave me power to carry on. As a foreign student, life here is not as easy as in China. He also cared about my life, and put pressure on me as less as possible. However, I am very sorry for him that I did not insist on learning Japanese. Maybe I have a "lazy cancer". On the Mitsubishi meeting, he needed to translate my English report to Japanese, and he even wrote the Japanese abstract for my doctor thesis. I am very lucky to have such a nice professor in Japan. I wish him to be happy every day.

I would like to thank to professor Dang Chaobin. He gave me a lot of suggestions to improve my research, and for each paper I wrote, he revised it very carefully. He has very serious and pure spirit on research, which can be a model for Chinese researchers. I hope I can learn more from him.

I would like to thank to my senior He Jiacheng. He gave me numerous help on my life and research. He solved most of my life problems in Japan with his superb Japanese. Meanwhile, when I had problems on research, he always gave me some effective suggestions. I hope we will have a bright future in Guangdong province.

I received a lot of nice help from my lab members. Particularly, tutor Champaign Mr. Higashi Tomohiro helped me a lot. In the three years, when I had Japanese or research problem, he perfectly solved it that I don't know how to express my gratitude besides Sushi. Lovely Mr. Ito Makoto gave me kindly help on all the lab equipment, and Mr. Inoue Shunnosuke helped me a lot to give and receive telephone calls and emails with Japanese companies, that I will keep shopping in his "supermarket". Miss Yu Hanru, Mr. Chen Zuozhou and Mr. Cao Xufa gave me kindly help on my life, and my Korea friend Mr. Hong Sung Joo guided me a lot in Japan and brought numerous happiness to me in the three years. Thanks to my Chinese junior Mr. Yuan Shangqing and Miss Zheng Chen, who took me to the hospital when I was sick. Thanks to four lovely secretaries: Ms. Chikuma Yuka, Ms. Yoshimi Sachiyo, Ms. Kawai Kyoko and Ms. Chikamatsu Chizuko. Thanks to Professor Feng Shiyu, who kindly introduced me to this lab. Thanks to my friend Miss. Hsu Ya, Mr. Sun Guodong, they gave me kindly help on my life in Japan.

This study was sponsored by the project "Development of Non-fluorinated Energy-Saving

Refrigeration and Air Conditioning Systems" of the New Energy and Industrial Technology Development Organization, Japan. The author is grateful for the support from Ministry of Education, Culture, Sports, Science and Technology, Japan, as well as China Scholarship Council.

At last, deepest gratitude goes to my beloved parents and my grandmother. My parents work very hard and try their best to give me a better life, and their love makes me felling warm in my heart. My grandmother is 90 years old. I hope she can live beyond 100 years. I am going to work soon, that I hope I can bring better life to my family.

.

References

[1] Tuo H. Flash gas bypass-a way to improve distribution of adiabatic two-phase refrigerant flow in headers of microchannel evaporators[M]. University of Illinois at Urbana-Champaign, 2013.

[2] C. Zilio, J. S. Brown, G. Schiochet, A. Cavallini, The refrigerant R1234yf in air conditioning systems, Energy 36.10 (2011): 6110-6120.

[3] S. Jarall, Study of refrigeration system with HFO-1234yf as a working fluid, International journal of refrigeration 35.6 (2012): 1668-1677.

[4] S. Mortada, A. Zoughaib, C. Arzano-Daurelle, D. Clodic, Boiling heat transfer and pressure drop of R-134a and R-1234yf in minichannels for low mass fluxes, International Journal of Refrigeration 35.4 (2012): 962-973.

[5] D. Del Col, S. Bortolin, D. Torresin, A. Cavallini, Flow boiling of R1234yf in a 1 mm diameter channel, International journal of refrigeration 36.2 (2013): 353-362.

[6] S. Saitoh, C. Dang, Y. Nakamura, E. Hihara, Boiling heat transfer of HFO-1234yf flowing in a smooth small-diameter horizontal tube, International journal of refrigeration 34.8 (2011): 1846-1853.

[7] Z. Anwar, B. Palm, R. Khodabandeh, Flow boiling heat transfer, pressure drop and dryout characteristics of R1234yf: experimental results and predictions, Experimental Thermal and fluid Science 66 (2015): 137-149.

[8] K.E. Gungor, R.H.S. Winterton, A general correlation for flow boiling in tubes and annuli, International Journal of Heat and Mass Transfer 29.3 (1986): 351-358.

[9] Mirmanto, J.S. Lewis, T.G. Karayiannis, Flow patterns and heat transfer measurements for flow boiling of water in a rectangular microchannel, Proceedings of the 3rd European Conference on Microfluidics (2012).

[10] M. Li, C. Dang, E. Hihara, Flow boiling heat transfer of HFO1234yf and R32 refrigerant mixtures in a smooth horizontal tube: Part I. Experimental investigation, Int. J. Heat Mass Transfer 55 (2012) 3437–3446.

[11] M. Li, C. Dang, E. Hihara, Flow boiling heat transfer of HFO1234yf and HFC32 refrigerant mixtures in a smooth horizontal tube: Part II. Prediction method, Int. J. Heat Mass Transfer 64 (2013) 591–608.

[12] J.R. Thome, Boiling in microchannels: a review of experiment and theory, International Journal of Heat and Fluid Flow 25.2 (2004): 128-139.

[13] J.R. Thome, State-of-the-art overview of boiling and two-phase flows in microchannels, Heat transfer engineering 27.9 (2006): 4-19.

[14] S.G. Kandlikar, Fundamental issues related to flow boiling in minichannels and microchannels, Experimental Thermal and Fluid Science 26.2 (2002): 389-407.

[15] W. Qu, I. Mudawar, Flow boiling heat transfer in two-phase micro-channel heat sinks—I. Experimental investigation and assessment of correlation methods, International Journal of Heat and Mass Transfer 46.15 (2003): 2755-2771.

[16] M.K. Khan, R. Kumar, P.K. Sahoo, Flow characteristics of refrigerants flowing through capillary tubes–a review, Applied Thermal Engineering 29.8 (2009): 1426-1439.

[17] P. Cheng, G. Wang, X. Quan, Recent work on boiling and condensation in microchannels, Journal of Heat Transfer 131.4 (2009): 043211.

[18] S.M. Kim, I. Mudawar, Universal approach to predicting saturated flow boiling heat transfer in mini/micro-channels–Part II. Two-phase heat transfer coefficient, International Journal of Heat and Mass Transfer 64 (2013): 1226-1238.

[19] K. Enoki, K. Miyata, H. Mori, K. Kariya, Y. Hamamoto, Boiling heat transfer and pressure drop of a refrigerant flowing vertically upward in small rectangular and triangular tubes, Heat Transfer Engineering 34.11-12 (2013): 966-975.

[20] K. Enoki, K. Miyata, H. Mori, K. Kariya, Y. Hamamoto, Flow patterns of the vapor-liquid two-phase flow in small tubes. Transactions of the Japan Society of Refrigerating and Air Conditioning Engineers (2013), 30(2), 155-167.

[21] T.H. Yen, M. Shoji, F. Takemura, Y. Suzuki, N. Kasagi, Visualization of convective boiling heat transfer in single microchannels with different shaped cross-sections, International Journal of Heat and Mass Transfer 49.21 (2006): 3884-3894.

[22] C. Tanaka, C. Dang, E. Hihara, Characteristics of flow boiling heat transfer in rectangular minichannels, Proceedings of the 15th International Heat Transfer Conference, Kyoto, Japan: IHTC.

[23] C. Keepaiboon, S. Wongwises, Two-phase flow patterns and heat transfer characteristics of R134a refrigerant during flow boiling in a single rectangular micro-channel, Experimental Thermal and Fluid Science 66 (2015): 36-45.

[24] U. Soupremanien, S. Le Person, M. Favre-Marinet, Y. Bultel, Influence of the aspect ratio on boiling flows in rectangular mini-channels, Experimental thermal and fluid science 35.5 (2011): 797-809.

[25] R.L. Webb, S-H. Jung, Air-side performance of enhanced brazed aluminum heat exchangers, ASHRAE Transactions, 98-2 (1992).

[26] P. Zhang, P.S. Hrnjak, Air-side performance evaluation of three types of heat exchangers in dry, wet and periodic frosting conditions, International journal of refrigeration 32.5 (2009): 911-921.

[27] M-H. Kim, C.W. Bullard, Air-side performance of brazed aluminum heat exchangers under dehumidifying conditions, International Journal of refrigeration 25.7 (2002): 924-934.

[28] M-H. Kim, B. Youn, C.W. Bullard, Effect of inclination on the air-side performance of a brazed aluminum heat exchanger under dry and wet conditions, International Journal of Heat and Mass Transfer 44.24 (2001): 4613-4623.

[29] M-H. Kim, S. Song, C.W. Bullard, Effect of inlet humidity condition on the air-side performance of an inclined brazed aluminum evaporator, International journal of refrigeration 25.5 (2002): 611-620.

[30] J. Wu, G. Ouyang, P. Hou, H. Xiao, Experimental investigation of frost formation on a parallel flow evaporator, Applied energy 88.5 (2011): 1549-1556.

[31] E. Moallem, L. Cremaschi, D.E. Fisher, S. Padhmanabhan, Experimental measurements of the surface coating and water retention effects on frosting performance of microchannel heat exchangers for heat pump systems, Experimental Thermal and Fluid Science 39 (2012): 176-188.

[32] Y. Xia, Y. Zhong, P.S. Hrnjak, A.M. Jacobi, Frost, defrost, and refrost and its impact on the air-side thermal-hydraulic performance of louvered-fin, flat-tube heat exchangers, International Journal of Refrigeration 29.7 (2006): 1066-1079.

[33] B. Xu, Q. Han, J. Chen, F. Li, N. Wang, D. Li, X. Pan, Experimental investigation of frost and defrost performance of microchannel heat exchangers for heat pump systems, Applied energy 103 (2013): 180-188.

[34] B. Xu, C. Zhang, Y. Wang, J. Chen, K. Xu, F. Li, N. Wang, Experimental investigation of the performance of microchannel heat exchangers with a new type of fin under wet and frosting conditions, Applied Thermal Engineering 89 (2015): 444-458.

[35] N.C. Dejong, A.M. Jacobi, An experimental study of flow and heat transfer in parallel-plate arrays: local, row-by-row and surface average behavior, International Journal of Heat and Mass Transfer 40.6 (1997): 1365-1378.

[36] T.A. Cowell, M.R. Heikal, A. Achaichia, Flow and heat transfer in compact louvered fin surfaces, Experimental Thermal and Fluid Science 10.2 (1995): 192-199.

[37] A. Achaichia, T.A. Cowell, Heat transfer and pressure drop characteristics of flat tube and louvered plate fin surfaces, Experimental Thermal and Fluid Science 1.2 (1988): 147-157.

[38] Shikazono, N., Okawa, D., Kobayashi, M., Kasagi, N., Waki, T., Kandori, I., and Hataya, S. “Research and Development of High-Performance Compact Finless Heat Exchanger,” Proceedings of 6th International Conference on Enhanced, Compact and Ultra-Compact Heat Exchangers: Science, Engineering and Technology, CHE2007-0017.

[39] Nakano, H., Onishi, H., Tada, Y., and Takimoto, A. “Heat Transfer Characteristics of Finless Tube Heat Exchanger under Frost Conditions with Mist Deposition,” Proceedings of Thermal Engineering Conference, pp. 253-254, (2007).

[40] Onishi, H., Mido, S., Tada, Y., and Takimoto A. “Heat Transfer Characteristics with Frosting of Flat Tube Heat Exchanger for Refrigerator-Performance Comparison with Fin-and-Tube Heat Exchanger,” The 46th Japanese National Heat Transfer Symposium, C1-311, (2009).

[41] Kaneko, A., Katsuta, M., and Hori, R. “Research of Heat transfer and pressure drop characteristic of Concavo-Convex Plate,” The 48th Japanese National Heat Transfer Symposium, G321, (2011).

[42] Onishi, H., Yonekura, H., Tada, Y., and Takimoto, A. “Heat transfer performance of finless flat tube heat exchanger with vortex generator,” 14th International Heat Transfer Conference, IHTC14-23232, pp. 799-807, (2010).

[43] He Y L, Zhang Y. Advances and outlooks of heat transfer enhancement by longitudinal vortex generators[J]. arXiv preprint arXiv:1602.00323, 2016.

[44] Wu J M, Tao W Q. Investigation on laminar convection heat transfer in fin-and-tube heat exchanger in aligned arrangement with longitudinal vortex generator from the viewpoint of field synergy principle[J]. Applied Thermal Engineering, 2007, 27(14): 2609-2617.

[45] Wu J M, Tao W Q. Numerical study on laminar convection heat transfer in a rectangular channel with longitudinal vortex generator. Part A: Verification of field synergy principle[J]. International Journal of Heat and Mass Transfer, 2008, 51(5): 1179-1191.

[46] Chen Y, Fiebig M, Mitra N K. Conjugate heat transfer of a finned oval tube with a punched longitudinal vortex generator in form of a delta winglet—parametric investigations of the winglet[J]. International Journal of Heat and Mass Transfer, 1998, 41(23): 3961-3978.

[47] Chen Y, Fiebig M, Mitra N K. Heat transfer enhancement of a finned oval tube with punched longitudinal vortex generators in-line[J]. International Journal of Heat and Mass Transfer, 1998, 41(24): 4151-4166.

[48] Chen Y, Fiebig M, Mitra N K. Heat transfer enhancement of finned oval tubes with staggered punched longitudinal vortex generators[J]. International Journal of Heat and Mass Transfer, 2000, 43(3): 417-435.

[49] Fiebig M, Valencia A, Mitra N K. Wing-type vortex generators for fin-and-tube heat exchangers[J]. Experimental Thermal and Fluid Science, 1993, 7(4): 287-295.

[50] Biswas G, Mitra N K, Fiebig M. Heat transfer enhancement in fin-tube heat exchangers by winglet type vortex generators[J]. International Journal of Heat and Mass Transfer, 1994, 37(2): 283-291.

[51] Wang C C, Lo J, Lin Y T, et al. Flow visualization of annular and delta winlet vortex generators in fin-and-tube heat exchanger application[J]. International Journal of Heat and Mass Transfer, 2002, 45(18): 3803-3815.

[52] Torii K, Kwak K M, Nishino K. Heat transfer enhancement accompanying pressure-loss reduction with winglet-type vortex generators for fin-tube heat exchangers[J]. International Journal of Heat and Mass Transfer, 2002, 45(18): 3795-3801.

[53] Pesteei S M, Subbarao P M V, Agarwal R S. Experimental study of the effect of winglet location on heat transfer enhancement and pressure drop in fin-tube heat exchangers[J]. Applied Thermal Engineering, 2005, 25(11): 1684-1696.

[54] Wang Q, Chen Q, Wang L, et al. Experimental study of heat transfer enhancement in narrow rectangular channel with longitudinal vortex generators[J]. Nuclear Engineering and Design, 2007, 237(7): 686-693.

[55] Leu J S, Wu Y H, Jang J Y. Heat transfer and fluid flow analysis in plate-fin and tube heat exchangers with a pair of block shape vortex generators[J]. International Journal of Heat and Mass Transfer, 2004, 47(19): 4327-4338.

[56] Chu P, He Y L, Lei Y G, et al. Three-dimensional numerical study on fin-and-oval-tube heat exchanger with longitudinal vortex generators[J]. Applied Thermal Engineering, 2009, 29(5): 859-876.

[57] He Y L, Chu P, Tao W Q, et al. Analysis of heat transfer and pressure drop for fin-and-tube heat exchangers with rectangular winglet-type vortex generators[J]. Applied Thermal Engineering, 2013, 61(2): 770-783.

[58] Bowers, C.D., T.A. Newell, and P.S. Hrnjak, Experimental investigation of two-phase refrigerant distribution in a microchannel manifold, ACRC Report TR-245 (2006), Univ. of Illinois, Urbana,USA.

[59] Peng, F. D. Cantrak, and P.S. Hrnjak, 2002. Refrigerant distribution in the inlet header of plate evaporators. SAE Congress (2002), Paper No.2002-01-0948.

[60] Cho, H., and K. Cho, Mass flow rate distribution and phase separation of R-22 in multi microchannel tubes under adiabatic condition, Microscale Thermalphys. Eng., 8(2) (2003): 527–533.

[61] Hwang, Y., D.H. Jin, and R. Radermacher, Refrigerant distribution in minichannel evaporator manifolds. HVAC&R Research, 13(4) (2007): 543-555.

[62] Vist, S, and J. Pettersen, Two-phase flow distribution in compact heat exchanger manifolds. Exp.Therm. Fluid Sci., 28(2-3) (2004): pp.209-215.

[63] Kim, H.H., E.J. Lee, H.W. Byun, Two-phase refrigerant distribution in a parallel flow minichannel heat exchanger having horizontal headers. Int. J. Heat Mass Transfer, 55(25-26) (2012): 7747-7759.

[64] Peng, F., and P.S. Hrnjak, Adiabatic developing two-phase refrigerant flow in manifolds of heat exchangers. ACRC Report TR-225 (2004), Univ. of Illinois, Urbana, USA.

[65] Marchitto, A., F. Devia, M. Fossa, G. Guglielmini, and C. Schenone, Experiments on two-phase flow distribution inside parallel channels of compact heat exchangers. Int. J. Multiphas. Flow, 34(2)(2008): 128-144.

[66] Shi, J., X. Qu, Z. Qi, and J. Chen, Investigating performance of microchannel evaporators with different manifold structures. Int. J. Refrig., 34(1) (2011): 292-302.

[67] Dshida, M, and P.S. Hrnjak, Evaluation of microchannel heat exchangers for a residential minisplit type air-conditioning/heat pump system. ACRC Report CR-67 (2008), Univ. of Illinois, Urbana, USA.

[68] Elbel, S. and P.S. Hrnjak, Flash gas bypass for improving the performance of transcritical R744 systems that use microchannel evaporators. Int. J Refrig., 27(7) (2004): 724 – 735.

[69] Beaver, A.C., J.M. Yin, C.W. Bullard, and P.S. Hrnjak, An experimental investigation of transcritical carbon dioxide systems for residential air-conditioning. ACRC Report CR-18 (1999), Univ. of Illinois, Urbana, USA.

[70] Elbel, S. and P.S. Hrnjak, Experimental and Analytical Validation of New Approaches to Improve Transcritical CO2 Environmental Control Units. ACRC Report CR-52 (2003), Univ. of Illinois, Urbana, USA.

[71] Revellin, R., V. Dupont, T. Ursenbacher, J.R. Thome, and I. Zun, Characterization of diabatic twophase flows in microchannels: Flow parameter results for R-134a in a 0.5 mm channel. Int. J. Multiphas. Flow, 32(7) (2006): 755-774.

[72] Bowers, C.D., and P.S. Hrnjak, Developing adiabatic two-phase flow. ACRC Report TR-267,

(2009): Univ. of Illinois, Urbana, USA.

[73] Kuo, C.J., and Y. Peles, Flow boiling instabilities in microchannels and means for mitigation by reentrant cavities. J. Heat Transfer, 130(7) (2008): 072402-10.

[74] Kew, P.A. and K. Cornwell, Correlations for prediction of flow boiling heat transfer in smalldiameter channels. Appl. Therm. Eng., 17(8-10) (1997): 705-715.

[75] Kandlikar, S. G., W.K. Kuan, D.A. Willistein, and H. Borrelli, Stabilization of flow boiling in microchannels using pressure drop elements and fabricated nucleation sites, J Heat Transfer, 128(4) (2006): 389–396.

[76] Qu, W. and I. Mudawar, Transport phenomena in two-phase micro-channel heat sinks. J. Electron.Packaging, 126(2) (2004): 213-224.

[77] Balasubramanian, P. and S.G. Kandlikar, Experimental study of flow patterns, pressure drop, and flow instabilities in parallel rectangular minichannels. Heat Transfer Eng., 26(3) (2005): 20-27.

[78] Kosar, A., C. J. Kuo, and Y. Peles, Suppression of boiling flow oscillations in parallel microchannels with inlet restrictors, J Heat Transfer, 128(3) (2006): 251–260.

[79] H.J. Lee, S.Y. Lee, Pressure drop correlations for two-phase flow within horizontal rectangular channels with small heights, International Journal of Multiphase Flow 27.5 (2001): 783-796.

[80] R.W. Lockhart, R.C. Martinelli, Proposed correlation of data for isothermal two-phase, two-component flow in pipes, Chem. Eng. Prog 45.1 (1949): 39-48.

[81] K. Mishima, T. Hibiki, Some characteristics of air-water two-phase flow in small diameter vertical tubes, International Journal of Multiphase Flow 22.4 (1996): 703-712.

[82] S. Saitoh, H. Daiguji, E. Hihara, Correlation for boiling heat transfer of R-134a in horizontal tubes including effect of tube diameter, International Journal of Heat and Mass Transfer 50.25 (2007): 5215-5225.

[83] B. Agostini, A. Bontemps, Vertical flow boiling of refrigerant R134a in small channels, International journal of heat and fluid flow 26.2 (2005): 296-306.

[84] S.S. Bertsch, E.A. Groll, S.V. Garimella, A composite heat transfer correlation for saturated flow boiling in small channels, International Journal of Heat and Mass Transfer 52.7 (2009): 2110-2118.

[85] Yoshinaga Y, Peng H, Dang C, et al. Experimental Study on Liquid Film Thickness of Annular Flow in Microchannels[J]. 2014.

[86] S.G. Kandlikar, S. Garimella, D. Li, S. Colin, M.R. King, Heat transfer and fluid flow in minichannels and microchannels. Elsevier, 2005.

[87] Torii K, Kwak K M, Nishino K. Heat transfer enhancement accompanying pressure-loss reduction with winglet-type vortex generators for fin-tube heat exchangers[J]. International Journal of Heat and Mass Transfer, 2002, 45(18): 3795-3801.